

إقرار

أنا الموقع أدناه مقدم الرسالة التي تحمل العنوان:

Dye-Sensitized Solar Cells Using TiO₂ as a Semiconducting Layer

أقر بأن ما اشتملت عليه هذه الرسالة إنما هي نتاج جهدي الخاص، باستثناء ما تمت الإشارة إليه حيثما ورد، وإن هذه الرسالة ككل، أو أي جزء منها لم يقدم من قبل لنيل درجة أو لقب علمي أو بحث لدى أية مؤسسة تعليمية أو بحثية أخرى.

DECLARATION

The work provided in this thesis, unless otherwise referenced, is the researcher's own work, and has not been submitted elsewhere for any other degree or qualification.

Student's name: **KAMAL S. EI-REFI**

اسم الطالب :

Signature:

التوقيع:

Date: 7-12-2013

التاريخ:

Islamic University of Gaza
Deanery of Higher Studies
Faculty of Science
Department of Physics



Dye-Sensitized Solar Cells Using TiO_2 as a Semiconducting Layer

الخلايا الشمسية ذات الأصباغ باستخدام ثاني أكسيد التيتانيوم كطبقة شبه موصلة

By

KAMAL S. EL-REFI

B.Sc. in Physics, Islamic University of Gaza

Supervisors

Dr. Taher M. El-Agez

Associate Professor of Physics

Dr. Sofyan A. Taya

Associate Professor of Physics

**Submitted to the Faculty of Science as a Partial Fulfillment of the Master Degree
of Science (M. Sc.) in Physics**

1434 – 2013



نتيجة الحكم على أطروحة ماجستير

بناءً على موافقة الدراسات العليا بالجامعة الإسلامية بغزة على تشكيل لجنة الحكم على أطروحة الباحث/
كمال صبحي سالم الريفي لنيل درجة الماجستير في كلية العلوم قسم الفيزياء وموضوعها:

الخلايا الشمسية ذات الأصباغ باستخدام ثاني أكسيد التيتانيوم كطبقة شبه موصلة Dye-Sensitized Solar Cells Using TiO₂ as a Semiconducting Layer

وبعد المناقشة التي تمت اليوم الاثنين 02 ذو الحجة 1434هـ، الموافق 2013/10/07م الساعة
الحادية عشرة صباحاً، اجتمعت لجنة الحكم على الأطروحة والمكونة من:

.....
.....

T. Ahmad M. ... 11/10/2013

.....
.....

.....
.....

مشرفاً ورئيساً

مشرفاً

مناقشاً داخلياً

مناقشاً خارجياً

د. سفيان عبد الرحمن تايه

د. ظاهر محمد العاجز

أ.د. محمد موسى شبات

د. ناجي مطلق الداودي

وبعد المداولة أوصت اللجنة بمنح الباحث درجة الماجستير في كلية العلوم / قسم الفيزياء.

واللجنة إذ تمنحه هذه الدرجة فإنها توصيه بتقوى الله ولزوم طاعته وأن يسخر علمه في خدمة دينه ووطنه.

والله ولي التوفيق،،،

مساعد نائب الرئيس للبحث العلمي و للدراسات العليا

.....
.....

أ.د. فؤاد علي العاجز

Dedication

*If was dedication expressed though a part of the
fulfillment of
dedication*

To

*Teacher and the source of human knowledge of our
Prophet Muhammad (peace be upon him)*

To

Like fatherhood Highest ... And my dear father

To

granule my heart first ... my mother compassionate

To

*Tenderness code .. To the mother of all people ... Dear
grandmother*

To

Love all the love My brothers and sisters

To

All friends and family

To

Of paved road in front of me to get to the peak of science

Dedicate this modest effort

KAMAL S. EL-REFI

ACKNOWLEDGMENTS

In the name of Allah to whom I am overwhelmed with gratitude for his continuous help and guidance throughout the path of knowledge. I would like to express my gratitude to all those who gave me the possibility to complete this thesis.

I am extremely indebted to supervisors Dr. Sofyan Taya and Dr. Taher El-Agez for their constant support and whose help, and encouragement helped me in all time of research for arranging and writing of this thesis.

Personally, I'd like to thank all those who have helped with their advice and efforts .

ABSTRACT

The dye-sensitized solar cell (DSSC) is one of the photochemical electric cells, which consists of the photoelectrode, the dye, the electrolyte, and the counter electrode. The advantage of DSSCs is the low cost of the solar energy conversion into electricity because of inexpensive materials and the relative ease of the fabrication processes..

In this work, DSSCs were prepared using TiO_2 as a semiconducting layer with twenty natural and eight chemical dyes. Thin films of TiO_2 were spread on transparent conducting FTO coated glass using doctor blade method. The absorption spectra of all dyes were performed. The J-V characteristic curves of the fabricated cells were measured and studied at different light intensities. All photovoltaic parameters of the cells were presented. The results revealed that the extract of Mirabelle plums and Eosin Y lead to the highest efficiency. Impedance spectroscopy was measured for three cells with natural dyes and the equivalent circuit was found. The *Ziziphus jujuba* is the best natural dye were use, has values J_{sc} of 3.90 mA/cm^2 , V_{oc} of 0.661 V , $P_{max}=1.239 \text{ mW}$, $F.F=0.480$, and $\eta = 1.032\%$. The best performance was obtained for cell dyed with chemical dye Eosin Y which has the following results, $J_{sc} = 1.23 \text{ mA/cm}^2$, $V_{oc}=0.63 \text{ V}$, $P_{max}= 0.44 \text{ mW/cm}^2$, $F.F=0.52$, and $\eta =0.34\%$.

Abstract in Arabic

ملخص الدراسة

الخلايا الشمسية ذات الأصباغ (DSSC) هي واحدة من الخلايا الكهروكيميائية الضوئية ، والذي تتكون من القطب الضوئي ، الصبغة ، المنحل بالكهرباء ، والقطب العداد (البلاتين). ميزة DSSCs هو انخفاض تكلفة تحويل الطاقة الشمسية إلى كهرباء بسبب مواد غير مكلفة، والسهولة النسبية في عمليات التصنيع. في هذا العمل ، تم إعداد DSSCs باستخدام ثاني أكسيد التيتانيوم (TiO_2) كطبقة شبه الموصلة مع عشرين من الأصباغ الطبيعية وثمانية الكيمائية . تم تحضير أفلام رقيقة من (TiO_2) على الزجاج المطلبي (FTO) باستخدام أسلوب شفرة الطيب . أجريت أطياف امتصاص كل الأصباغ . وتم قياس منحنيات مميزة J-V من الخلايا المصنعة و درس في شدة إضاءة مختلفة . وعرضت جميع المتغيرات الضوئية للخلايا . وكشفت النتائج أن مستخلص السدر و يوزين γ يؤدي إلى أعلى كفاءة . وقد تم قياس مقاومة التحليل الطيفي لثلاث خلايا من الأصباغ الطبيعية و تم ايجاد الدائرة المكافئة . و السدر هو أفضل صبغة طبيعية استخدمت، و النتائج هي

$$J_{sc} = 3.90 \text{ mA/cm}^2 , V_{oc} = 0.661 \text{ V} , P_{max}=1.239 \text{ mW} , F.F=0.480 , \eta = 1.032\%.$$

تم الحصول على أفضل أداء لخلية مصبوغة مع الصبغة الكيمائية يوزين γ الذي يحتوي على النتائج التالية،

$$J_{sc}=1.23 \text{ mA/cm}^2 , V_{oc}=0.63 \text{ V} , P_{max}= 0.44 \text{ mW/cm}^2 , F.F=0.52 , \eta =0.34\%.$$

CONTENTS

Dedication.....	ii
ACKNOWLEDGMENTS.....	iii
ABSTRACT.....	iv
List of Figure Captions.....	viii
List of Table Captions	xv

CHAPTER ONE : INTRODUCTION AND STATE OF THE ART

1.1.Energy Sources	1
1.1.1.Non-Renewable Energy Sources.....	1
1.1.2.Renewable Energy Sources.....	1
1.2.Solar Irradiation and Availability of Solar Electricity.....	1
1.3 Types of Solar Energy Conversion.....	3
a. Thermal Solar Energy Conversion.....	3
b. Thermoelectric Solar Energy Conversion.....	3
c. Photoelectric Solar Energy Conversion.....	3
d. Chemical Solar Energy Conversion.....	4
1.4. Solar Electricity.....	4
1.5.Types of Solar Cells.....	4
1.5.1.Single-Crystalline and Polycrystalline Silicon Solar Cells.....	4
1.5.2.Thin Film Solar Cells.....	6
1.5.3.Photoelectrochemical Solar Cells.....	6
1.6. Gaza and Electricity Problem	7
1.7. State of the Art	8
1.8. Semiconductors and Light Absorption.....	9

CHAPTER TWO : DYE SENSITIZED SOLAR CELLS

Introduction.....	11
2.1 Materials of the Dye-Sensitized Solar Cells.....	11

2.1.1. Substrates.....	12
2.1.2 Nanoparticle Electrodes.....	12
2.1.3. Sensitizing Dyes	13
2.1.4. Electrolytes	14
2.1.5. Counter-Electrode Catalysts	14
2.1.6. Electrical Contacts.....	15
2.1.7. Sealing of Dye Sensitized Solar cell	15
2.2. Operating Principle	16
2.3. Parameters of Solar Cells.....	18
2.4. The Simple Electrical Model of a Solar Cell.....	20
2.5. Impedance Spectroscopy.....	22
2.5.1. Basic Knowledge for Understanding Impedance Spectroscopy.....	22
2.5.1.1. Introduction.....	22
2.5.1.2. Nyquist and Bode Plots.....	23
2.5.1.3. Equivalent Circuit Models	24
2.5.2. Electrochemical Elements	26
2.5.2.1. Lumped Elements	26
2.5.2.1.1. Resistance	26
2.5.2.1.2. Capacitance	27
2.5.2.1.3. Inductance	27
2.5.2.2. Frequency-Dependent Elements	27
2.5.2.2.1 Warburg Resistance	27
2.5.2.2.2. Constant Phase Element (CPE)	28

CHAPTER THREE : EXPERIMENTAL WORK

3.1. Natural Dyes as Photosensitizers for Dye Sensitized Solar Cells.....	30
3.1.1 Material Used in Preparing Solar Cells.....	30
3.1.2. Experimental.....	30
3.1.2.1 Natural Dyes Extraction	30
3.1.2.2. Preparation of Dye Sensitized Solar Cells	31

3.1.3. Cell Characterizations	33
3.1.3.1. Measuring Absorption Spectra of Natural Dyes.....	33
3.1.3.2. J-V Measurements.....	33
3.1.4. Electrochemical Impedance Spectroscopy.....	34
3.2. Chemical Dyes as Photosensitizers for Dye Sensitized Solar Cells.....	34
3.2.1 Material Used in Preparing Solar Cells.....	34
3.2.2 Chemical Dyes Preparation	35
CHAPTER FOUR : RESULTS AND DISCUSSION	
4.1. Natural Dyes as Photosensitizers for Dye Sensitized Solar Cells.....	38
4.1.1 Absorption Spectra of Natural Dyes.....	38
4.1.2. Photovoltaic Parameters of Natural Dye Sensitized Solar Cells..	49
4.2. Chemical Dyes as Photosensitizers for Dye Sensitized Solar Cells.....	79
4.2.1 Absorption Spectra of Chemical Dyes.....	79
4.2.2 Photovoltaic Properties of Chemical Dye Sensitized Solar Cells	83
4.3 Results and Discussions of Electrochemical Impedance Spectroscopy	95
CHAPTER FIVE:	
Conclusion	105
References	107

List of Figure Captions

CHAPTER ONE

- Figure 1.1 Spectral distribution of solar radiation. 3
- Figure 1.2 Light absorption by semiconductor. The impinging photon induces an electron transition from the valence band into the conduction band if $h\nu \geq E_g$. 10

CHAPTER TWO

- Figure 2.1. Materials of dye sensitized solar cell 11
- Figure 2.2. The working principle of the dye-sensitized nanostructured solar cell. 19
- Figure 2.3. Voltage – current characteristics of a solar cell. Shaded area represents the maximum achievable output power. 21
- Figure 2.4. Equivalent circuit of a solar cell including series and shunt resistances. 21
- Figure 2.5. A Nyquist plot (complex-plane diagram). 24
- Figure 2.6. A Bode modulus, and phase plots. 24

CHAPTER THREE

- Figure 3.1 Doctor blade method to spread the TiO_2 paste on FTO coated glass. 32
- Figure 3.2 A side view of the TiO_2 film under magnification of 100x. 32
- Figure 3.3 A top view of the TiO_2 film under magnification of 40x. 33

CHAPTER FOUR

- Figure 4.1 The absorption spectrum of the extract of Cream using ethyl alcohol. 39
- Figure 4.2 The absorption spectrum of the extract of Apricot using ethyl alcohol. 40
- Figure 4.3 The absorption spectrum of the extract of Figs using ethyl alcohol. 40

Figure 4.4	The absorption spectrum of the extract of Apple using ethyl alcohol.	41
Figure 4.5	The absorption spectrum of the extract of Sage using ethyl alcohol.	41
Figure 4.6	The absorption spectrum of the extract of Thyme using ethyl alcohol.	42
Figure 4.7	The absorption spectrum of the extract of Mint using ethyl alcohol.	42
Figure 4.8	The absorption spectrum of the extract of Ziziphus jujuba using ethyl alcohol.	43
Figure 4.9	The absorption spectrum of the extract of Orange using ethyl alcohol.	43
Figure 4.10	The absorption spectrum of the extract of Shade tree using ethyl alcohol.	44
Figure 4.11	The absorption spectrum of the extract of Basil using ethyl alcohol.	44
Figure 4.12	The absorption spectrum of the extract of Berries using ethyl alcohol.	45
Figure 4.13	The absorption spectrum of the extract of Mirabelle plums using ethyl alcohol.	45
Figure 4.14	The absorption spectrum of the extract of Victoria plums using ethyl alcohol.	46
Figure 4.15	The absorption spectrum of the extract of Paech using ethyl alcohol.	46
Figure 4.16	The absorption spectrum of the extract of Mango using ethyl alcohol.	47
Figure 4.17	The absorption spectrum of the extract of Pomegranate using ethyl alcohol.	47
Figure 4.18	The absorption spectrum of the extract of Bananas using ethyl alcohol.	48
Figure 4.19	The absorption spectrum of the extract of Guava using ethyl alcohol.	48
Figure 4.20	The absorption spectrum of the extract of Fluoridation using ethyl alcohol.	49

Figure 4.21	Current density–voltage curves for the DSSCs sensitized by Cream at different light intensities.	50
Figure 4.22	Power - voltage characteristics of the DSSCs sensitized by Cream at different light intensities.	50
Figure 4.23	Current density–voltage curves for the DSSCs sensitized by Apricot at different light intensities.	51
Figure 4.24	Power - voltage characteristics of the DSSCs sensitized by Apricot at different light intensities.	51
Figure 4.25	Current density–voltage curves for the DSSCs sensitized by Figs at different light intensities.	52
Figure 4.26	Power - voltage characteristics of the DSSCs sensitized by Figs at different light intensities.	52
Figure 4.27	Current density–voltage curves for the DSSCs sensitized by Apples at different light intensities.	53
Figure 4.28	Power - voltage characteristics of the DSSCs sensitized by Apples at different light intensities.	53
Figure 4.29	Current density–voltage curves for the DSSCs sensitized by Sage at different light intensities.	54
Figure 4.30	Power - voltage characteristics of the DSSCs sensitized by Sage at different light intensities.	54
Figure 4.31	Current density–voltage curves for the DSSCs sensitized by Thyme at different light intensities.	55
Figure 4.32	Power - voltage characteristics of the DSSCs sensitized by Thyme at different light intensities.	55
Figure 4.33	Current density–voltage curves for the DSSCs sensitized by Mint at different light intensities.	56
Figure 4.34	Power - voltage characteristics of the DSSCs sensitized by Miant at different light intensities.	56
Figure 4.35	Current density–voltage curves for the DSSCs sensitized by Ziziphus jujuba at different light intensities.	57
Figure 4.36	Power - voltage characteristics of the DSSCs sensitized by Ziziphus jujuba at different light intensities.	57
Figure 4.37	Current density–voltage curves for the DSSCs sensitized by Orange at different light intensities.	58

Figure 4.38	Power - voltage characteristics of the DSSCs sensitized by Orange at different light intensities.	58
Figure 4.39	Current density–voltage curves for the DSSCs sensitized by Shade tree at different light intensities.	59
Figure 4.40	Power - voltage characteristics of the DSSCs sensitized by Sade tree at different light intensities.	59
Figure 4.41	Current density–voltage curves for the DSSCs sensitized by Basil at different light intensities.	60
Figure 4.42	Power - voltage characteristics of the DSSCs sensitized by Basil at different light intensities.	60
Figure 4.43	Current density–voltage curves for the DSSCs sensitized by Mirbelle plums at different light intensities.	61
Figure 4.44	Power - voltage characteristics of the DSSCs sensitized by Mirbelle plums at different light intensities.	61
Figure 4.45	Current density–voltage curves for the DSSCs sensitized by Mirbelle plums at different light intensities.	62
Figure 4.46	Power - voltage characteristics of the DSSCs sensitized by Mirbelle plums at different light intensities.	62
Figure 4.47	Current density–voltage curves for the DSSCs sensitized by Victoria plums at different light intensities.	63
Figure 4.48	Power - voltage characteristics of the DSSCs sensitized by Victoria plums at different light intensities.	63
Figure 4.49	Current density–voltage curves for the DSSCs sensitized by peach at different light intensities.	64
Figure 4.50	Power - voltage characteristics of the DSSCs sensitized by Peach at different light intensities.	64
Figure 4.51	Current density–voltage curves for the DSSCs sensitized by Mango at different light intensities.	65
Figure 4.52	Power - voltage characteristics of the DSSCs sensitized by Mango at different light intensities.	65
Figure 4.53	Current density–voltage curves for the DSSCs sensitized by Pomegranate at different light intensities.	66
Figure 4.54	Power - voltage characteristics of the DSSCs sensitized by Pomegranat at different light intensities.	66

Figure 4.55	Current density–voltage curves for the DSSCs sensitized by Bananas at different light intensities.	67
Figure 4.56	Power - voltage characteristics of the DSSCs sensitized by Bananas at different light intensities.	67
Figure 4.57	Current density–voltage curves for the DSSCs sensitized by Guava at different light intensities.	68
Figure 4.58	Power - voltage characteristics of the DSSCs sensitized by Guava at different light intensities.	68
Figure 4.59	Current density–voltage curves for the DSSCs sensitized by Fluoridation at different light intensities.	69
Figure 4.60	Power - voltage characteristics of the DSSCs sensitized by Fluoridation at different light intensities.	69
Figure 4.61	The absorption spectrum of the extract of Eosin using ethyl alcohol as a solvent.	79
Figure 4.62	The absorption spectrum of the extract of Aniline blue using ethyl alcohol as a solvent.	80
Figure 4.63	The absorption spectrum of the extract of Bromophenol blue using ethyl alcohol as a solvent.	80
Figure 4.64	The absorption spectrum of the extract of Alcian blue using ethyl alcohol as a solvent.	81
Figure 4.65	The absorption spectrum of the extract of Methyl blue using ethyl alcohol as a solvent.	81
Figure 4.66	The absorption spectrum of the extract of Crystal Violet using ethyl alcohol as a solvent.	82
Figure 4.67	The absorption spectrum of the extract of Fast Green using ethyl alcohol as a solvent.	82
Figure 4.68	The absorption spectrum of the extract of Carbol Fuchsin using ethyl alcohol as a solvent.	83
Figure 4.69	Current density–voltage curves for the DSSC sensitized by Eosin Y at different light intensities.	84
Figure 4.70	Power - voltage characteristics of the DSSC sensitized by Eosin Y at different light intensities.	84

Figure 4.71	Current density–voltage curves for the DSSC sensitized by Aniline blue at different light intensities.	85
Figure 4.72	Power - voltage characteristics of the DSSC sensitized by Aniline blue at different light intensities.	85
Figure 4.73	Current density–voltage curves for the DSSC sensitized by Bomopheol blue at different light intensities.	86
Figure 4.74	Power - voltage characteristics of the DSSC sensitized by Bomopheol blue at different light intensities.	86
Figure 4.75	Current density–voltage curves for the DSSC sensitized by Alcian blue at different light intensities.	87
Figure 4.76	Power - voltage characteristics of the DSSC sensitized by Alcian blue at different light intensities.	87
Figure 4.77	Current density–voltage curves for the DSSC sensitized by Methyl blue at different light intensities.	88
Figure 4.78	Power - voltage characteristics of the DSSC sensitized by Methyl blue at different light intensities.	88
Figure 4.79	Current density–voltage curves for the DSSC sensitized by Crystal Violet at different light intensities.	89
Figure 4.80	Power - voltage characteristics of the DSSC sensitized by Crysatl Violet at different light intensities.	89
Figure 4.81	Current density–voltage curves for the DSSC sensitized by Fast green at different light intensities.	90
Figure 4.82	Power - voltage characteristics of the DSSC sensitized by Fast green at different light intensities.	90
Figure 4.83	Current density–voltage curves for the DSSC sensitized by Corbol Fuchsin at different light intensities.	91
Figure 4.84	Power - voltage characteristics of the DSSC sensitized by Corbol Fuchsin at different light intensities.	91
Figure 4.85	Nyquist curve for the DSSCs sensitized by Berries.	95
Figure 4.86	Bode modulus for the DSSCs sensitized by Berries.	96

Figure 4.87	Bode modulus for the DSSCs sensitized by Berries.	96
Figure 4.88	The equivalent circuit for DSSCs sensitized by Berries.	97
Figure 4.89	The equivalent circuit for DSSCs sensitized by Berries with replaced CPE with pseudo capacitance.	97
Figure 4.90	Nyquist curve for simulated values, measured data points.	98
Figure 4.91	Nyquist curve for the DSSCs sensitized by Mirabelle plums.	99
Figure 4.92	Bode modulus for the DSSCs sensitized by Mirabelle plums.	99
Figure 4.93	Bode modulus for the DSSCs sensitized by Mirabelle plums.	100
Figure 4.94	The equivalent circuit for DSSCs sensitized by Mirabelle plums.	100
Figure 4.95	The equivalent circuit for DSSCs sensitized by Mirabelle plums ethyl alcohol with replaced CPE with pseudo capacitance.	101
Figure 4.96	Nyquist curve for simulated values, measured data points.	101
Figure 4.97	Nyquist curve for the DSSC sensitized by Peach.	102
Figure 4.98	Bode modulus for the DSSCs sensitized by Peach.	102
Figure 4.99	Bode modulus for the DSSCs sensitized by Peach.	103
Figure 4.100	The equivalent circuit for DSSCs sensitized by Peach.	103
Figure 4.101	The equivalent circuit for DSSCs sensitized by Peach with replaced CPE with pseudo capacitance..	104
Figure 4.102	Nyquist curve for simulated values, measured data points.	104

List of Table Captions

CHAPTER TWO

Table 2.1 Common circuit elements used in equivalent circuit modele. 25

Table 2.2 Physical meaning of the coefficient Q. 29

CHAPTER THREE

Table 3.1 The name of natural dyes were used. 31

Table 3.2 Structure of chemical dyes. 35

CHAPTER FOUR

Table 4.1 Photovoltaic parameters of the DSCs sensitized by natural dyes 74

Table 4.2 Photovoltaic parameters of the fabricated DSSCs. 93

CHAPTER ONE

INTRODUCTION AND STATE OF THE ART

1.1. Energy Sources

Many types of energy are used in our life including oil energy, coal energy, solar energy, wind energy, and others. Energy sources have been classified into non-renewable and renewable sources.

1.1.1. Non-Renewable Energy Sources

Fossil fuels such as coal and natural gas are the main sources of energy used by humans. This type of fuel was formed by the decomposition of living organisms buried in the ground millions of years ago. This type of energy continues to drop and is expected to run out through several decades. They have a direct impact on human health and cause many diseases such as lung cancer, tract infections aerobic and many others. They also lead to the pollution of air, water, and soil. Moreover, they raise the air temperature around the earth's surface. As a result it is necessary that humans find new energy sources to meet their growing needs.

1.1.2. Renewable Energy Sources

Renewable energy comes from natural resources such as sunlight, wind, rain, tides, and geothermal heat. The renewable energy sources are clean sources of energy and do not lead to pollution. On the other hand, renewable energy sources, have few disadvantages such as they are intermittent and have high cost.

1.2. Solar Irradiation and Availability of Solar Electricity

The intensity of solar radiation in the earth's distance from the sun is approximately 1353 W/m^2 , a number also called the solar constant [1]. The solar radiation is emitted from the sun's photosphere at 6000°K temperature, which gives it a spectral distribution resembling closely that of a black body at the corresponding temperature as shown in the Fig. 1.1. [2]. Passing through the earth's atmosphere, the solar radiation is attenuated by scattering from air molecules, aerosols and dust particles, as well as by absorption by the air molecules, in particular oxygen, ozone, water vapor,

and carbon dioxide. This gives a characteristic fingerprint to the solar radiation spectrum on the earth's surface.

The available solar irradiation in a certain place depends on the latitude, the altitude and the climatic type in a yearly basis, the season, the time of day, and the weather conditions in a specific time. The total yearly solar irradiation on horizontal surface is 700-1000 kWh/m² in North Europe, 900-1300 kWh/m² in Middle Europe, 1300-1800 kWh/m² in South Europe, 1800-2300 kWh/m² in the equator, and 2000-2500 kWh/m² in the so called "solar belt" i.e. between 20° and 30° latitude [3]. An order of magnitude estimate of the usefulness of these yearly solar energy densities, converted to electricity with a grid-connected PV system, can be made by comparing these to an area related yearly electricity consumption of a typical detached house. In Finland, a typical electricity consumption for a 4 person family living in a detached house with floor area of 120 m² and using electric heating is 18500 kWh/year[4]. The yearly solar irradiation falling to the same horizontal area in North Europe conditions (about 1000 kWh/m²/year), converted to solar electricity with total PV system efficiency of 10% amounts to about 12000 kWh/m², i.e. about 65% of the yearly electricity consumption of the examined typical family.

In a large scale, the determination of the actual practical grid-connected PV potential is of course a far more complicated task, since factors such as type of the buildings, roof shapes, tilt angles, shading questions, ages of the buildings, and other technical questions have to be concerned. By an analysis of the building stock, Gutschner and Nowak [5] estimated that 16% of the electricity consumption of urban area (City of Zürich) and almost half of the consumption of a rural area (Canton of Fribourg) could be met by solar electricity generated by building-integrated photovoltaics covering the available roof-top area having a good solar yield (more than 80% of the maximum annual solar irradiation).

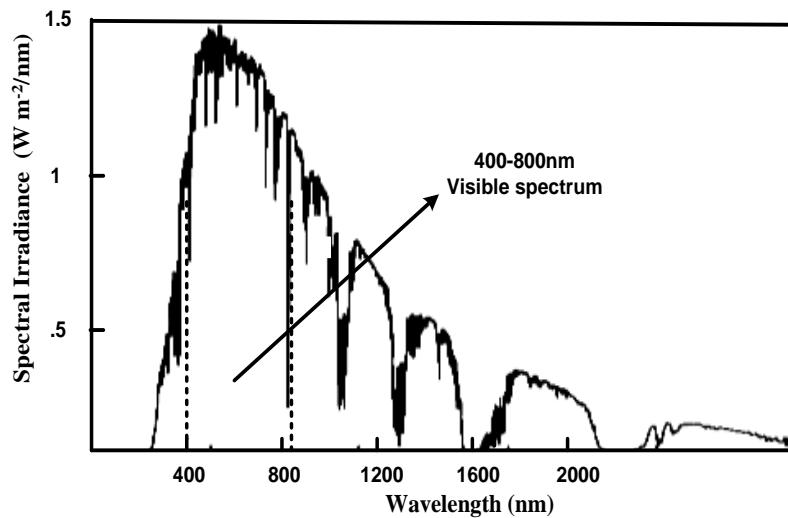


Figure 1.1. Spectral distribution of solar radiation.

1.3. Types of Solar Energy Conversions

Four different types of solar energy conversion methods are currently available for this purpose

a. Thermal Solar Energy Conversion

This type is observed in the form of black panels on rooftops, and is only used to heat water directly for domestic purposes. This type is not very effective in winter due to the low density of solar radiation. It is widely used all over the world including Gaza Strip.

b. Thermoelectric Solar Energy Conversion

It is well known that electricity are produced by turbines which are rotated by steam produced by heated water using conventional fuels. Solar energy can be converted to heat, and this heat energy is used to boil water which in turn rotates the steam turbine.

c. Photoelectric Solar Energy Conversion

This type of energy conversion makes use of devices called solar cells. Direct conversion of solar energy into electricity is the best known type of solar energy

conversion. The rise in the cost of solar cells is the main factor that limits the wide range use of solar electricity.

d. Chemical Solar Energy Conversion

This track represents the conversion of solar energy into chemical energy and is very important because its ability to overcome the problems of long-term storage and energy transfer.

1.4 Solar Electricity

Solar electricity is a growing energy technology today and solar cells have found markets in a variety of applications ranging from consumer electronics and small scale distributed power systems to centralized megawatt scale power plants. Direct utilization of solar radiation to produce electricity is close to an ideal way to utilize the nature's renewable energy flow. Generating electricity from the sun radiation has many features over other energy generation techniques. The high cost of solar cells has been a significant obstacle for the implementation of the solar electricity in a large scale. There is therefore an urgent need for the development of new materials and concepts for the solar cell technology to reduce this cost.

Nanotechnology researches have recently exhibit high interest in the field of solar energy conversion. Developing nanoscale materials and utilizing them in the field of solar cells and systems that could potentially lead to realization of low-cost solar cells in the future have received an increasing interest. These materials include for example different types of synthetic organic materials and inorganic nanoparticles. The solar cells based on these materials are called for example organic solar cells or molecular solar cells.

1.5. Types of Solar Cells

1.5.1 Single-Crystalline and Polycrystalline Silicon Solar Cells

Over 95% of all the solar cells produced worldwide are composed of the semiconductor material Silicon (Si). As the second most abundant element in earth's crust, silicon has the advantage, of being available in sufficient quantities, and additionally processing the material does not burden the environment. To produce a solar cell, the semiconductor is contaminated or "doped". "Doping" is the intentional introduction of chemical elements, with which one can obtain a surplus of either

positive charge carriers (p-conducting semiconductor layer) or negative charge carriers (n-conducting semiconductor layer) from the semiconductor material. If two differently contaminated semiconductor layers are combined, then a so-called p-n-junction results on the boundary of the layers. At this junction, an interior electric field is built up which leads to the separation of the charge carriers that are released by light. Through metal contacts, an electric charge can be tapped. If the outer circuit is closed, meaning a consumer is connected, then direct current flows.

The crystalline silicon is often referred to as the first generation photovoltaic technology. The first silicon solar cell was developed by Chapin, Fuller, and Pearson at the Bell Telephone Laboratories in the mid 1950's, and it had already about 6% efficiency [6]. Today the silicon solar cells dominate the photovoltaic (PV) market by 82% and the recorded efficiency for a laboratory cell is 24.7% [7], while the efficiency of the commercial crystalline silicon solar panels is in the best case about 15% [8]. The main reason why Si has dominated the PV market is that high quality Si has been already produced at large quantities by the semiconductor industry. The processing of crystalline silicon wafers is high-level semiconductor technology, and as such expensive and very capital intensive. This also adds directly to the cost of the photovoltaic modules, so that the cost of processed silicon wafers contribute to fifty percent of the total manufacturing cost of the module [9]. A big question for the Si photovoltaic technology is the availability of highly purified Si. The PV industry has been using mainly low cost reject material from the semiconductor industry. This has created a problematic dependence on the volatile semiconductor market causing fluctuations also in the cost of Si material for the solar cells. In fact, it is generally seen that the dominance of the standard Si PV technology in the growing PV market can be realized only by production of special solar cell grade silicon. Yet the first efforts to produce such material have been unsuccessful because of the high purity requirements and the small market for the special silicon at the moment. The crystalline silicon technology is relatively mature and has still has a large cost reduction potential. It seems to be generally understood however, that the cost reduction can be achieved only by increasing manufacturing volume. From the manufacturers' point of view this is coupled to the need for the special solar cell grade silicon supply and from the market's point of view not very easy to achieve at present

PV system costs without governmental subsidies for customers to create artificial markets for the solar electricity.

1.5.2. Thin Film Solar Cells

The second generation photovoltaics consists of thin film solar cell materials such as amorphous silicon (a-Si), cadmium telluride (CdTe), copper indium gallium diselenide (CIGS), and thin film crystalline silicon. A thin-film solar cell (TFSC), also called a thin-film photovoltaic cell (TFPV), is a solar cell that is made by depositing one or more thin layers (thin film) of photovoltaic material on a substrate. The thickness range of such a layer is wide and varies from a few nanometers to tens of micrometers. Many different photovoltaic materials are deposited with various deposition methods on a variety of substrates. Thin-film solar cells are usually categorized according to the photovoltaic material. Silicon cells are approximately 10 cm by 10 cm large (recently also 15 cm by 15 cm). A transparent anti-reflection film protects the cell and decreases reflective loss on the cell surface.

The driving force for the development of thin film solar cells has been their potential for the reduction of manufacturing costs. While silicon solar panels are assembled from individual cells processed from about 100 cm² silicon wafers, thin film semiconductor materials can be deposited onto large surfaces, which is beneficial for volume production. Also as direct band gap semiconductors, the thin film semiconductor materials have much higher absorption coefficient than silicon, and therefore typically less than 1µm thick semiconductor layer is required, which is 100-1000 times less than that for Si. The amount of expensive semiconductor material is thus reduced, or on the other hand, more expensive semiconductors can be used in the thin films.

1.5.3. Photoelectrochemical Solar Cells

The oldest type of photovoltaic cell is the photoelectrochemical solar cell, used already by Becquerel for the discovery of the photovoltaic effect in 1839. In the photoelectrochemical solar cell a semiconductor-electrolyte junction is used as a photoactive layer. While energy conversion efficiencies exceeding 16% have been achieved with the photoelectrochemical solar cells utilizing semiconductor photoelectrodes [10], instability of these solar cells by photocorrosion has left them without practical importance. Furthermore, the photoelectrochemical solar cells using

some semiconductor materials as in the commercial solar cells, such as Si, CuInSe₂ or GaAs does not offer any real advantages over the established solid state solar cells. In **1991**, the dye-sensitized solar cell (DSSC) was developed by Grätzel [11] which was named "Grätzel Cell". DSSC is considered the third generation of photovoltaic devices for the conversion of visible light into electric energy. These new types of solar cells are based on the photosensitization produced by the dyes on wide band-gap semiconductors such as TiO₂. This sensitization is produced by the dye absorption of part of the visible light spectrum. DSSCs are low cost solar cells because of inexpensive materials and the relative ease of the fabrication processes. Recent studies have shown that metal oxides such as TiO₂ and ZnO have been successfully used as photo-anode when a dye is adsorbed in the interior of the porous layer of the semiconductor.

The use of natural pigments as sensitizing dyes for the conversion of solar energy into electricity is very interesting because, on one hand they enhance the economical aspect and on the other hand, they produce significant benefits from the environmental. Natural pigments extracted from fruits and vegetables, such as chlorophyll, have been extensively investigated as DSSC sensitizers [12].

The efficiency is determined by two main factors: (i) the maximum photocurrent density called short circuit current (J_{SC}) related to the charge injection rate from the dye highest occupied molecular orbital (HOMO) to the semiconductor conduction bands and (ii) the open circuit potential (V_{OC}). The highest efficiency of DSSCs sensitized by Ruthenium complexes adsorbed on nanocrystalline TiO₂ has reached 11–12% but they are still not suitable for the high cost.

1.6. Gaza and Electricity Problem

Electricity demand in Gaza strip can reach up to 360 megawatts (MW). At its current operating capacity, the Gaza Power Plant (GPP) can produce up to 80 MW; supplemented by 120 MW purchased from Israel and 22 MW from Egypt, the total amount of electricity available can meet approximately two-thirds of the demand.

The chronic electricity deficit affecting Gaza over the past few years has disrupted the delivery of basic services and many fields in the daily life. Since February 2012, the situation has further deteriorated following a sharp decline in the amount of fuel brought into Gaza from Egypt and used to operate the GPP. The generating capacity and reliability of the GPP has been significantly impaired over the past six years by

additional factors. These include the destruction of six transformers by an Israeli airstrike in 2006; the restrictions on the import of spare parts, equipment, and fuel in the context of Israel's blockade. The resulting decline has been exacerbated by the poor state of the distribution network, which results in significant electricity losses. To cope with the long blackouts, service providers and private households have resorted to back-up generators, which are unreliable due to their dependence on scarce fuel and spare parts. Private mobile generators can be particularly unsafe, environmentally polluting, and are not affordable by the poorest. Medical services, including life-saving interventions, are at risk of collapsing due to an imminent exhaustion of the fuel reserves used to operate back-up generators and to run ambulances. Constant fluctuations in power supply have resulted in the malfunctioning of sensitive medical equipment, disrupting medical services. The insufficient supply of electricity and fuel to operate water pumps and wells has caused a further reduction in the availability of running water in most households. This has increased people's reliance on private uncontrolled water suppliers and lowered hygiene standards. Wastewater plants have also shortened treatment cycles, thus increasing the pollution level of partially treated sewage discharged into the sea. There is also the risk of back-flow of sewage onto streets. The fuel and electricity shortages have negatively affected livelihoods, in particular agricultural activities.

1.7. State of Art

The use of dye-sensitization in photovoltaics was considered a breakthrough at the early 1990's in the Laboratory of Photonics and Interfaces in the EPFL Switzerland. By the successful combination of nanostructured electrodes and efficient charge injection dyes professor Grätzel and his co-workers developed a solar cell with energy conversion efficiency exceeding 7% in 1991 [11]. This solar cell is called the dye sensitized nanostructured solar cell or the Grätzel cell after its inventor since then an increasing interest has been shown in the fabrication and development of DSSCS.

In 2004, dye-sensitized solar cells (DSSC) were assembled by using natural dyes extracted from black rice, capsicum, erythrina, variegata flower, rosa xanthina, and kelp as sensitizers [14]. The I_{SC} ranging from 1.142 mA to 0.225 mA, the V_{OC} ranging from 0.551 V to 0.412 V, the fill factor ranging from 0.52 to 0.63, and P_{max} ranging

from 58 μW to 327 μW were obtained from the DSSC sensitized with natural dye extracts.

In 2007, some experimental data for analyzing the various dye's absorption spectra, which can be applied in the DSSC have been presents [15]. The analysis of dyes focused on the natural dyes which are extracted by the plants and compared with the chemical. The results showed that the natural dyes have the wider absorption spectra than the chemical synthesis due to the more various constituents in the natural dyes. In 2009, The performances of natural dye-sensitized solar cells assembled by using natural dyes extracted from spinach, amaranth and a mixture of them were investigated. In the sun, the Voc of cells sensitized by spinach extract was 450 mA, while those sensitezed by the mixture showed a Voc above 500 mV [16]. In 2010, twenty natural dyes, extracted from natural materials such as flowers, leaves, fruits, traditional Chinese medicines, and beverages, were used as sensitizers to fabricate DSSCs. The photoelectrochemical performance of the DSCs based on these dyes showed that the open circuit voltages (Voc) varied from 0.337 to 0.689 V, and the short circuit photocurrent densities (Jsc) ranged from 0.14 to 2.69mAcm⁻²[17].

1.8. Semiconductors and Light Absorption

Semiconductors are interesting solar cell materials because they have near-optimal band gaps. When a semiconductor is exposed to light of energy larger than the band gap energy ($h\nu \geq E_g$), an electron from the valence band can be exited into the conduction band (see Figure 1.2). This process creates non-equilibrium carriers in pairs, so that $D_n=D_p$, where D_n and D_p are the excess concentrations of electrons and holes, compared to the equilibrium concentrations (n_0 and p_0), and is called the intrinsic or fundamental absorption. The amount of light absorbed by a semiconductor is given by Lambert's law of extinction:

$$I = I_0 e^{-\beta x}, \quad (1.1)$$

where x is the coordinate, I_0 is the intensity of non-reflected light incident on the surface of the semiconductor at $x=0$, and β is the linear coefficient of light absorption. The dimension of this coefficient is the inverse of length, thus, β^{-1} is often arbitrarily called the depth or length of penetration and is a measure of distance over which the incident light attenuates e times.

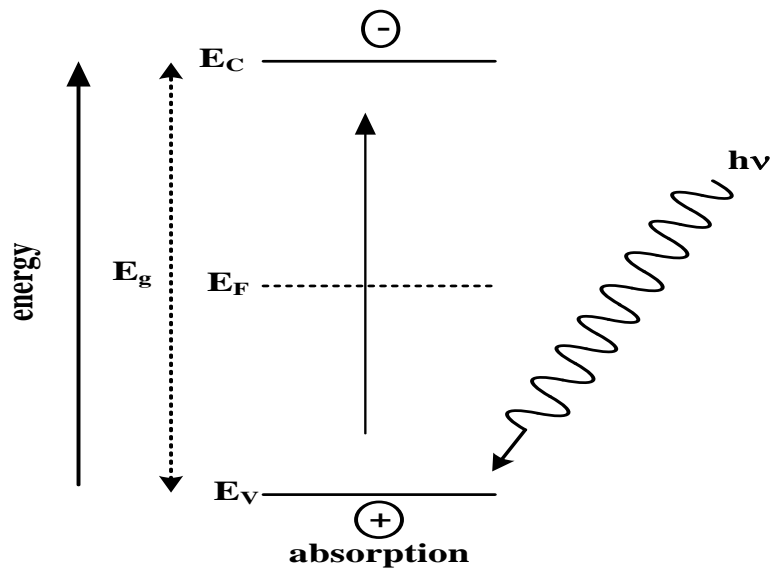


Figure 1.2. Light absorption by a semiconductor. The impinging photon induces an electron transition from the valence band into the conduction band if $h\nu \geq E_g$.

CHAPTER TWO

DYE- SENSITIZED SOLAR CELLS

In this chapter, the operational principle of dye-sensitized solar cells (DSSCs) are presented. The materials used to fabricate DSSCs are explained in details and the principle of operation is investigated. Moreover, the DSSC parameters (short circuit current, open circuit voltage, optimum voltage, optimum current, fill factor and efficiency) are also presented

Introduction:

Grätzel developed dye-sensitized solar cell in 1991 which was called the "Grätzel Cell" It is the third generation of photovoltaic devices for the conversion of visible light into electric energy. The principle of operation of DSSC is based on the photosensitization produced by the dyes adsorbed on the surface of wide band-gap semiconductor.

2.1 Materials of the Dye-Sensitized Solar Cell:

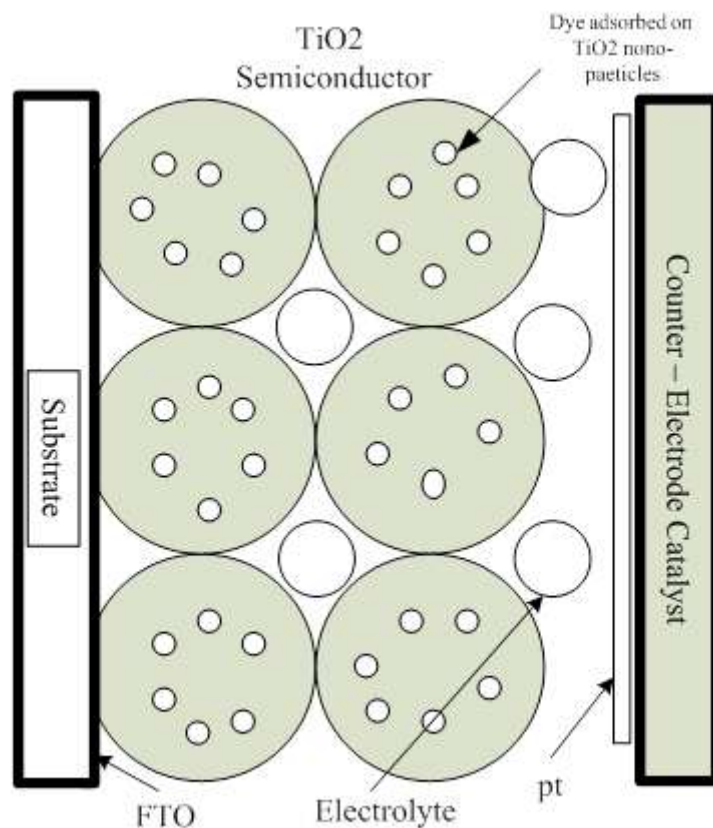


Figure 2.1. The assembly of the Dye-Sensitized Solar Cell

2.1.1 Substrates

The electrodes of the standard DSSC are prepared from transparent conducting oxide (TCO) coated on glass substrates, between which the cell is assembled. Fluorine-doped tin oxide ($\text{SnO}_2:\text{F}$) and indium tin oxide ($\text{In}_2\text{O}_3:\text{Sn}$ or ITO) are the most frequently used TCOs in thin film photovoltaic cells. The standard preparation procedure of the nanostructured TiO_2 electrode includes sintering of the deposited TiO_2 film at 450-500°C. As the only TCO coating stable at these temperatures, the $\text{SnO}_2:\text{F}$ has been the material of choice for DSSCs [17]. The choice of sheet resistance of the SnO_2 -coated glass plates is a compromise between conflicting beneficial properties of the TCO-coated glass: the higher the conductance the lower the transmittance and vice versa. The conducting coating of the substrate works as a current collector and the substrate material itself behaves both as a support structure to the cell and as a sealing layer between the cell and the ambient air.

2.1.2 Nanoparticle Electrodes:

Stable oxide semiconductors cannot absorb visible light because they have relatively wide band gaps. Sensitization of wide band gap oxide semiconductor materials, such as TiO_2 , Zinc Oxide (ZnO), and SnO_2 , with photosensitizers, such as organic dyes, natural dyes, that can absorb visible light has been extensively studied in relation to the development of photography technology since the late nineteenth century [19].

- **TiO_2 Semiconductor**

TiO_2 is a wide band gap ($E_g = 3.2$ eV) semiconductor. It is widely used as a pigment in paper and paint industry, an excipient in pharmaceuticals, and as a raw material of cosmetics. It is cheap to be produced and the preparation of particles of very small size is fairly easy. The TiO_2 has three crystallite structures: anatase, rutile and brookite, of which brookite are very difficult to obtain. Rutile absorbs light in the near UV-region, band gap excitations lead to generation of holes, and this causes long term instability of the solar cell. Anatase is dominant in low temperatures (<800 °C). TiO_2 has some properties of the most important, such as molar mass: 79.86g/mol, melting point: 1843°C, boiling point: 2972°C and refractive index: 2.614 at 587.6 nm. The

densities are 3.89 g/cm^3 and 4.26 g/cm^3 for anatase and rutile respectively. Rutile absorbs 4% of the incoming light in the near-UV region, and band gap excitation generates holes that act as strong oxidants reducing the long-term stability of the dye-sensitized solar cells. The third crystalline form of TiO_2 , brookite, is difficult to produce and is therefore not of practical interest for the DSSC. The band-gaps of the crystalline forms are 3.2 eV (the absorption edge at 388 nm) for anatase and 3.0 eV (the absorption edge at 413 nm) for rutile [20].

2.1.3 Sensitizing Dyes

To achieve a high light-to-energy conversion efficiency in a DSSC, the properties of the dye molecule as attached to the semiconductor particle surface are essential. Such desirable properties can be summarized as:

- Interfacial properties: good adsorption to the semiconductor surface
- Practical properties: e.g. high solubility to the solvent used in the dye impregnation.
- Stability: the adsorbed dye molecule should be stable enough in the working environment (at the semiconductor-electrolyte interface) to sustain about 20 years of operation at exposure to natural daylight, i.e. at least 10^8 redox turnovers [21].
- Kinetics: the process of electron injection from the excited state of the dye to the conduction band of the semiconductor should be fast enough to outrun competing unwanted relaxation and reaction pathways. The excitation of the molecule should be preferentially of the metal to ligand charge transfer (MLCT) type.
- Absorption: the dye should absorb light at wavelenghts up to about 920 nanometers, i.e. the energy of the excited state of the molecule should be about 1.35 eV above the electronic ground state corresponding to the ideal band gap of a single band gap solar cell [22].
- Energetic: to minimize energy losses and to maximize the photovoltage, the excited state of the adsorbed dye molecule should be only slightly above the conduction band edge of the TiO_2 , but yet above enough to present an energetic driving force for the electron injection process. For the same reason, the ground

state of the molecule should be only slightly below the redox potential of the electrolyte.

2.1.4 Electrolytes

The electrolyte is used to transport the electrons back to the dye molecules. The electrolyte consists of redox couple (I_3^-/I^-) in a solvent such as acetonitrile (ACN). The performance achievable with acetonitrile is nevertheless greater due to lower viscosity. The ideal characteristics of the redox couple for the DSSC electrolyte are [23]:

1. redox potential thermodynamically (energetically) favorable with respect to the redox potential of the dye to maximize cell voltage;
2. high solubility to the solvent to ensure high concentration of charge carriers in the electrolyte;
3. high diffusion coefficients in the used solvent to enable efficient mass transport;
4. absence of significant spectral characteristics in the visible region to prevent absorption of incident light in the electrolyte;
5. high stability of both the reduced and oxidized forms of the couple to enable long operating life;
6. highly reversible couple to facilitate fast electron transfer kinetics;
7. chemically inert toward all other components in the DSSC.

2.1.5 Counter-Electrode Catalyst

The function of counter electrode in DSSCs is to reduce triiodide to iodide. The plain FTO layer does this rather poorly, so a small amount of platinum is deposited to the electrode to catalyze the reaction. Charge transfer resistance, R_{ct} is a measure of the electrode performance in an electron transfer process. The platinized counter electrode has resistance of $1\Omega/cm^2$, while the resistance of plain electrode is seven orders of magnitude larger [24, 25].

2.1.6 Electrical Contacts

To keep the resistive losses in the transparent conduction oxide coating layer reasonably low, the longest distance from a photoactive point to a current collector should not exceed about 1 cm. For example, silver paint and adhesive copper tape can be used to extend the contact area of the current collector to fulfill this geometric requirement. In test cells, alligator clips can be easily attached to these conductor strips. An iodine-based electrolyte is highly corrosive, attacking most metals, such as silver, aluminum, copper, nickel, and even gold, and can thus be particularly problematic when it is used in designing an electrical contacting of single cells in an integrated DSSC module.

2.1.7 Sealing of Dye-Sensitized Solar Cell

Being directly related to the long-term stability of the cells, sealing a DSSC seems to be one of the main technological challenges of the DSSC technology. A suitable sealing material should at least:

1. be leak-proof to the electrolyte components and impermeable to both ambient oxygen and water vapor.
2. be chemically inert towards the electrolyte and other cell components.
3. be committed well to the glass substrate and transparent conduction oxide coating.

2.2 Operating Principle

The operation of photovoltaic cell can be generally divided into three basic steps

- 1- Light absorption.
- 2- Charge separation.
- 3- Charge collection.

The efficiency of a solar cell depends on the efficiency of each of these elements and is maximized by the materials selection and the cell design.

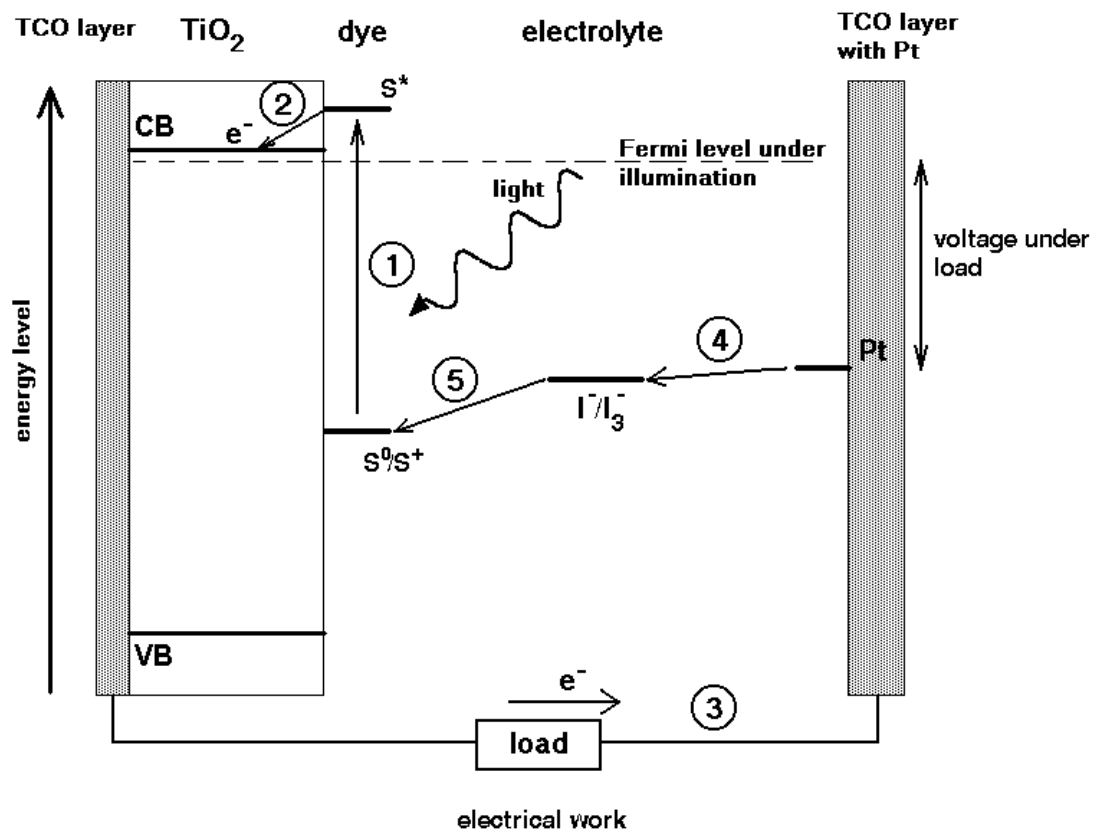


Figure 2.1. The working principle of the dye-sensitized nanostructured solar cell.

The operation of the dye sensitized solar cell is shown in the Fig 2.1.

A photon is absorbed by the dye molecule and this leads to the excitation of the dye to an electronically excited state (S^*)



The excited dye molecule injects an electron into the conduction band of the TiO_2 electrode and is oxidized (S^+)



The original state of the dye (S) is subsequently restored by the electron from the electrolyte through the reduction of iodide



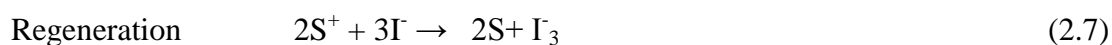
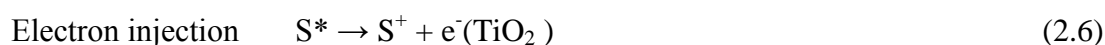
The regeneration of dye from iodide prevents the capture of the conduction band electrons through the dye oxidation. The iodide is in turn regenerated at the counter electrode by reducing tri-iodide as follows



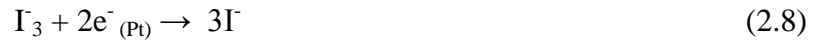
The circle is completed by migration through the external load. The maximum photovoltage obtained is the difference between the fermi level of semiconductor under illumination and redox potential of the mediating redox couple, depicted by ΔV . Ideally the device generates electrical energy from light without suffering any permanent chemical transformation [26].

The operating cycle can be summarized in chemical reaction terminology as

Anode:



Cathode:



Cell:



2.3 Parameters of Solar Cells

The important parameters of the DSSC are short circuit current (I_{sc}), open circuit voltage (V_{oc}), optimum voltage (V_m), optimum current (I_m), fill factor (FF) and efficiency (η) have to be obtained the parameters can be carried out from J-V curve of DSSCs under illumination as shown in figure 2.2.

- **Short Circuit Current I_{sc} :**

If the output voltage is zero, the cell is said to be short circuited. The short circuit current is equal to the absolute number of photons converted to hole-electron pairs. The I_{sc} is depends on the thickness of the electrode, the adsorbed dye molecule, diffusion electrolytes, dipping time, temperature of the cell, and dye loading.

- **Open Circuit voltage V_{oc} :**

If the output current is zero, the cell is open circuited and the voltage of the cell is called the open circuit voltage, is depends on wide band gap of semiconductors, redox potential, and the ground state of the dye molecule.

- **Optimum voltage V_m :**

V_m is the voltage at the optimum operating point at which the DSSC output power is maximum, is depends on bonds between the dye molecule and TiO_2 film, and dying temperature and time.

- **Optimum Current I_m :**

I_m is the current at the optimum operating point which the DSSC output power is maximum, is depends on the intensity of incident light, and connection between material interfaces.

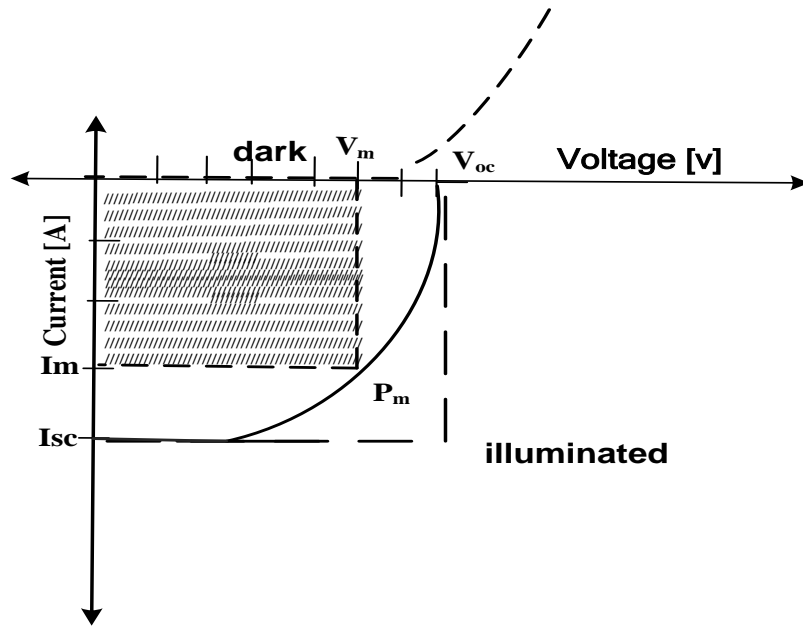


Figure 2.2. Voltage –current characteristics of a solar cell. Shaded area represents the maximum achievable output power.

- **Fill Factor FF :**

The fill factor is an important part of the efficiency of the cell. High V_{oc} and I_{sc} are essential in achieving high efficiencies, but paired with a low fill factor, the overall efficiency of the cell will remain low. The ratio of peak output power $V_m I_m$ to $V_{oc} I_{sc}$ is called the fill factor (FF) of a solar cell.

$$FF = \frac{I_m \times V_m}{I_{sc} \times V_{oc}} = \frac{P_m}{I_{sc} \times V_{oc}} \quad , \quad (2.10)$$

where P_m is maximum power. The meaning of fill factor can be understood from its graphical representation. It indicates how much area underneath the I–V characteristic curve is filled by the rectangle described by $V_m I_m$ (shaded area in Fig. 2.2) in relation to the rectangle $V_{oc} I_{sc}$. The theoretically maximum obtainable FF is a function of the open circuit potential, the higher the V_{oc} the higher FF. Fill factors for optimized solar cells are typically within the range of 0.6–0.75.

- **Efficiency η :**

The energy conversion of a solar cell is defined as the ratio of the output power of the cell and incident irradiance. Maximum efficiency is reached when power delivered to the load is P_{\max} . Incident optical power is normally specified as the solar power on the surface of the earth which is approximately $1\text{mW}/\text{mm}^2$. Spectral distribution of sunlight is close to a blackbody spectrum at 6000°C minus the atmospheric spectrum [27]. The maximum efficiency can be calculated from the J-V curve according to the relation :

$$\eta = \frac{I_m \times V_m}{P_{(light)}} = FF \frac{I_{sc} \times V_{oc}}{P_{(light)}}, \quad (2.11)$$

where $P_{(light)}$ is the energy of the light shining on the a solar cell and is obtained when the light intensities of the whole spectral range are integrated. I_{sc} is directly proportional to the incident optical power $P_{(light)}$ while V_{oc} increases logarithmically with the incident power [28]. So the overall efficiency of solar cell is expected to increase logarithmically with incident power. The efficiency of the solar cell depends on the temperature of the cell, and which is even more important, on the quality of the illumination, i.e., the total light intensity and the spectral distribution of the intensity. For this reason, a standard measurement condition has been developed to facilitate comparable testing of the solar cells between different laboratories. Specific solar radiation conditions are defined by the Air Mass(AM) value. The Standard Test Condition (STC) for solar cells is the Air Mass 1.5 spectrum, an incident power density of 1000 W m^{-2} , and temperature of the cell is 25°C . The output power of the solar cell at these conditions is the nominal power of the cell, or module, and is reported in peak watts, W_p . In practice, special solar simulator light sources are used for the standard measurements [29].

2.4 The Simple Electrical Model of a Solar Cell

The equivalent circuit corresponding to a solar cell is shown in the Figure (2.3).A solar cell can be thought as a combination of a current source and diode in the solar cell having two resistant R_s , series resistors, and R_{sh} , parallel resistant,. The cell

would be an ideal cell if R_s is zero, and R_{sh} to be infinitely large. In fact this is not a practical case.

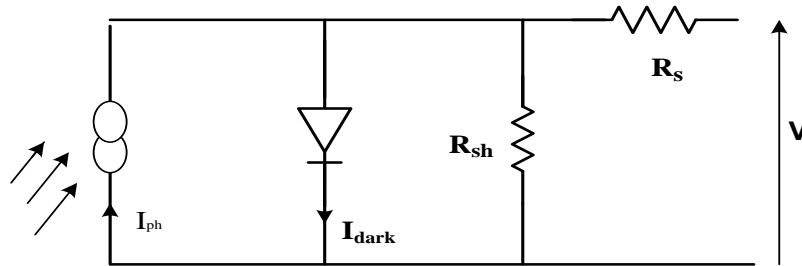


Figure 2.3. Equivalent circuit of a solar cell including series and shunt resistances.

The R_s is composed of the electric resistance of different material in the cell and interfaces between them. The resistance of the TCO layer has the biggest influence on resistance. The shunt resistance measures the resistance between the electrodes of the cell through undesirable routes example from TiO_2 film to electrolyte. It is desired to be as high as possible. The diode model does not represent the dye solar cell very well. The internal structure of the DSSC is more complex than that of silicon solar cell. But the concepts of the series and parallel resistances can also be applied to the DSSC. The resistance can be measured using impedance spectroscopy.

Series and parallel resistances reduce the fill factor as shown in Figure (2.4). For an efficient cell we need R_s to be as small and R_{sh} to be as large as possible.

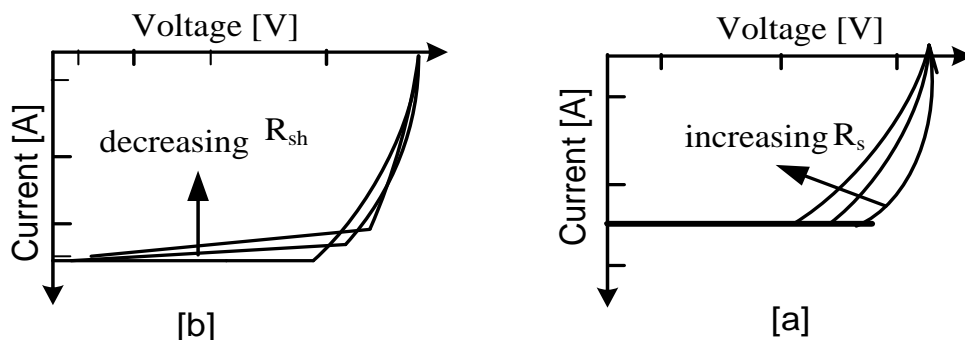


Figure 2.4. Effect of (a)reducing parallel resistances and (b) increasing series.

The effect of R_s and R_{sh} is shown in the Fig 2.4. The effect of decreasing R_{sh} and increasing R_s is to reduce the area of the maximum power rectangle compared to that with area $I_{sc}V_{oc}$.

2.5. Impedance Spectroscopy

Impedance Spectroscopy (IS) has become a major tool for investigating the properties and quality of dye-sensitized solar cell devices. This section provides an introduction of IS interpretation methods focusing on the analysis of DSSC impedance data.

2.5.1. Basic Knowledge for Understanding Impedance Spectroscopy

2.5.1.1. Introduction

Ohm's law defines the resistance, R , in terms of the ratio between voltage V and current I . Its use is limited to the ideal resistor for a DC system, which is independent of frequency. The relationship between the resistance, current, and voltage can be expressed as

$$R = V/I \quad (2.12)$$

However, real electrochemical systems exhibit much more complex behaviours. They are not simply resistive. The electrochemical double layer adds a capacitive term. Other electrode processes, such as diffusion, are time and/or frequency dependent. Therefore, for an actual electrochemical system, impedance is used instead of resistance. The impedance of an electrochemical system $Z(\omega)$ is the AC response of the system being studied to the application of sinusoidal signal imposed upon the system. The form of the current–voltage relationship of the impedance in an electrochemical system can also be expressed as

$$Z(\omega) = V(t)/I(t), \quad (2.13)$$

where $V(t)$ and $I(t)$ are the measured voltage and current in an AC system and ω is the frequency of the AC signal. The technique that measures the AC impedance of a circuit element or an electric circuit is called AC impedance spectroscopy. The impedances of a resistor (Z_R), a capacitor (Z_C), and an inductor (Z_L) for a sinusoidal system can be expressed, respectively, as follows:

$$Z_R(\omega) = V(t)/I(t) = R \quad (2.14)$$

$$Z_C(\omega) = V(t) / I(t) = 1/i\omega C \quad (2.15)$$

$$Z_L(\omega) = V(t) / I(t) = i\omega L \quad (2.16)$$

If AC impedance spectroscopy is used in an electrochemical system, this technique is generally called electrochemical impedance spectroscopy, known as EIS. The impedance of an electrochemical system can also be expressed typically in cartesian coordinates:

$$Z(\omega) = Z' + iZ'' , \quad (2.17)$$

where Z' and Z'' are the real and imaginary parts of the impedance, respectively. In polar coordinates, this becomes

$$Z(\omega) = |Z|e^{i\theta} , \quad (2.18)$$

where $|Z| = \sqrt{(Z')^2 + Z''^2}$ is the modulus and θ is the phase corresponding to a given frequency.

2.5.1.2. Nyquist and Bode Plots

Generally, the impedance spectrum of an electrochemical system can be presented in Nyquist and Bode plots, which are representations of the impedance as a function of frequency[29,30]. A Nyquist plot is displayed for the experimental data set $Z(Z'_i, Z''_i, \omega_i)$, ($i = 1, 2, \dots, n$) of n points measured at different frequencies, with each point representing the real and imaginary parts of the impedance ($Z'_i \sim Z''_i$) at a particular frequency ω_i . A Bode plot is an alternative representation of the impedance. There are two types of Bode diagram, $\log |Z| \sim \log \omega$ (or $|Z| \sim \log \omega$) and $\theta \sim \log \omega$, describing the frequency dependencies of the modulus and phase, respectively. A Bode plot is normally depicted logarithmically over the measured frequency range because the same number of points is collected at each decade. Both plots usually start at a high frequency and end at a low frequency, which enables the initial resistor to be found more quickly. The most common graphical representation of experimental impedance is a Nyquist plot (complex-plane diagram), which is more illustrative than a Bode plot. However, a Bode plot sometimes can provide additional information. Some typical Nyquist plots for an electrochemical system are shown in Figure 2.5.

The usual result is a semicircle, with the high-frequency part giving the solution resistance and the width of the semicircle giving the charge-transfer resistance.

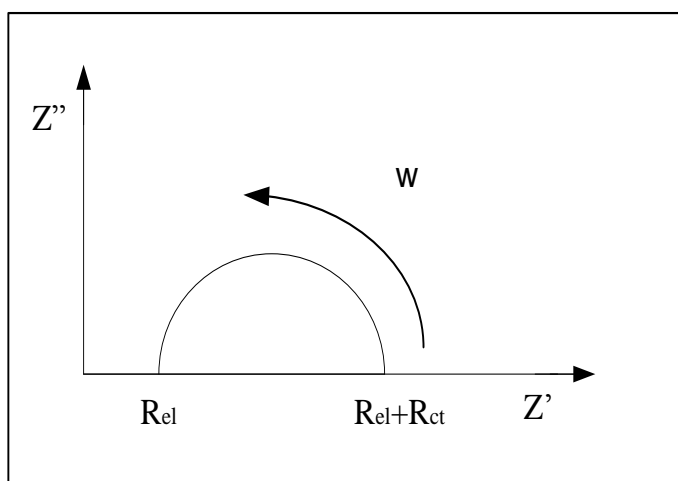


Fig 2.5. A Nyquist plot (complex-plane diagram).

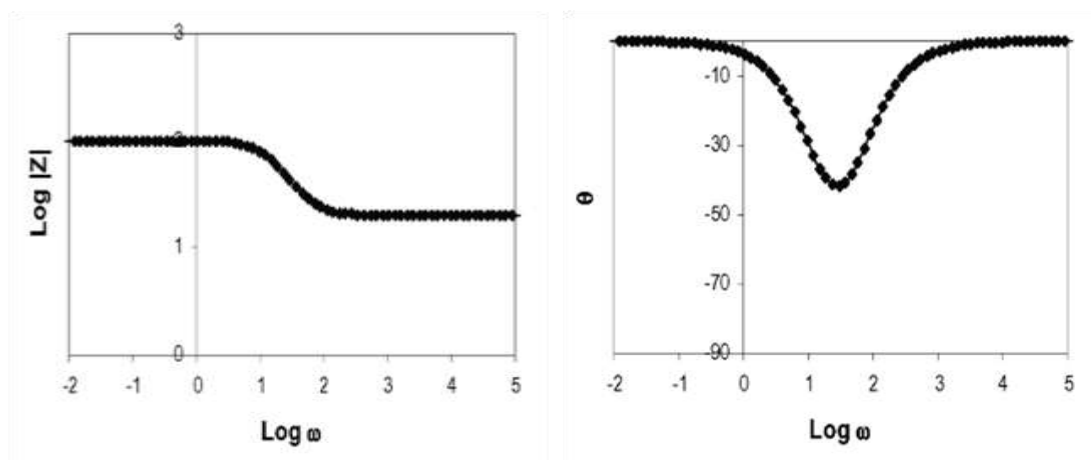



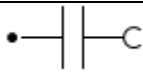



Fig 2.6. A Bode modulus, and phase plots.

2.5.1.3. Equivalent Circuit Models

EIS data analysis is commonly carried out by fitting it to an equivalent electric circuit model. An equivalent circuit model is a combination of resistances, capacitances, and/or inductances, as well as a few specialized electrochemical elements (such as Warburg diffusion elements and constant phase elements), which produces the same response as the electrochemical system does when the same excitation signal is

imposed. Equivalent circuit models can be partially or completely empirical. In the model, each circuit component comes from a physical process in the electrochemical cell and has a characteristic impedance behavior. The shape of the model's impedance spectrum is controlled by the style of electrical elements in the model and the interconnections between them (series or parallel combinations). The size of each feature in the spectrum is controlled by the circuit elements' parameters. However, although many powerful numerical analysis software are available to fit the spectra and give the best values for equivalent circuit parameters, analysis of the impedance data can still be troublesome, because specialized electrochemical processes such as Warburg diffusion or adsorption also contribute to the impedance, further complicating the situation. To set up a suitable model, one requires a basic knowledge of the cell being studied and a fundamental understanding of the behaviour of cell elements. The equivalent circuit should be as simple as possible to represent the electrochemical system and it should give the best possible match between the model's impedance and the measured impedance of the system, whose equivalent circuit contains at least an electrolyte resistance, a double-layer capacity, and the impedance of the Faradaic or non-Faradaic process [32]. Some common equivalent circuit elements for an electrochemical system are listed in Table 2.1. A detailed description of these elements will be introduced in subsection 2.5.2.

Table 2.1. Common circuit elements used in equivalent circuit models

Equivalent element	Symbol	Expression
Resistance		$Z_R = R$
Capacitance		$Z_C = \frac{-i}{(\omega c)}$
Inductance		$Z_L = i\omega L$
Constant phase element		$Z_Q = \frac{1}{Y_o (i\omega)^n}$
Warburg impedance		$Z_W = \frac{1}{Y_o \sqrt{i\omega}}$

2.5.2. Electrochemical Elements

The electrolyte/interface and associated electrochemical processes can be treated as an electric circuit consisting of electrical elements, including resistors, capacitors, constant phase elements, and so on. Although the commonly used electrical elements have already been described in subsection 2.5.1, the following subsection provides a brief review to preface the ensuing discussion of EIS equivalent circuits and their related DSSC processes.

2.5.2.1. Lumped Elements

2.5.2.1.1. Resistance

The electrical element resistance, R , is described in the time domain based on Ohm's law:

$$V = RI \quad (2.19)$$

where V is the voltage drop across R and I is the current passing through it. In the frequency domain, its impedance has only a real part:

$$Z_R(\omega) = R \quad (2.20)$$

(i.e., $Z' = R$ and $Z'' = 0$). Resistance in electrochemical systems includes ionic resistance, electronic resistance, charge-transfer resistance, and mass transfer resistance. The ionic resistance is sometimes expressed as ionic conductivity, using the unit of siemens per centimetre (S/cm), which is the reciprocal of the resistivity:

$$\sigma = \frac{1}{\rho}, \quad (2.21)$$

where ρ is the resistivity expressed as $\Omega \cdot \text{cm}$. Electronic resistance is normally used to describe the movement of electrons within a conducting media, such as metal wires or conducting polymers. In DSSCs, the electronic resistance is usually omitted because it is very small in comparison with the ionic resistance. Charge-transfer resistance is the resistance that occurs when electrons transfer at the electrode/electrolyte interface. The charge-transfer resistance is dependent on the reaction, the electrode surface, and the electrode potential. In general, an increase in over potential leads to a decrease in charge-transfer resistance.

2.5.2.1.2. Capacitance

If a layer of non-conductive medium is sandwiched between two electrodes and electricity passes through this assembly, electric charge will be stored at both electrodes. This assembly is called a capacitor. The capacitor is measured by its capacitance (C), which is represented by the stored electric charge, divided by the voltage drop across the two electrodes:

$$C = \frac{Q}{V} = \epsilon_0 \epsilon_r \frac{A}{d}, \quad (2.22)$$

where Q is the charge, V is the voltage difference between the two electrodes, ϵ_0 is the permittivity of a vacuum, ϵ_r is the dielectric constant or relative permittivity of the insulator used, A is the electrode area, and d is the distance between the electrodes. The impedance $Z_C(\omega)$ of the capacitor is given by the following equation:

$$Z_C = \frac{-i}{(\omega C)}. \quad (2.23)$$

2.5.2.1.3. Inductance

Inductance (L) is the magnetic field generated when a current is passed through an inductor, typically a wire coil. The strength of the magnetic field is measured in henries (H). The impedance of an inductor $Z_L(\omega)$ is given as

$$Z_L = i\omega L, \quad (2.24)$$

where L is inductance of inductor.

2.5.2.2. Frequency-Dependent Elements

2.5.2.2.1 Warburg Resistance

Warburg resistance[33] represents the resistance related to mass transfer in an electrochemical process. The resistance is frequency dependent, and consists of both resistance and capacitance. The impedance of the Warburg resistance ($Z_w(\omega)$) is written as

$$Z_{\omega} = \frac{1}{Y_{\circ} \sqrt{i\omega}} \quad (2.25)$$

where $Y_{\circ} = \frac{1}{\sigma}$, The Warburg impedance can be considered as a resistance ($R_f = \frac{\sigma}{\sqrt{\omega}}$) connected with a capacitance ($C_f = \frac{\sigma}{\sqrt{\omega}}$) in series. Since the impedance of the real part equals that of the imaginary part, in Nyquist spectra the Warburg impedance is represented by the 45 ° line following the semicircle (charge transfer and double-layer circuit).

2.5.2.2.2. Constant Phase Element (CPE) :

The constant phase element (CPE) is a non-intuitive circuit element that was discovered in the course of investigations into responses from real systems. In general, a Nyquist plot (also called a Cole–Cole plot or complex impedance plane plot) should be a semicircle with the centre on the x-axis. However, the observed plot for some real systems was indeed the arc of a circle but with the centre located somewhere below the x-axis. A CPE's impedance is given by

$$Z_{\omega} = \frac{1}{Y_{\circ} (i\omega)^n} \quad (2.26)$$

where Y_{\circ} is a factor of proportionality having numerical values, and n is the CPE exponent that characterizes the phase shift. For integral values of n ($n = 1, 0, -1$), the CPE represents C, R, and L, respectively. For $n = 0.5$, it gives the Warburg impedance. The physical meanings of the coefficient Q for $n = 1, 0, -1$, and 0.5 are listed in Table 2.2.

Table 2.2. Physical meaning of the coefficient Q

N	CPE designation	Q (meaning)	units
1	Capacitance	C	$F = \Omega^{-1}S$
0	Resistance	R^{-1}	Ω^{-1}
-1	Inductance	L^{-1}	$H^{-1} = \Omega^{-1}S^{-1}$
0.5	Warburg Resistance	σ	$\Omega S^{-1/2}$

For $n = 1 - \varepsilon$, where $0 < \varepsilon \leq 0.2$, the CPE corresponds to distortion of the capacitance due to electrode surface roughness or distribution/accumulation of charge carriers. For $n = 0.5 \pm \varepsilon$, where $0 < \varepsilon \leq 0.1$, the CPE is related to diffusion, with deviations from Fick's second law. For $n = 0 \pm \varepsilon$, where $0 < \varepsilon \leq 0.2$, the CPE represents distorted resistance. For $n < 0$, the CPE describes inductive energy accumulation. Therefore, the CPE is a generalized element. Several factors can contribute to the CPE: surface roughness, varying thickness or composition, non-uniform current distribution, and a distribution of reaction rates (non-homogeneous reaction rates on the electrode surface) [34].

CHAPTER THREE

EXPERIMENTAL WORK

In this chapter, DSSCs were prepared using natural and synthetic dyes as photosensitizers. The TiO₂ layer was dyed using twenty natural dyes and eight chemical dyes. The absorption spectra of all dyes were performed. The J-V characteristic curves of the fabricated cells were measured. Electrochemical impedance spectroscopy was measured for three cells.

3.1 Natural Dyes as Photosensitizers for Dye Sensitized Solar Cell

3.1.1 Material Used in Preparing Solar Cells

- a. Fluorine-doped SnO₂,conductive plates with sheet resistance 15 Ω/cm²,and transmission >80% (Xinyan Tech. Ltd, Hong Kong).
- b. TiO₂ nano particles with 10-25 nm (US Research Nanomaterial, Lnc, USA)
- c. Natural dyes extracted from several plants leaves listed in table 3.1
- d. A counter electrode fabricated from FTO-coated glass, with sputtering a platinum catalyst layer
- e. A redox (I⁻/I₃⁻) electrolyte solution. The electrolyte solution is composed of 2ml acetonitrile (ACN), 8ml propylene carbonate (p-carbonate), 0.668gm (KI), and 0.0634gm (I₂).
- f. Electrical contact between working and counter electrodes is achieved using alligator clips

3.1.2 Experimental

3.1.2.1 Natural Dyes Extraction

Twenty plant leaves were collected from various plants. The raw natural materials were first washed by distilled water, dried at 40 °C, then crushed into fine powder using a mortar. These crushed powders were immersed in ethyl alcohol at room temperature and in the dark for one day. After filtration of the solutions, natural dyes were obtained. The natural leaves used in this study are tabulated in table 3.1.

Table 3.1. Natural dyes used in this study were extracted from the leaves of the following plants

No. of dye	Name of dye	No. of dye	Name of dye
ND.1	Cream قشطة	ND.11	Basil ريحان
ND.2	Apricot مشمش	ND.12	Berries توت
ND.3	Figs تين	ND.13	Mirabelle plums برفوق اصفر
ND.4	Apples تفاح	ND.14	Victoria plums برفوق احمر
ND.5	Sage المريمية	ND.15	Peach خوخ
ND.6	Thyme زعتر	ND.16	Mango مانجا
ND.7	Mint نعناع	ND.17	Pomegranate رمان
ND.8	Ziziphus jujuba عناب	ND.18	Bananas موز
ND.9	Orange برتقال	ND.19	Guava جوافة
ND.10	Shade tree شجرة الظل	ND.20	Fluoridation فلورة

3.1.2.2 Preparation of Dye Sensitized Solar Cells

FTO conductive glass substrate were cut into pieces of dimensions 1.6cm×1.6cm. The glass was cleaned in a detergent solution using an ultrasonic bath for 9 min, rinsed with water and ethanol, and then dried in an oven at 60 °C for 30 min.

The TiO₂ paste was prepared by adding of 50 mg TiO₂ nano-powder and 50 mg polyethyleneglycol then grinding the mixture for half an hour until a homogeneous paste was obtained. Films of the prepared TiO₂ past were doctor bladed on the transparent conducting FTO coated glass. To make thin films, two pieces of tape were used as shown in the Figure 3.1

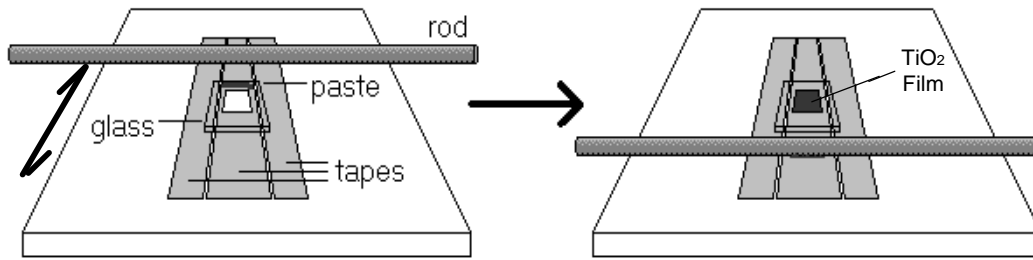


Figure 3.1. Doctor blade method to spread the TiO_2 paste on the FTO coated glass.

After the paste was spread, the films were left to dry for 5 minutes before removing the tape, and placing the film in an oven at 70°C for 30 min and left to dry. The films were then sintered at 450°C for 40 min and then were cooled to about 70°C . The thickness of the sintered films was measured using Olympus microscope and it was found about $22\mu\text{m}$, as shown in the Figure 3.2.

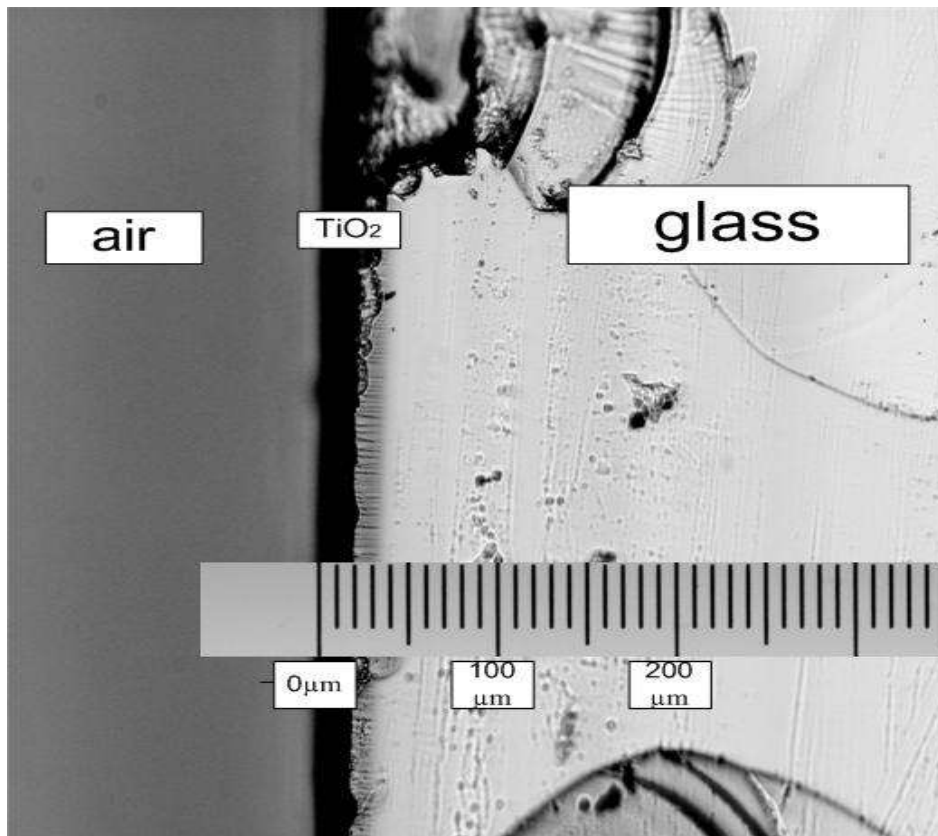


Figure 3.2. A side of the TiO_2 film under magnification of 100x.

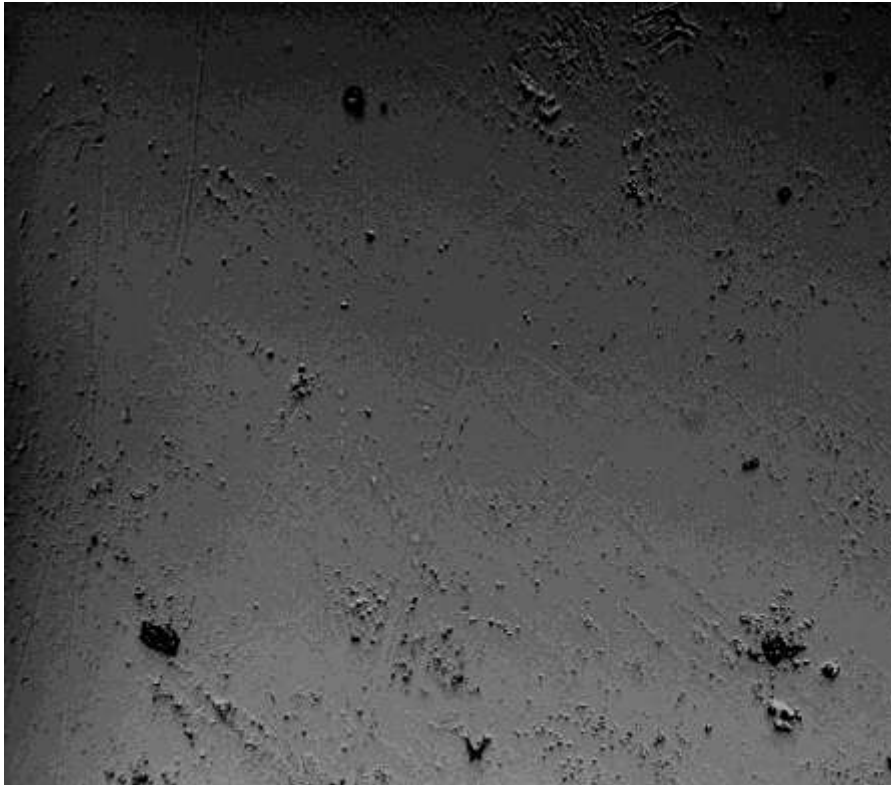


Figure 3.3. A top view of the TiO_2 film under magnification of 40x.

The sintered films were dyed for 16 hr under dark. The dyed TiO_2 electrode and platinum counter electrode were assembled to form a solar cell by sandwiching a redox (I^-/I_3^-) electrolyte solution.

3.1.3 Cell Characterization

3.1.3.1 Measuring Absorption Spectra of Natural Dyes.

The absorption spectra measurements of the extracted pigments in ethyl alcohol solution were performed using a UV-VIS spectrophotometer (Thermoline Geneays 6). The wavelength range of absorption spectra analysis extends from 350 to 800 nm.

3.1.3.2 J-V Measurements:

Because solar radiation is not always available and its magnitude differs according to location and surroundings, a solar simulator is usually used in the solar cell performance measurement. Using a simulator the measured cell gets constant irradiation and the environment condition can be controlled. In my work, high pressure mercury arc lamp was used. A voltage in the range -1 to 1 is applied to the solar cell and the resulting current is measured using NI USB6251 data acquisition

card in combination of a labview program. J-V – curves were measured in different solar irradiations using high pressure mercury arc lamp.

3.1.4 Electrochemical Impedance Spectroscopy

Electrochemical impedance spectroscopy (EIS) measurements can be performed with the Autolab instruments in combination with the frequency response analyzer (FRA). In a typical electrochemical impedance measurement, the FRA module generates a sine wave with a user -defined frequency and a small amplitude. This signal is superimposed on the applied DC potential or current on the cell. The AC voltage and current components are analyzed by the two FRA channels and the transfer function, the total impedance Z , is calculated, together with the phase angle shift and the real and imaginary components of the total impedance.

Electrochemical impedance spectroscopy was measured for three cells using Autolab device. After analyzing the results. The equivalent circuit for each cell was found. Three cells were prepared using Berries, Mirabelle plums, and Peach as sensitizers as described in section 3.1 The AC amplitude was set to 10 mV for all measurements. All the measurements were carried out with the NOVA software. The impedance was measured and plotted to obtain Nyquist and Bode plots.

3.2 Chemical Dyes as Photosensitizers for Dye Sensitized Solar Cell

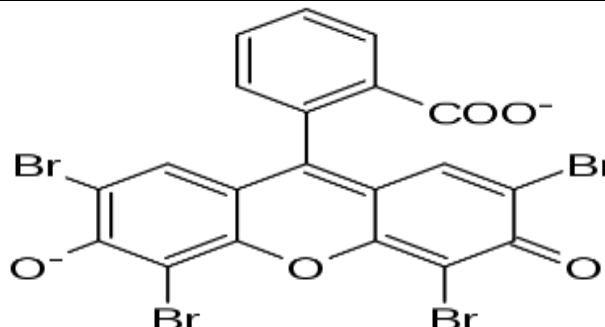
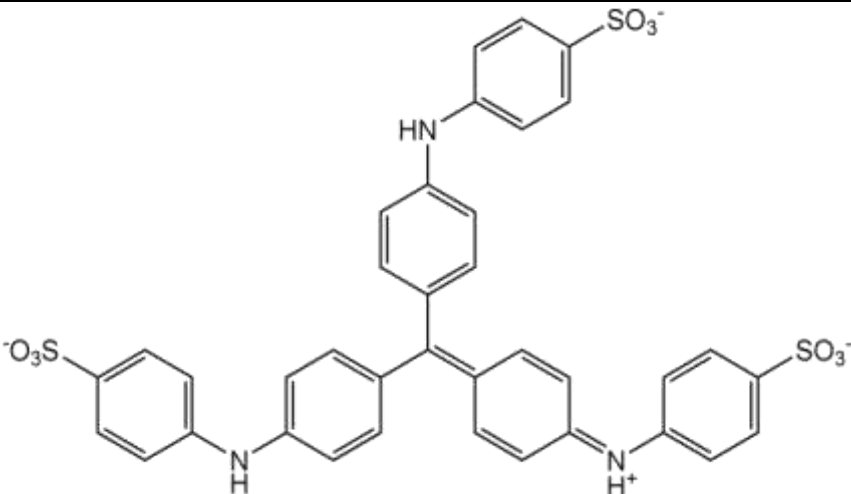
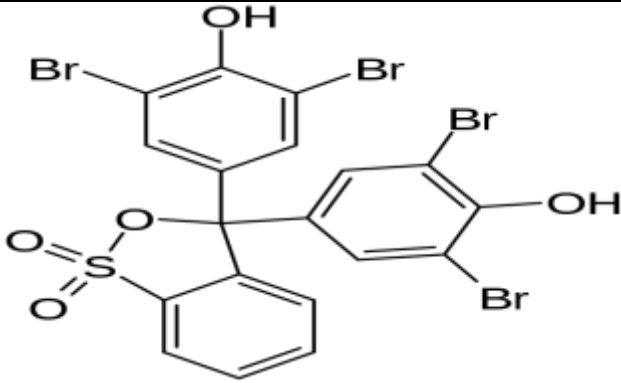
3.2.1 Material Used in Preparing Solar Cells

The same materials mentioned in subsection 3.1.1 are used to fabricate DSSCs. The main difference between these cells and those fabricated in here is the sensitizer. In this part, we use eight synthetic dyes as photosensitizers. These dyes are EosinY, Aniline Blue, Bromophenol Blue, Alcian Blue, Methyl Orange, Crystal Violet, Fast Green, and Carbol Fuchsin. The structures of these chemicals are shown in Table 3.2.

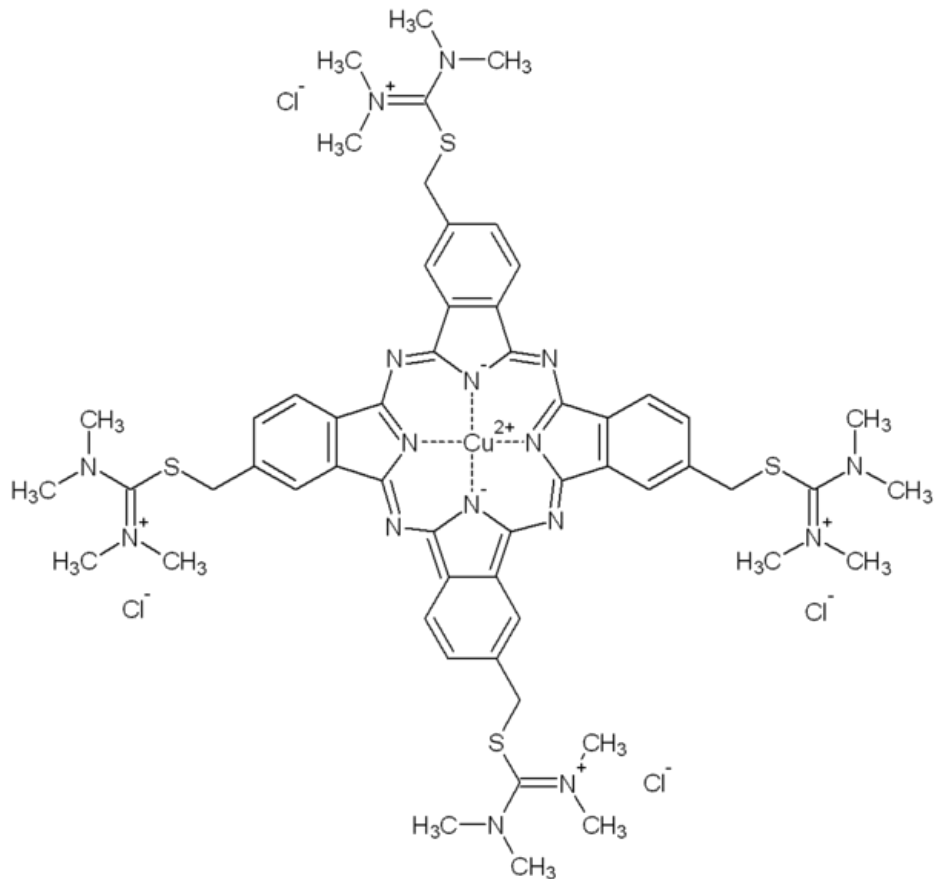
3.2.2 Chemical Dyes Preparation

Eight chemical dyes were used as shown in table 3.2. The dyeing solution was prepared by adding 0.004 gm of dye powder to 20ml of ethyl alcohol. The solutions was left at room temperature.

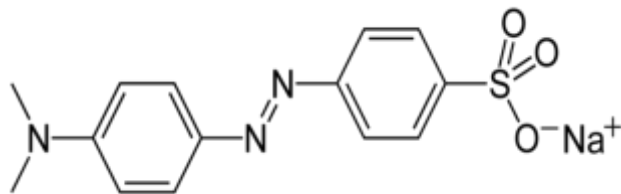
Table 3.2. Structures of the chemical dyes

Name of dye	Structure of dye
Eosin Y	
Aniline Blue	
Bromophenol Blue	

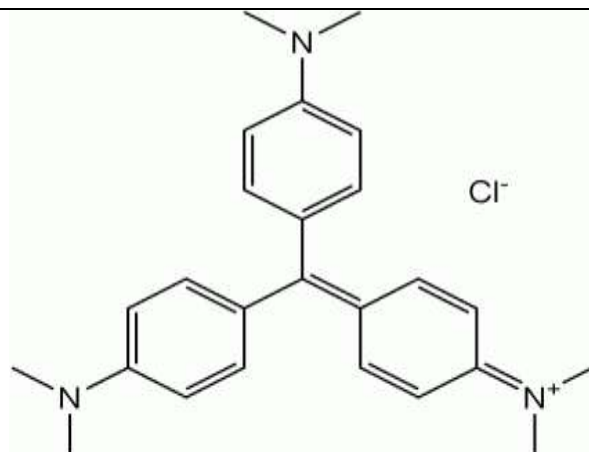
Alcian Blue

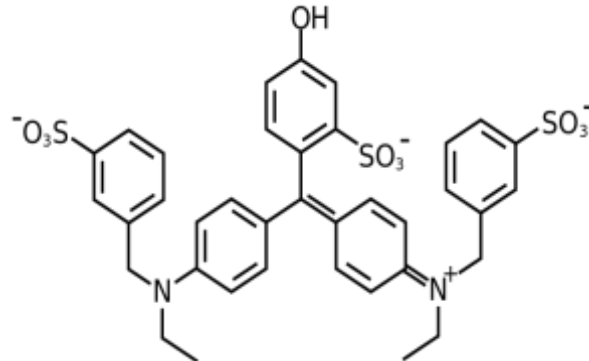
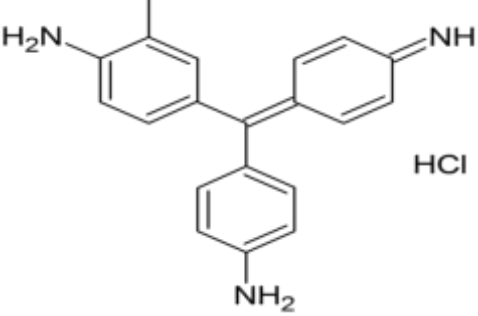


Methyl Orange



Crystal Violet



<p>Fast Green</p>	
<p>Carbol Fuchsin</p>	

CHAPTER FOUR

RESULTS AND DISCUSSION

In this chapter, the absorption spectra of all dyes were presented. The J-V characteristic curves of the fabricated cells were studied. The output power were calculated and plotted versus the voltage of the cell. Short circuit current J_{sc} , open circuit voltage V_{oc} , maximum absorption wavelength, maximum power P_{max} , fill factor F.F, and power conversion efficiency η were all presented.

4.1 Natural Dyes as Photosensitizers for Dye Sensitized Solar Cell

4.1.1 Absorption spectra of Natural Dyes

Figures 4.1 through 4.20 show the UV–VIS absorption spectra of 20 natural dyes extracted from the leaves of Cream, Apricot, Figs, Apples, Sage, Thyme, Mint, Ziziphus jujube, Orange, Shade tree, Basil, Berries, Mirabelle plums, Victoria plums, Peach, Mango, Pomegranate, Bananas, Guava, and Fluoridation in ethyl alcohol as a solvent. From Fig. 4.1, it can be seen that there is absorption peak at about 414.8 nm and 664.2 nm for the extract of Cream. As can be seen from Fig. 4.2, there is an absorption peak at about 394.2 nm and three small peak at 665.4 nm, 535.2 nm, and 505.6nm for the extract of Apricot. Fig. 4.3 shows that there is an absorption peak at about 413.4 nm and small peak at about 663 nm for the extract of Figs. Fig. 4.4 reveals that the extract of Apples has an absorption peak at about 406 nm and a small peak at about 664 nm. The absorption spectrum of Sage is shown in Fig. 4.5. In this case the figure shows two peaks at 414.5nm and 663. nm. Figure 4.6 shows that the extract of Thyme exhibits absorption peaks at 412.2 nm and 664.4 nm. As Fig. 4.7 shows, Mint extract has absorption peaks in the visible light region at 411.2 nm and 666.5 nm. Figure 4.8 shows the absorption spectrum of Ziziphus jujube. As can be seen from the figure, the Ziziphus jujube extract shows two peaks at 368 nm and at 408.8nm and a small peak at 665.4 nm. From Fig. 4.9 it can be seen that there is an absorption peak at about 415.3 nm and a small peak at about 663.2 nm for the extract of Orange. From Fig. 4.10, it can be seen that there are two absorption peaks at about 412.2 nm and 663.4 nm for the extract of Shade tree. As can be seen from Fig. 4.11, there in an absorption peak at about 410 nm and another peak at 664.3 nm for the extract of Basil. Fig. 4.12 shows that there is an absorption peak at about 412.2 nm

and small peak at about 664.3 nm for the extract of Berries. Figure 4.13 shows that the extract of Mirabelle plums exhibits an absorption peak at 665.7 nm. As Fig. 4.14 shows Victoria plums extract has an absorption peaks in the visible light region at 666 nm. Figure 4.15 reveals that the extract of Peach has an absorption peak at 665 nm. Figure 4.16 reveals that the extract of Mango has absorption peaks at 461.4 nm and peak at 664.1 nm. From Fig. 4.17 it can be seen that there is an absorption peak at about 401 nm and a small peak at about 665.3 nm for the extract of Pomegranate. As can be seen from Fig. 4.18 there is an absorption peak at about 472.2 nm and another peak at 664.3 nm for the extracts Bananas. As Fig. 4.19 shows Guava extract has an absorption peak in the visible light region at 665.1 nm. Finally, from Fig. 4.20, it can be seen that there is an absorption peak at about 403 nm and a small peak at about 665.4 nm for the extracts of Fluoridation. Generally, it is found that most of the dyes have absorption peaks at about 400 nm and small peaks at about 667 nm. This is due to that all samples are plant leaves and the existing pigment is chlorophyll.

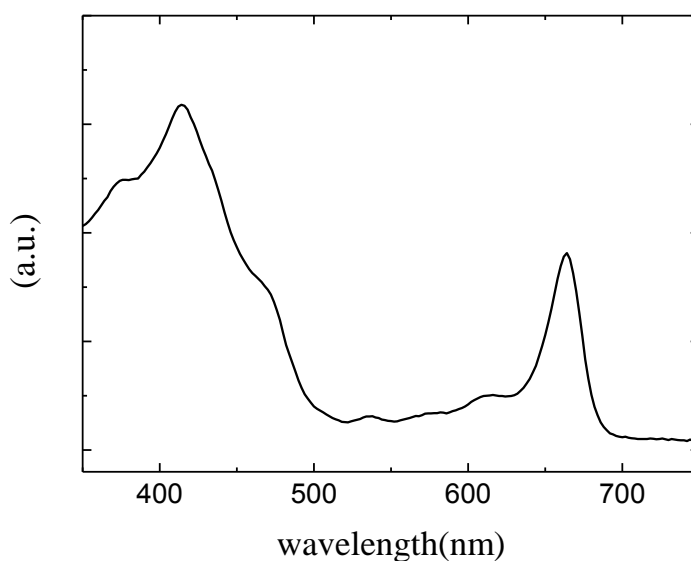


Figure 4.1. The absorption spectrum of the extract of Cream using ethyl alcohol as a solvent

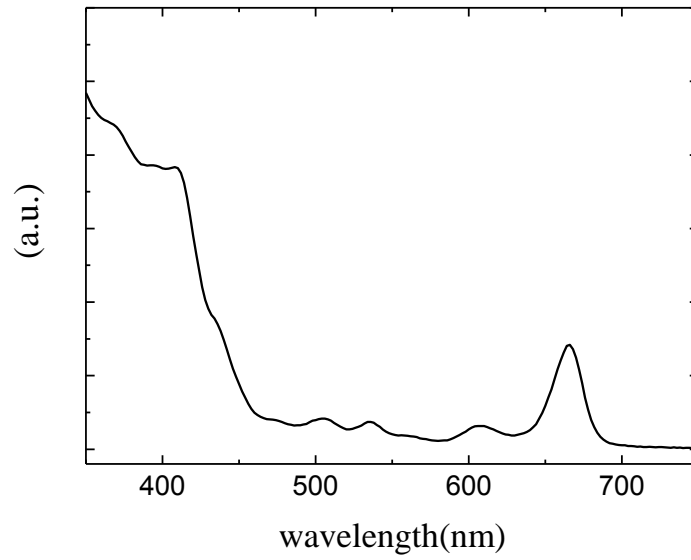


Figure 4.2. The absorption spectrum of the extract of Apricot using ethyl alcohol as a solvent

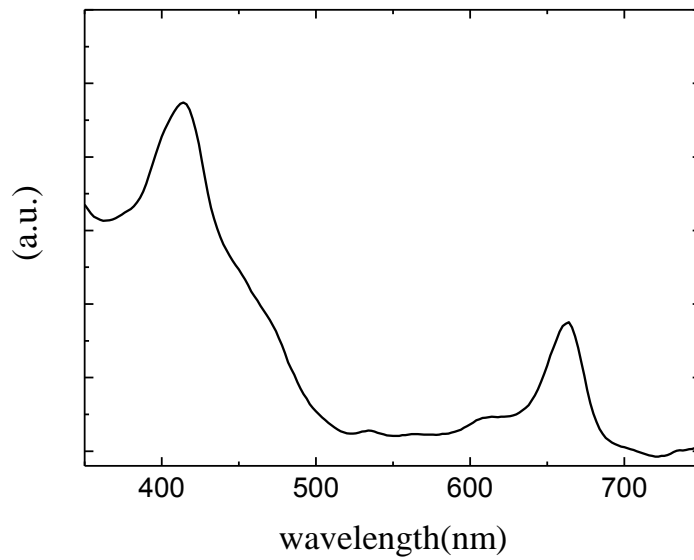


Figure 4.3. The absorption spectrum of the extract of Figs using ethyl alcohol as a solvent

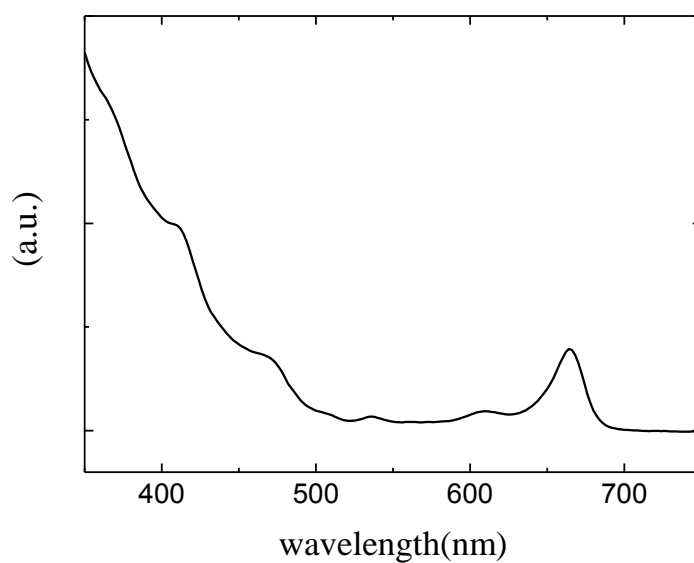


Figure 4.4. The absorption spectrum of the extract of Apples using ethyl alcohol as a solvent

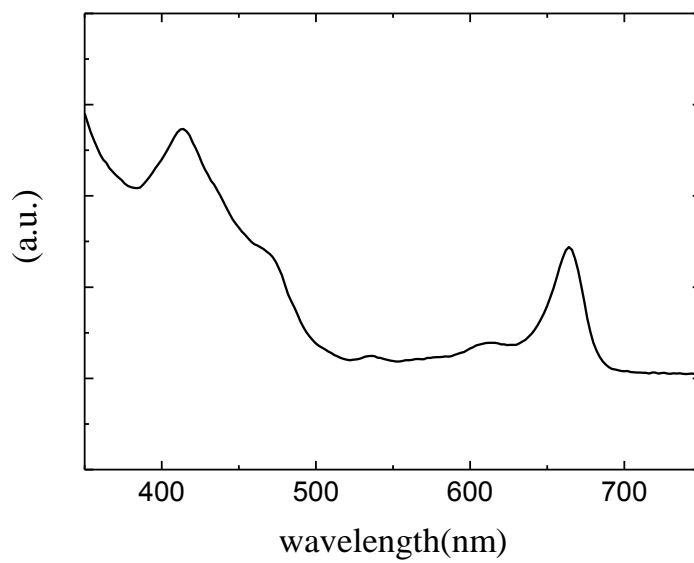


Figure 4.5. The absorption spectrum of the extract of Sage using ethyl alcohol as a solvent.

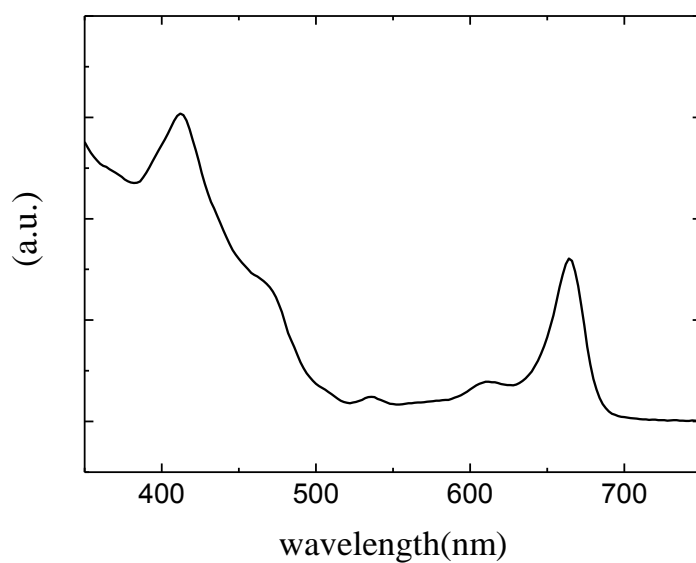


Figure 4.6. The absorption spectrum of the extract of Thyme using ethyl alcohol as a solvent.

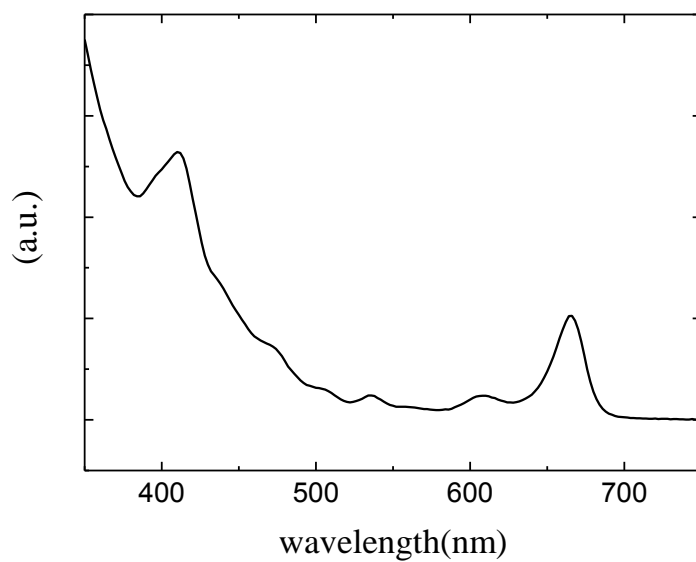


Figure 4.7. The absorption spectrum of the extract of Mint using ethyl alcohol as a solvent.

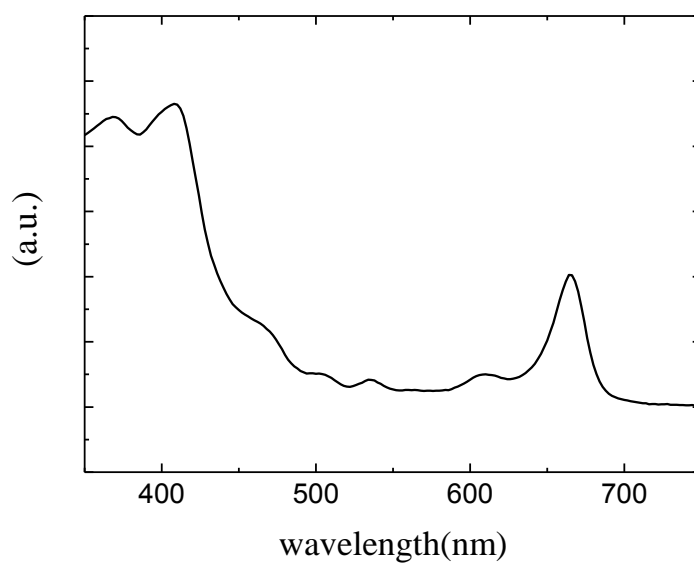


Figure 4.8. The absorption spectrum of the extract of *Ziziphus jujuba* using ethyl alcohol as a solvent.

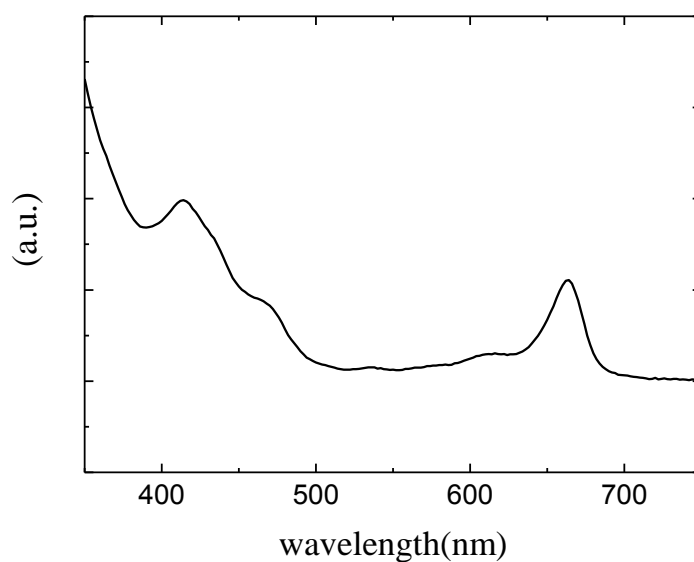


Figure 4.9. The absorption spectrum of the extract of Orange using ethyl alcohol as a solvent.

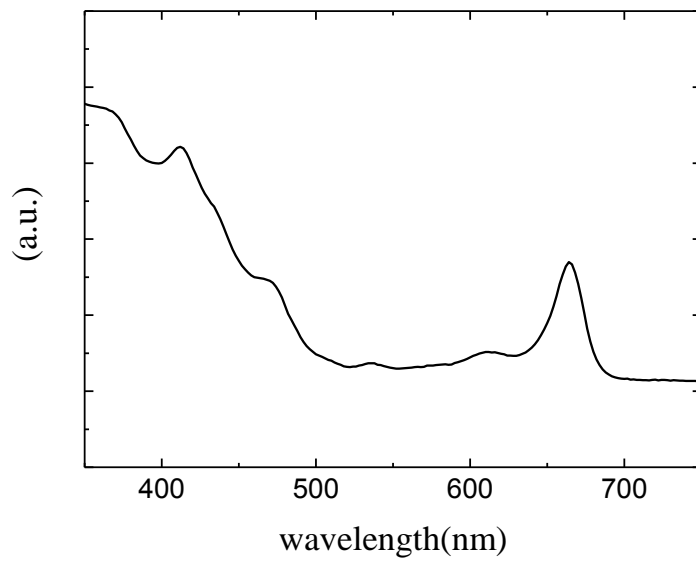


Figure 4.10. The absorption spectrum of the extract of Shade tree using ethyl alcohol as a solvent.

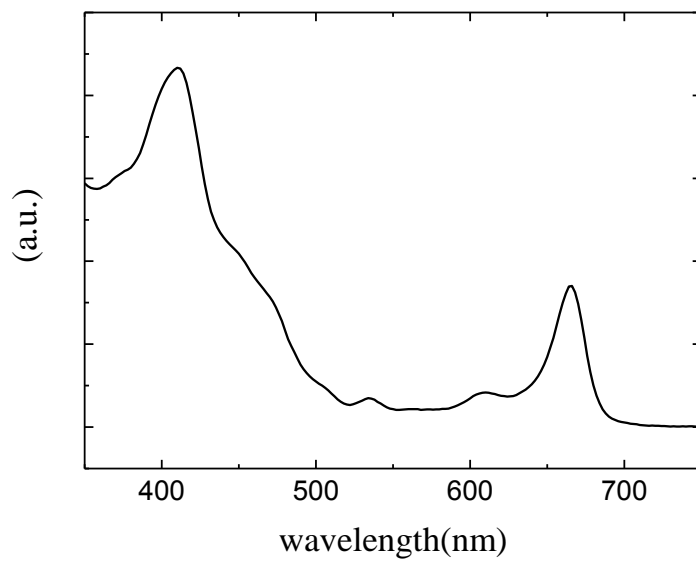


Figure 4.11. The absorption spectrum of the extract of Basil using ethyl alcohol as a solvent.

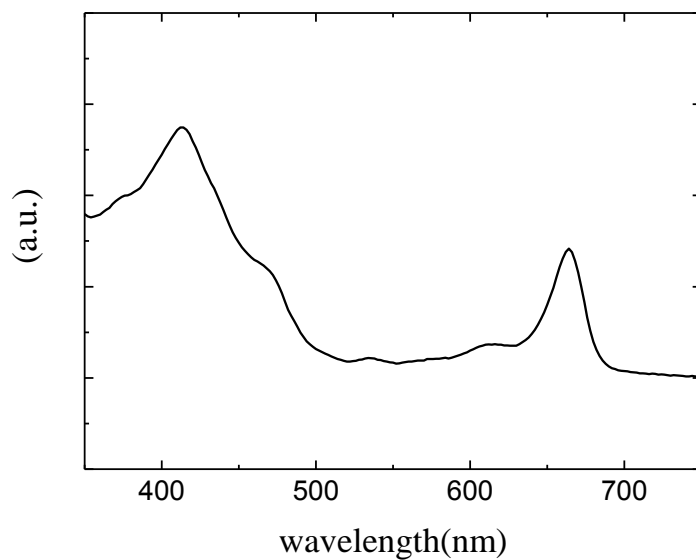


Figure 4.12. The absorption spectrum of the extract of Berries using ethyl alcohol as a solvent.

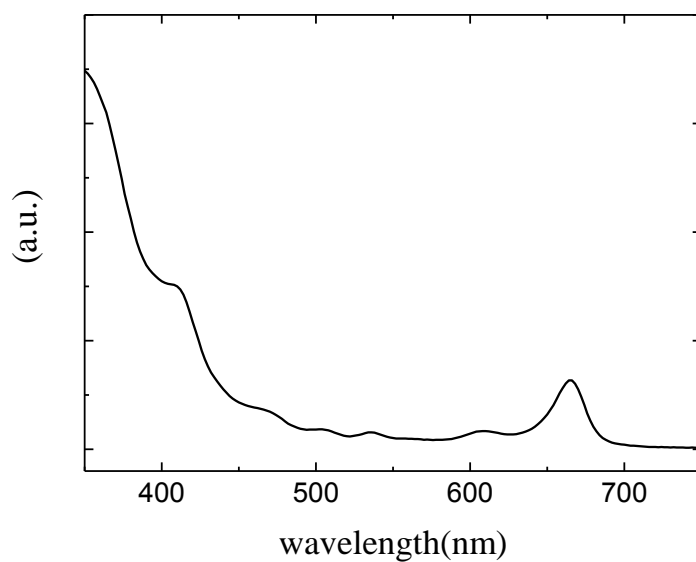


Figure 4.13. The absorption spectrum of the extract of Mirabelle plums using ethyl alcohol as a solvent

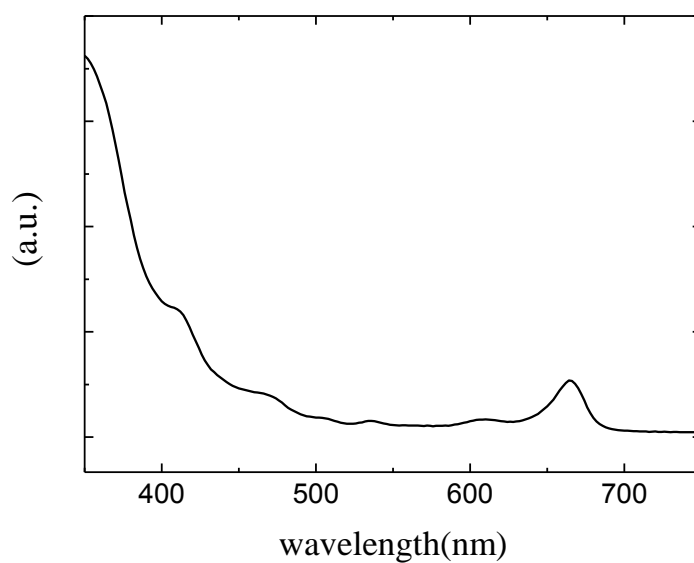


Figure 4.14. The absorption spectrum of the extract of Victoria plums using ethyl alcohol as a solvent.

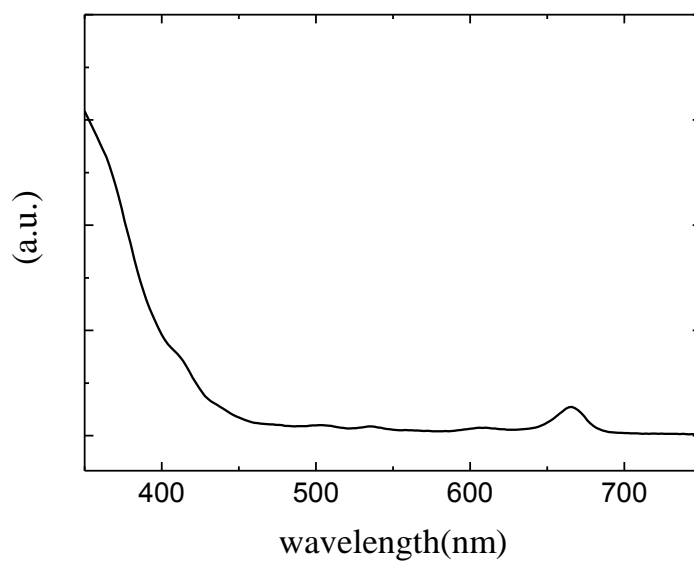


Figure 4.15. The absorption spectrum of the extract of Peach using ethyl alcohol as a solvent.

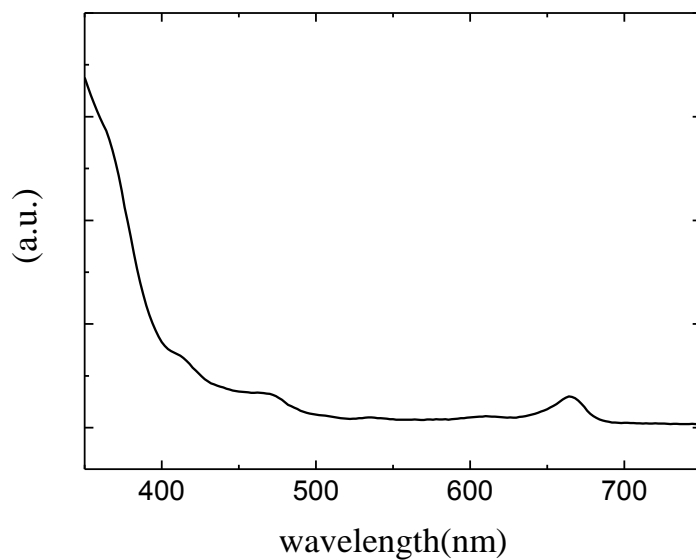


Figure 4.16. The absorption spectrum of the extract of Mango using ethyl alcohol as a solvent.

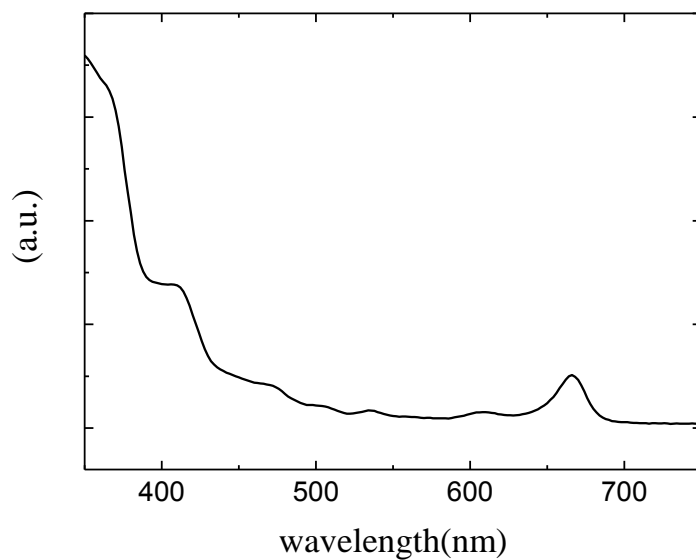


Figure 4.17. The absorption spectrum of the extract of Pomegranate using ethyl alcohol as a solvent.

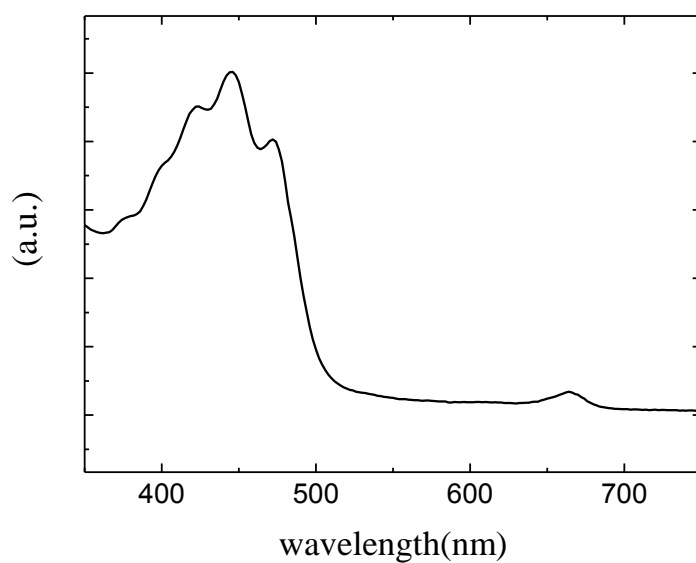


Figure 4.18. The absorption spectrum of the extract of Bananas using ethyl alcohol as a solvent.

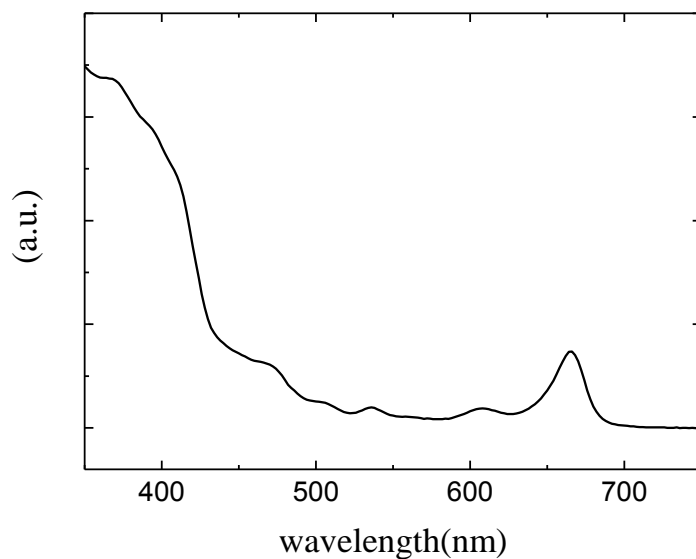


Figure 4.19. The absorption spectrum of the extract of Guava using ethyl alcohol as a solvent.

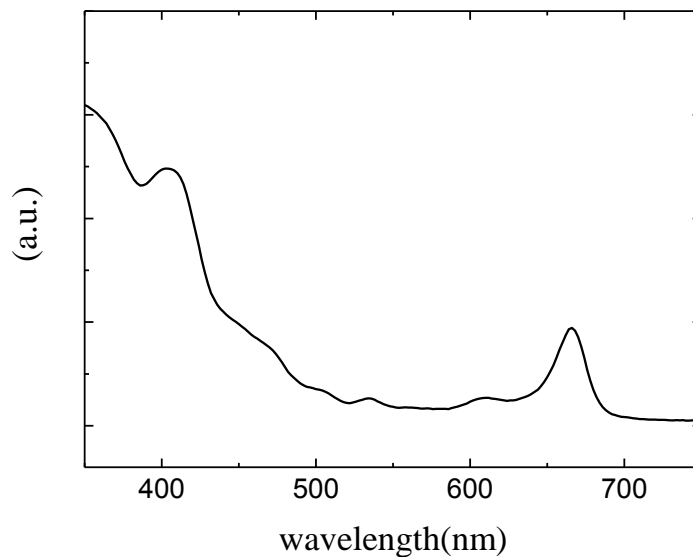


Figure 4.20. The absorption spectrum of the extract of Fluoridation using ethyl alcohol as a solvent.

4.1.2 Photovoltaic Parameters of Dye Sensitized Solar Cells

Electrical measurements results of the DSSCs sensitized using the extracts of 20 natural dyes described above are presented. For each DSSC, the measured current density J versus the voltage V is presented at three different light intensities (1200W/m^2 , 1000W/m^2 , and 800W/m^2). The power is calculated and plotted versus the voltage for each DSSC at the three intensities. Through the study and analysis of these curves and of each DSSC all the cell parameter can be determined. Figures 4.21, 4.23, 4.25, 4.27, 4.29, 4.31, 4.33, 4.35, 4.37, 4.39, 4.41, 4.43, 4.45, 4.47, 4.49, 4.51, 4.53, 4.55, 4.57, and 4.59 show, respectively, the J-V characteristic curves obtained for the fabricated DSSC using the extracts of Cream, Apricot, Figs, Apples, Sage, Thyme, Mint, Ziziphus jujube, Orange, Shade tree, Basil, Berries, Mirabelle plums, Victoria plums, Peach, Mango, Pomegranate, Bananas, Guava, and Fluoridation listed in table 3.1. Each figure shows the results obtained under three different light intensities (1200W/m^2 , 1000W/m^2 , and 800W/m^2). Figures 4.22, 4.24, 4.26, 4.28, 4.30, 4.32, 4.34, 4.36, 4.38, 4.40, 4.42, 4.44, 4.46, 4.48, 4.50, 4.52, 4.54, 4.56, 4.58, and 4.60 show, respectively, the calculated power versus the voltage at three different light intensities for the fabricated cell.

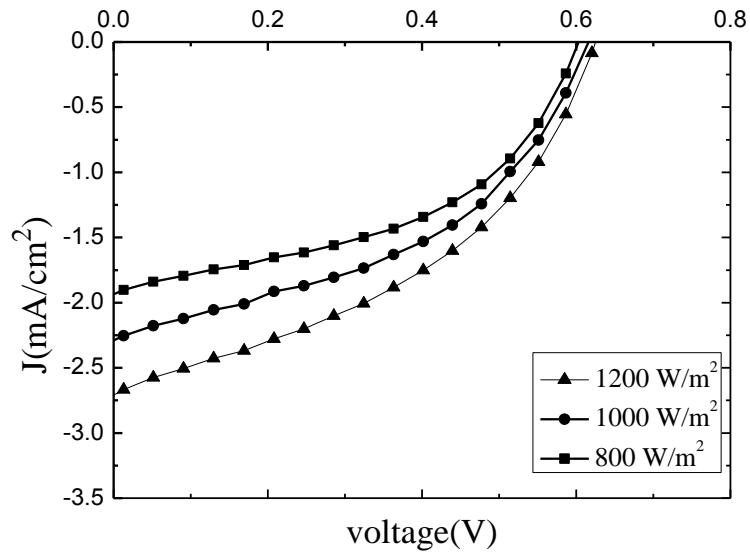


Figure 4.21. Current density–voltage characteristic curves for the DSSCs sensitized by Cream at different light intensities.

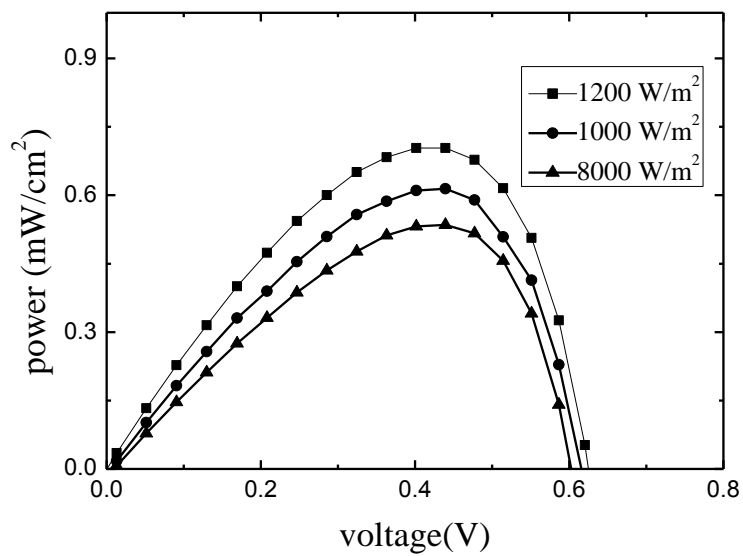


Figure 4.22. Power - voltage characteristics curves of the DSSCs sensitized by Cream at different light intensities.

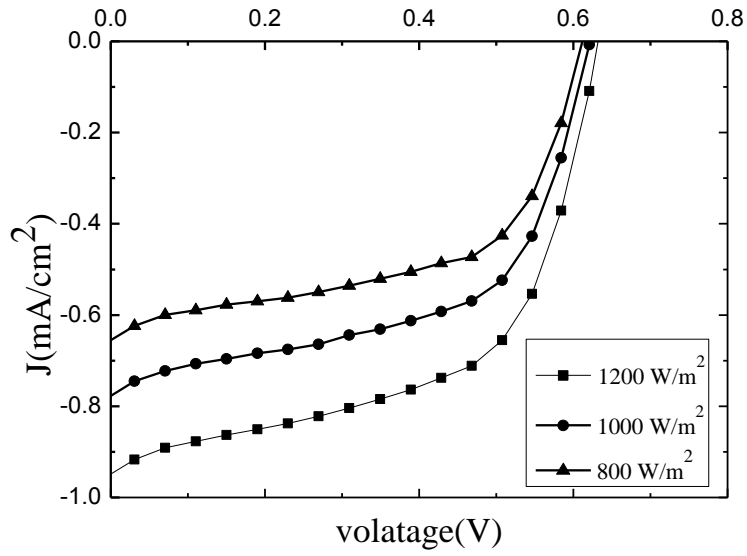


Figure 4.23. Current density–voltage characteristics curves for the DSSCs sensitized by Apricot at different light intensities.

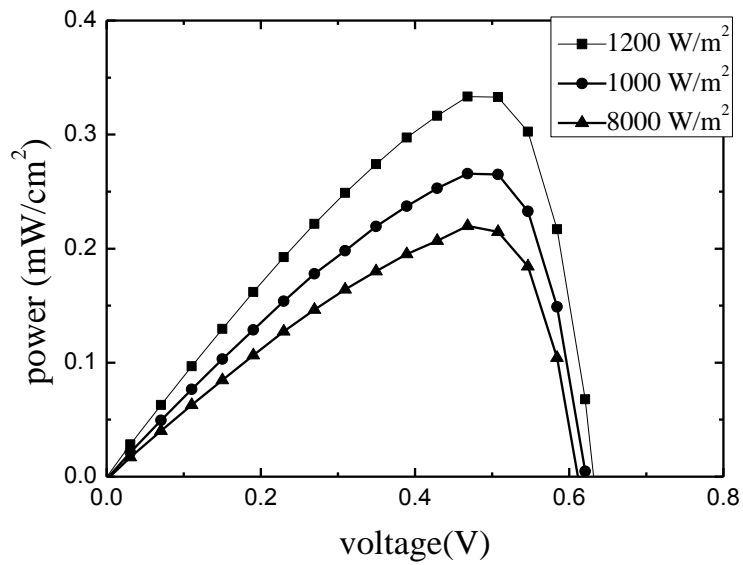


Figure 4.24. Power - voltage characteristics curves of the DSSCs sensitized by Apricot at different light intensities.

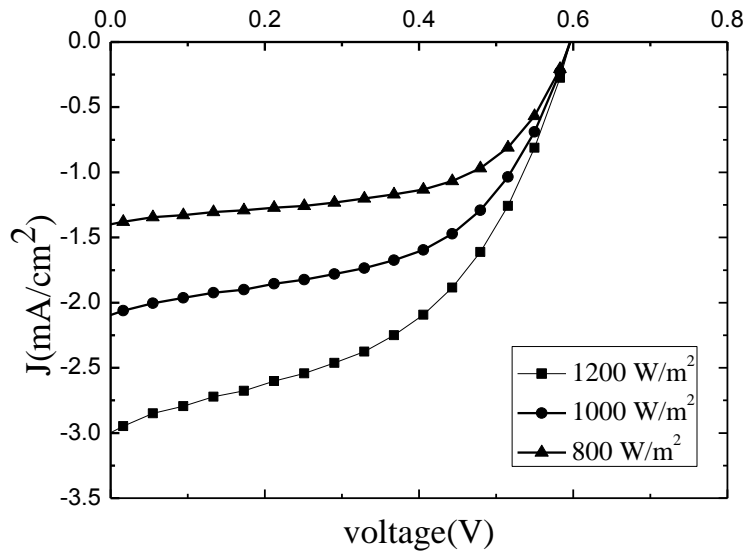


Figure 4.25 Current density–voltage characteristics curves for the DSSCs sensitized by Figs at different light intensities.

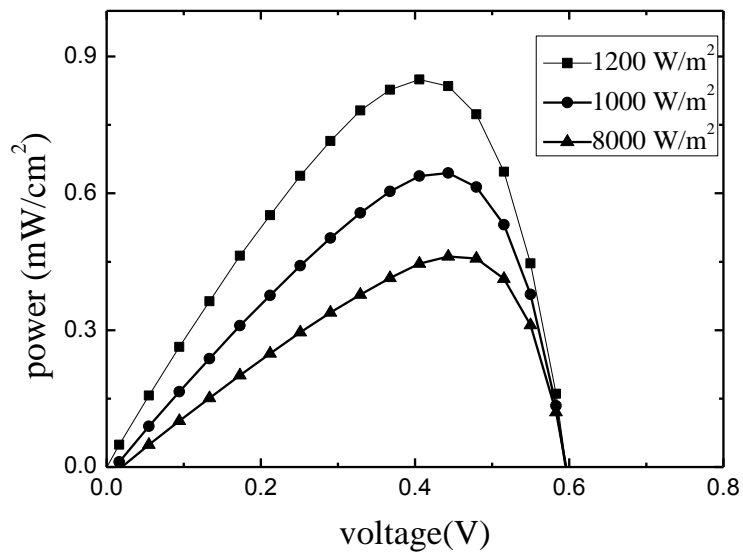


Figure 4.26. Power - voltage characteristics curves of the DSSCs sensitized by Figs at different light intensities.

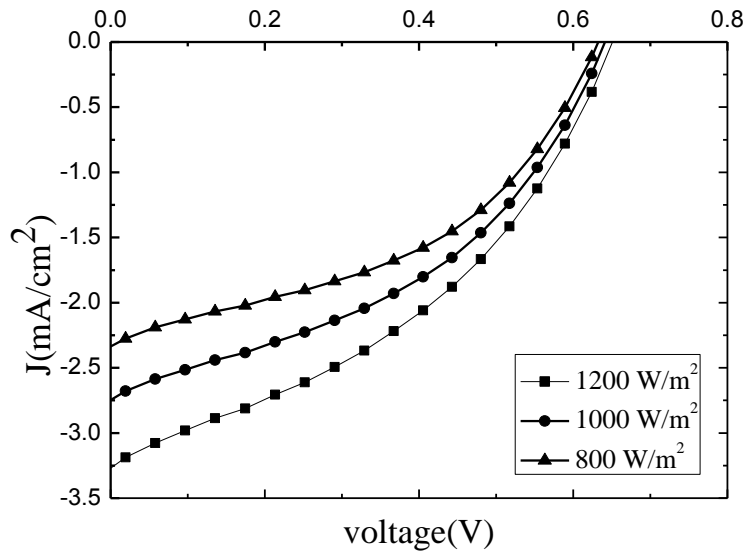


Figure 4.27. Current density–voltage characteristics curves for the DSSCs sensitized by Apples at different light intensities.

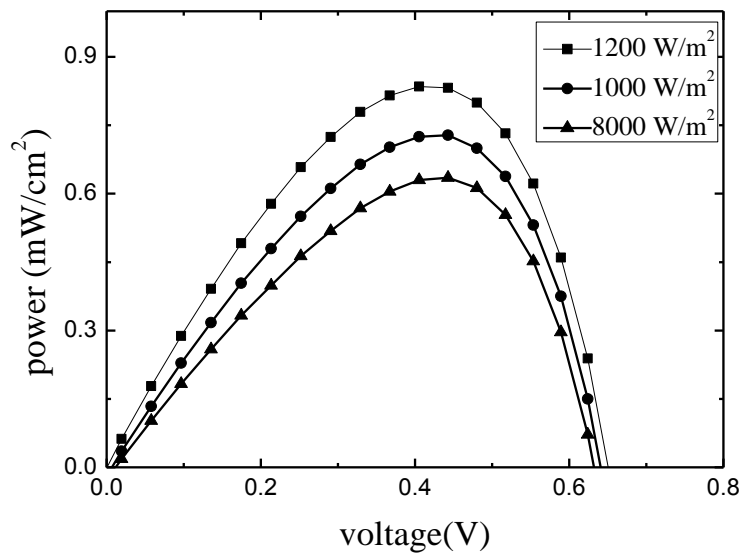


Figure 4.28. Power - voltage characteristics curves of the DSSCs sensitized by Apples at different light intensities.

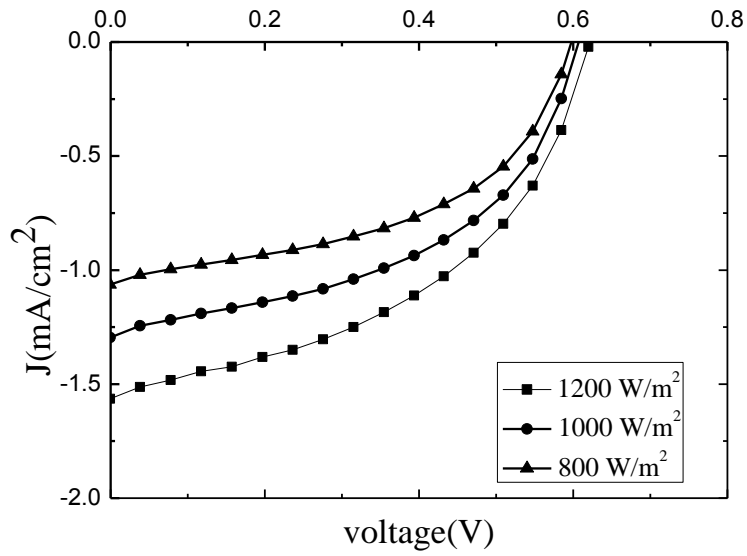


Figure 4.29. Current density–voltage characteristics curves for the DSSCs sensitized by Sage at different light intensities.

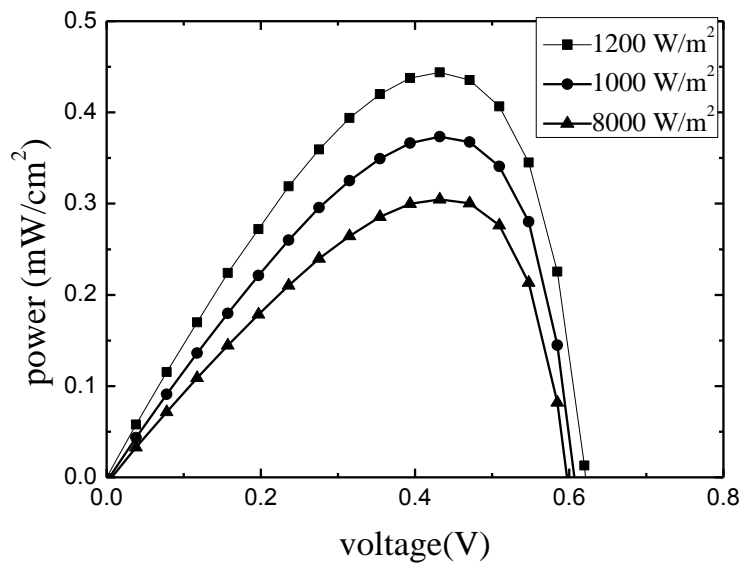


Figure 4.30. Power - voltage characteristics curves of the DSSCs sensitized by Sage at different light intensities.

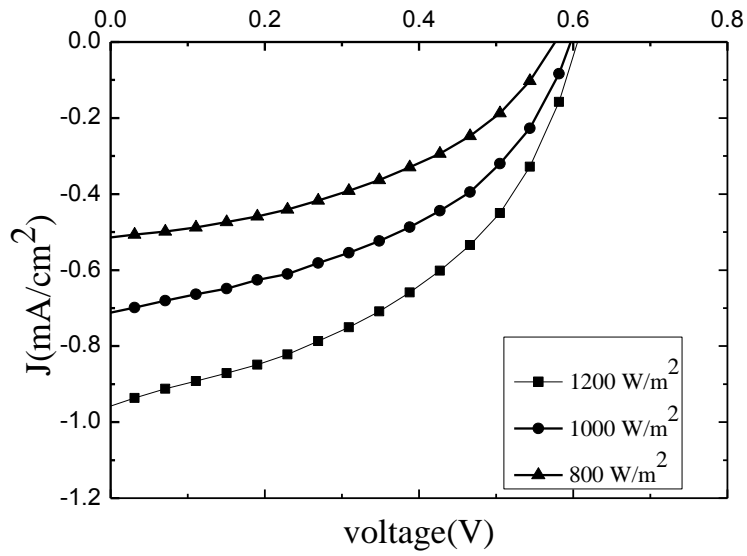


Figure 4.31. Current density–voltage characteristics curves for the DSSCs sensitized by Thyme at different light intensities.

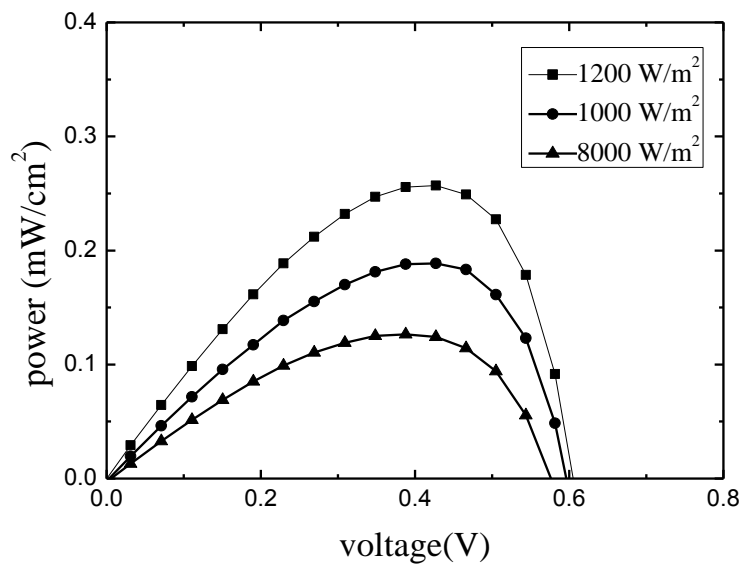


Figure 4.32. Power - voltage characteristics curves of the DSSCs sensitized by Thyme at different light intensities.

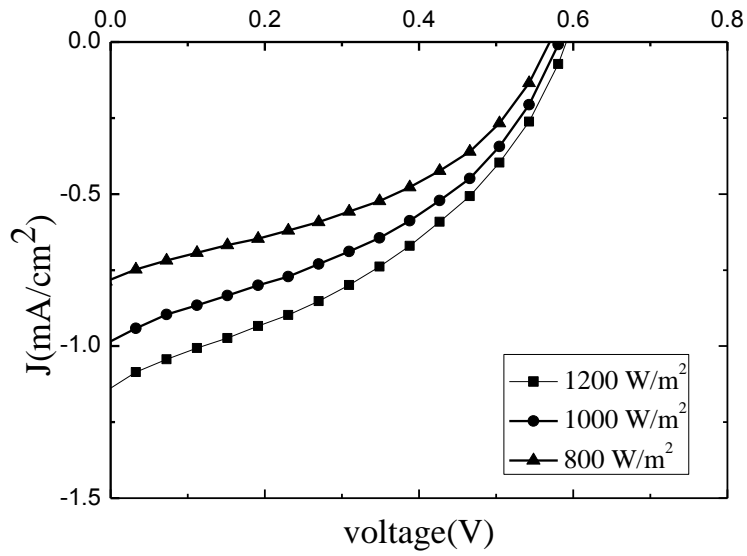


Figure 4.33. Current density–voltage characteristics curves for the DSSCs sensitized by Mint at different light intensities.

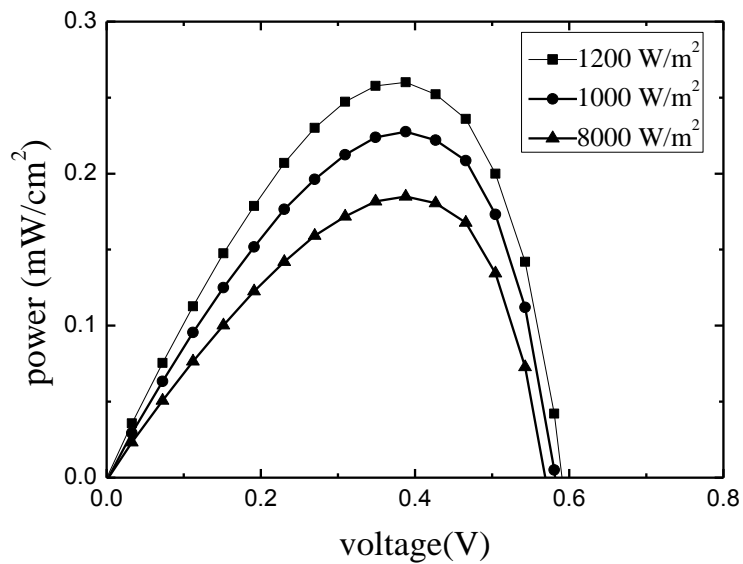


Figure 4.34. Power - voltage characteristics curves of the DSSCs sensitized by Mint at different light intensities.

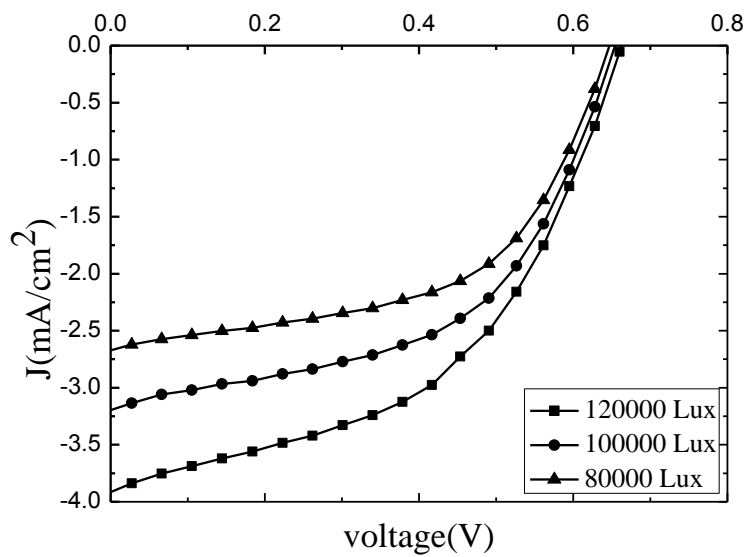


Figure 4.35. Current density–voltage characteristics curves for the DSSCs sensitized by Ziziphus jujube at different light intensities.

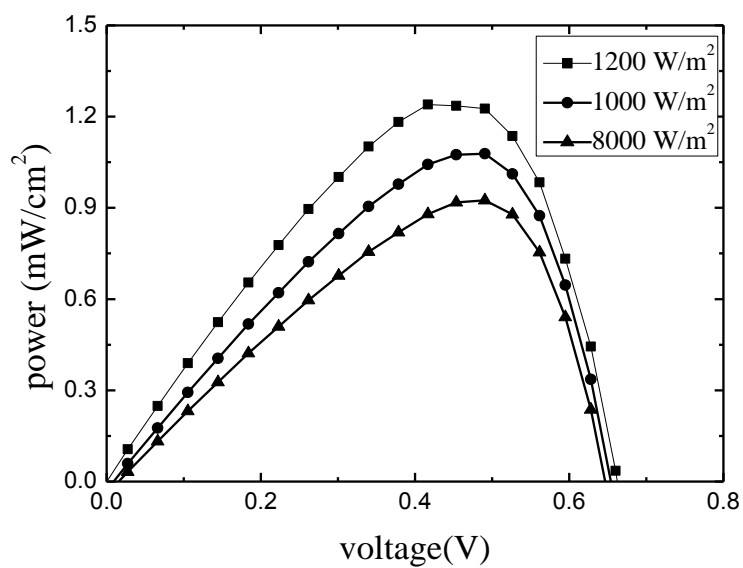


Figure 4.36. Power - voltage characteristics curves of the DSSCs sensitized by Ziziphus jujube at different light intensities.

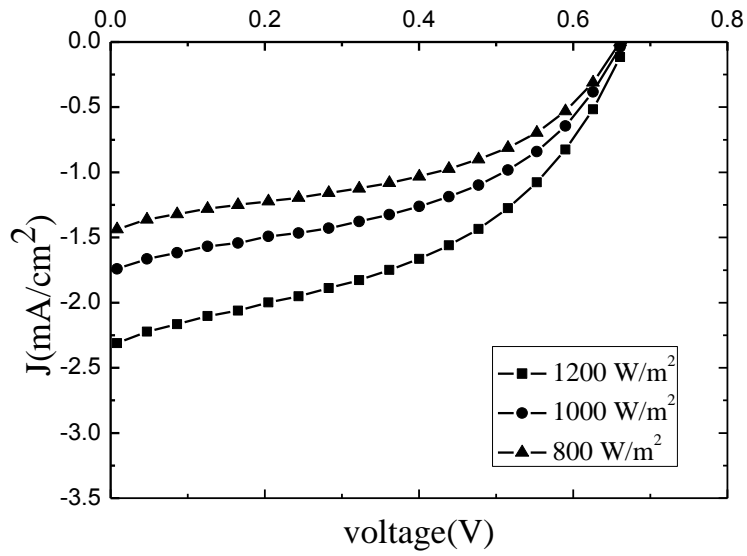


Figure 4.37. Current density–voltage characteristics curves for the DSSCs sensitized by Orange at different light intensities.

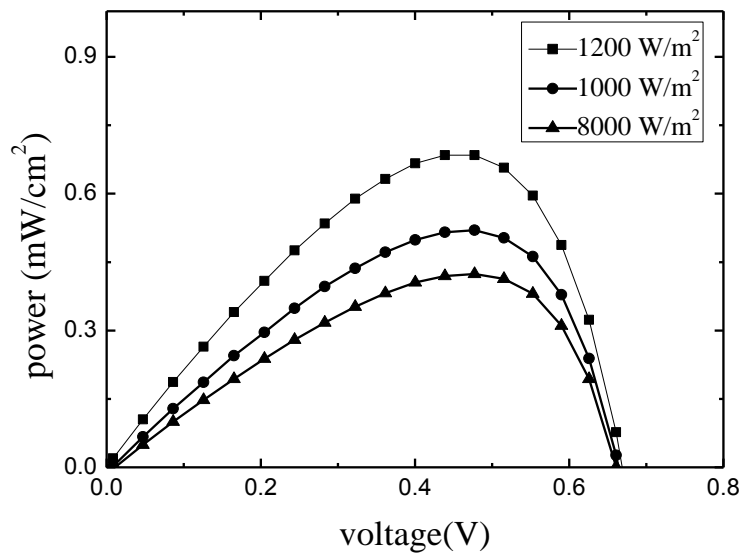


Figure 4.38. Power - voltage characteristics curves of the DSSCs sensitized by Orange at different light intensities.

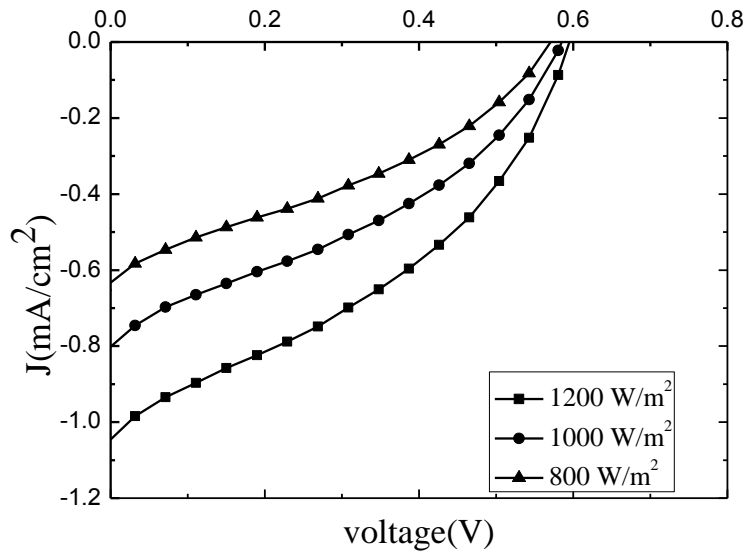


Figure 4.39. Current density–voltage characteristics curves for the DSSCs sensitized by Shade tree at different light intensities.

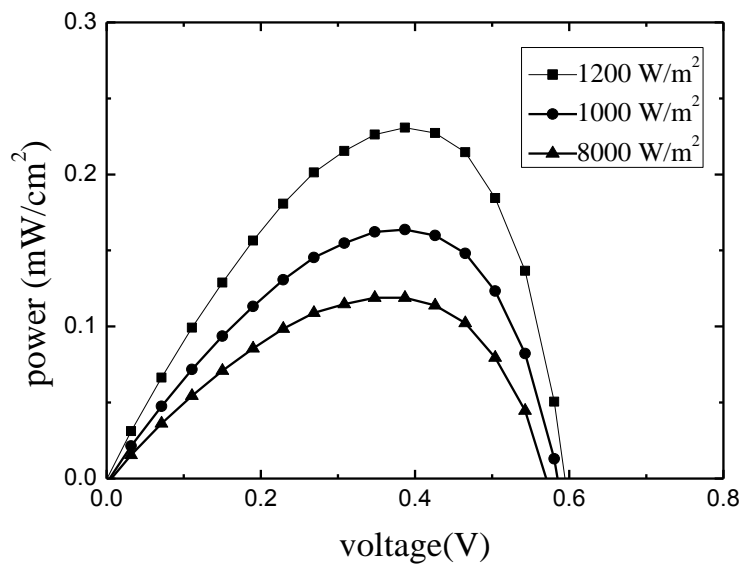


Figure 4.40. Power - voltage characteristics curves of the DSSCs sensitized by Shade tree at different light intensities.

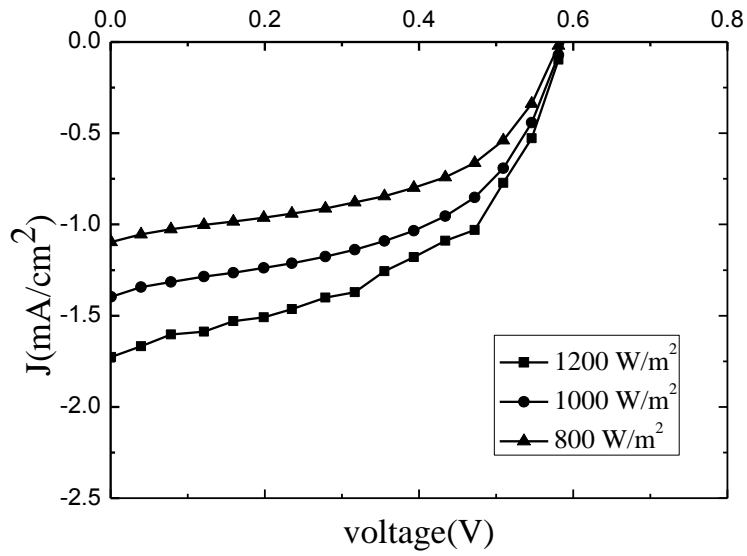


Figure 4.41 Current density–voltage characteristics curves for the DSSCs sensitized by Basil at different light intensities.

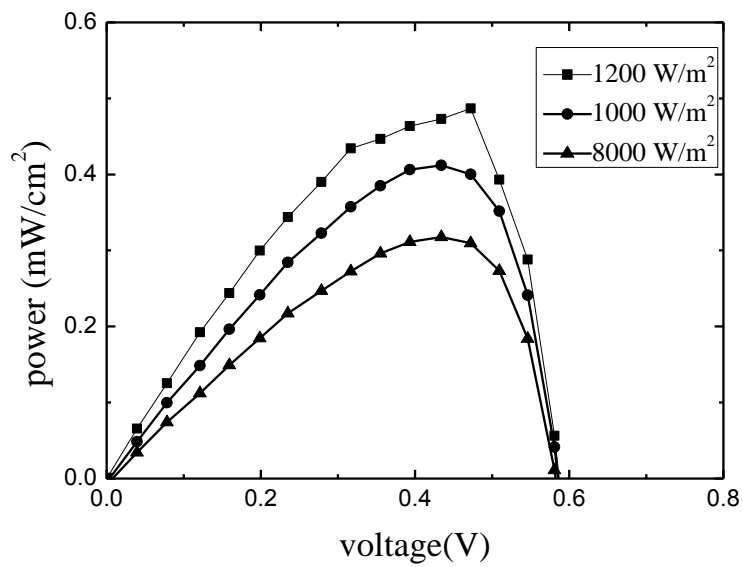


Figure 4.42. Power - voltage characteristics curves of the DSSCs sensitized by Basil at different light intensities.

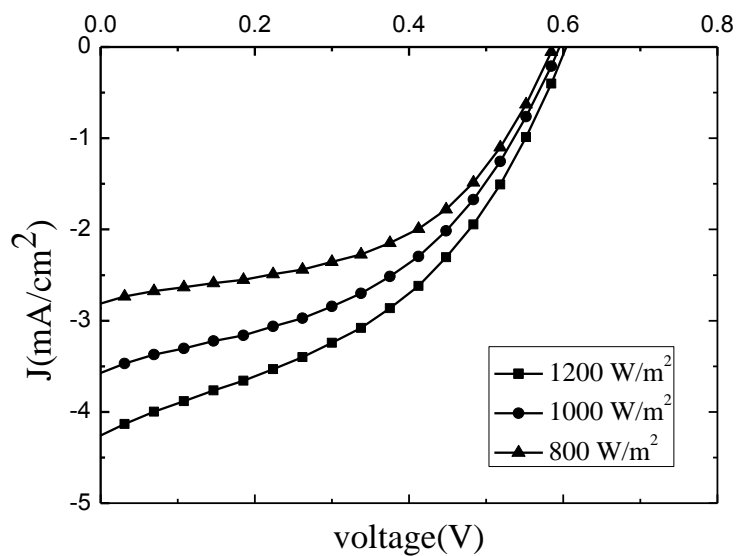


Figure 4.43. Current density–voltage characteristics curves for the DSSCs sensitized by Berries at different light intensities.

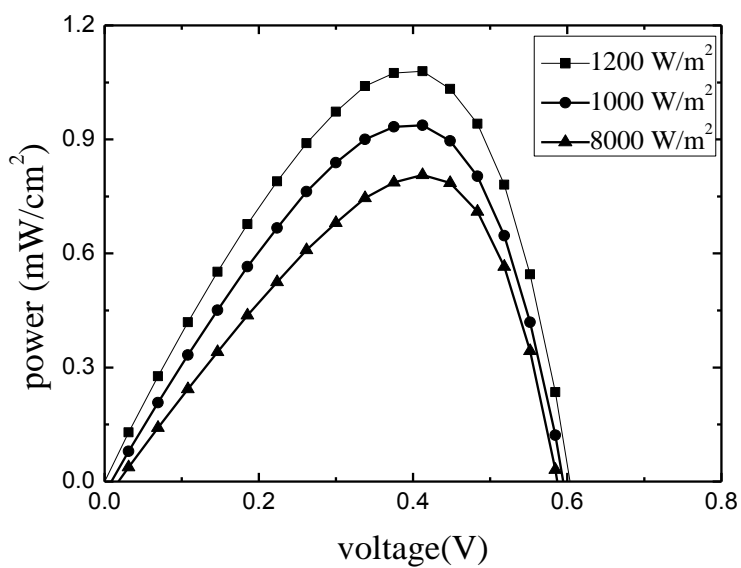


Figure 4.44. Power - voltage characteristics curves of the DSSCs sensitized by Berries at different light intensities.

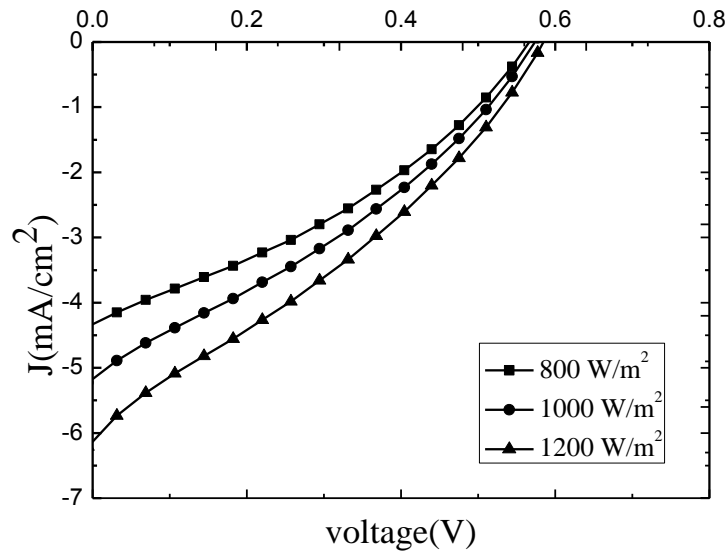


Figure 4.45. Current density–voltage characteristics curves for the DSSCs sensitized by Mirabelle plums at different light intensities.

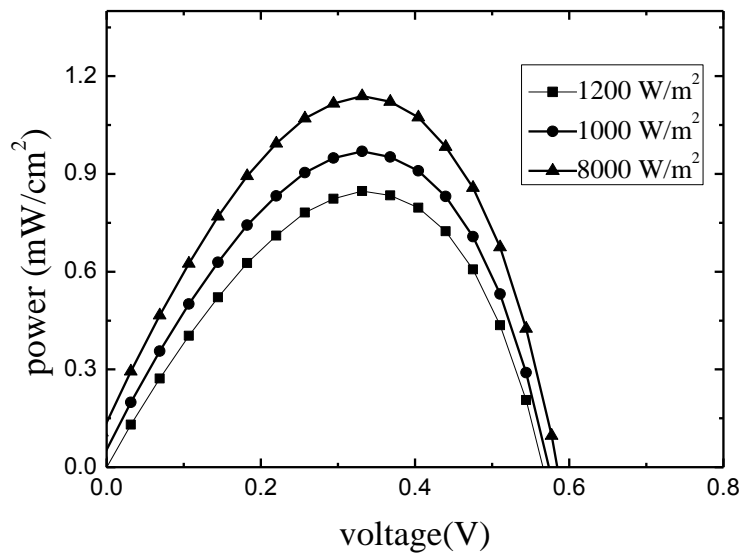


Figure 4.46. Power - voltage characteristics curves of the DSSCs sensitized by Mirabelle plums at different light intensities.

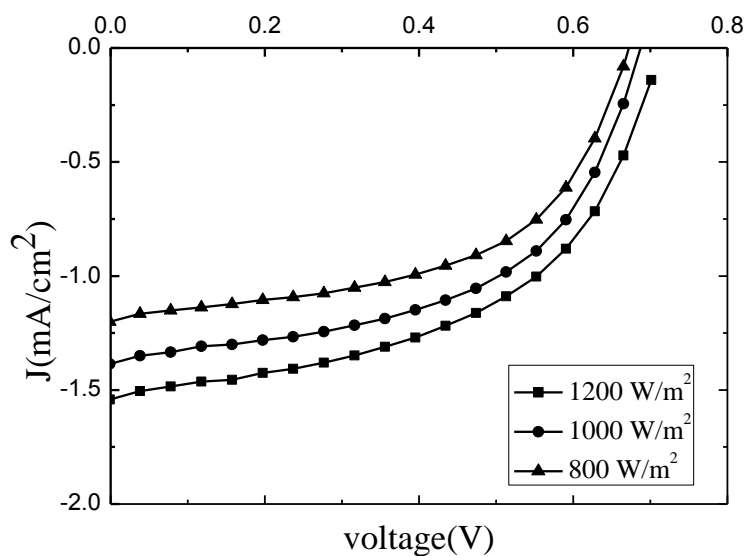


Figure 4.57. Current density–voltage characteristics curves for the DSSCs sensitized by Victoria plums at different light intensities.

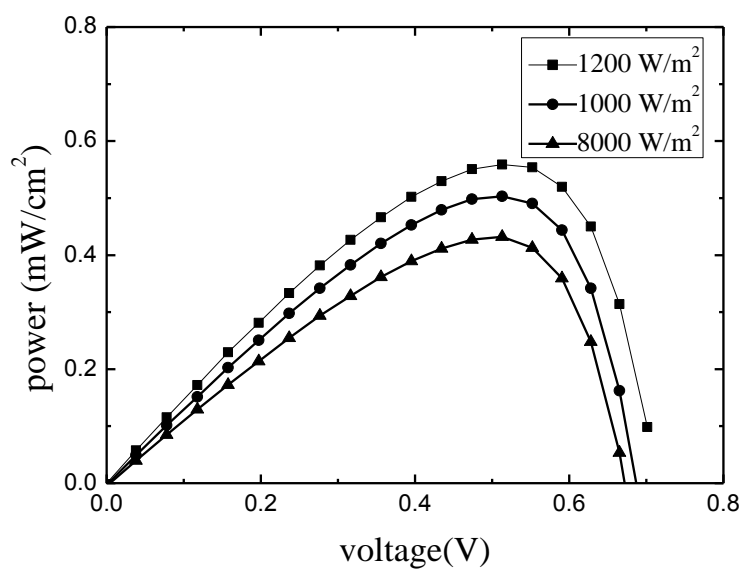


Figure 4.48. Power - voltage characteristics curves of the DSSCs sensitized by Victoria plums at different light intensities.

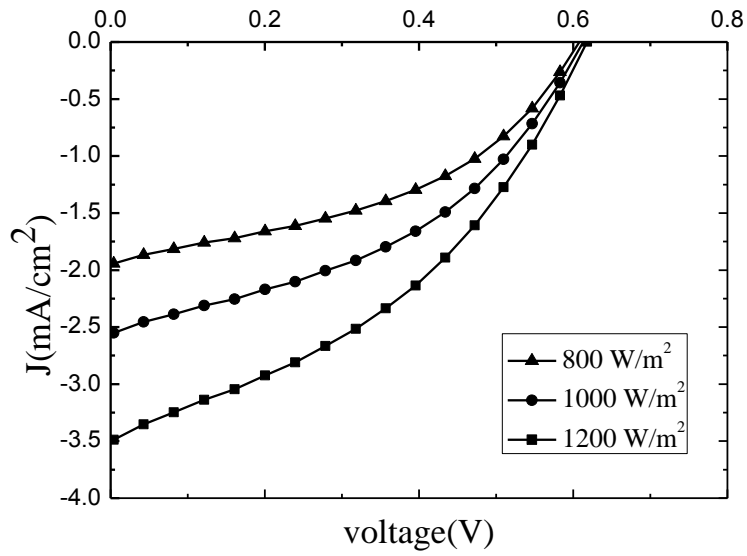


Figure 4.49. Current density–voltage characteristics curves for the DSSCs sensitized by peach at different light intensities.

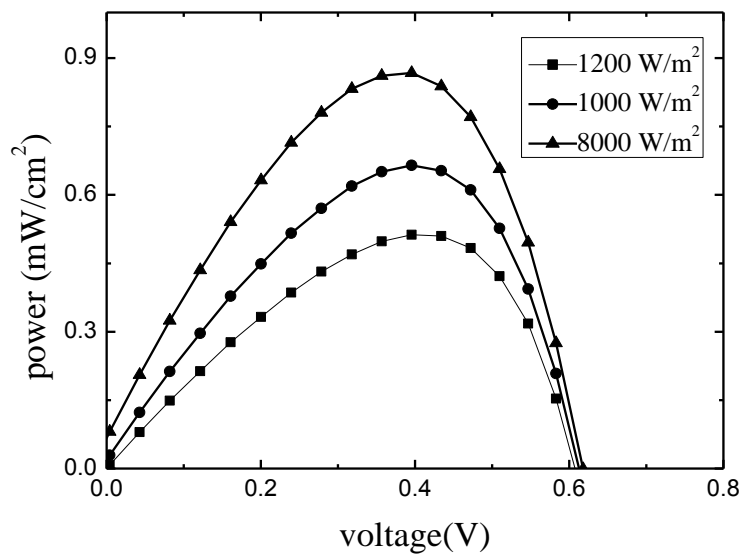


Figure 4.50. Power - voltage characteristics curves of the DSSCs sensitized by peach at different light intensities.

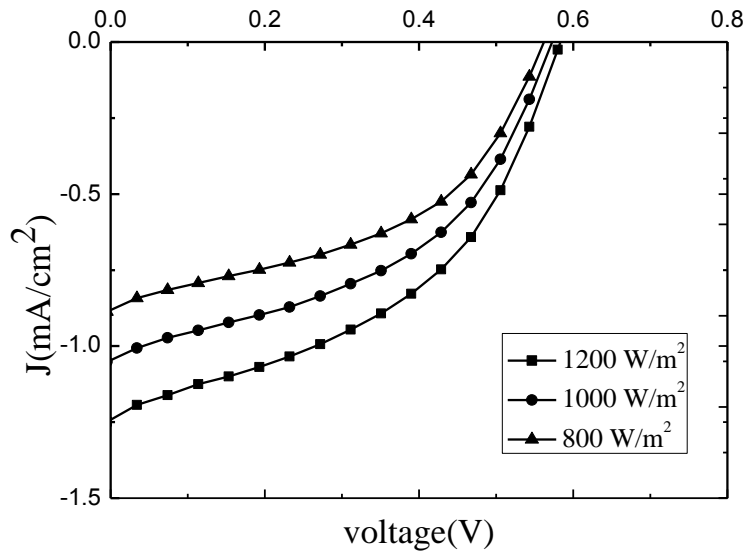


Figure 4.51. Current density–voltage characteristics curves for the DSSCs sensitized by Mango at different light intensities.

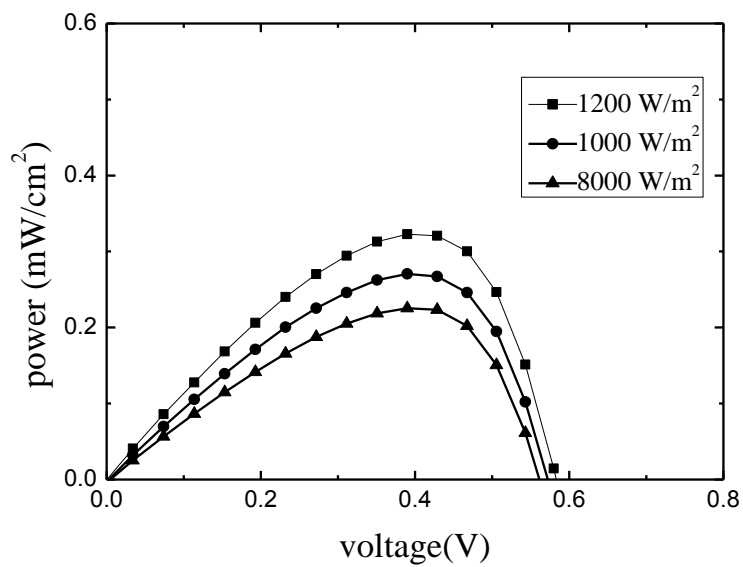


Figure 4.52. Power - voltage characteristics curves of the DSSCs sensitized by Mango at different light intensities.

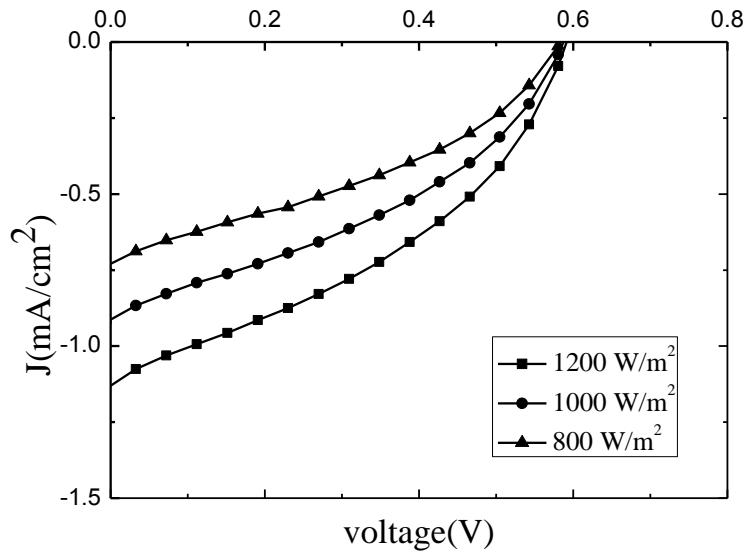


Figure 4.53. Current density–voltage characteristics curves for the DSSCs sensitized by Pomegranate at different light intensities.

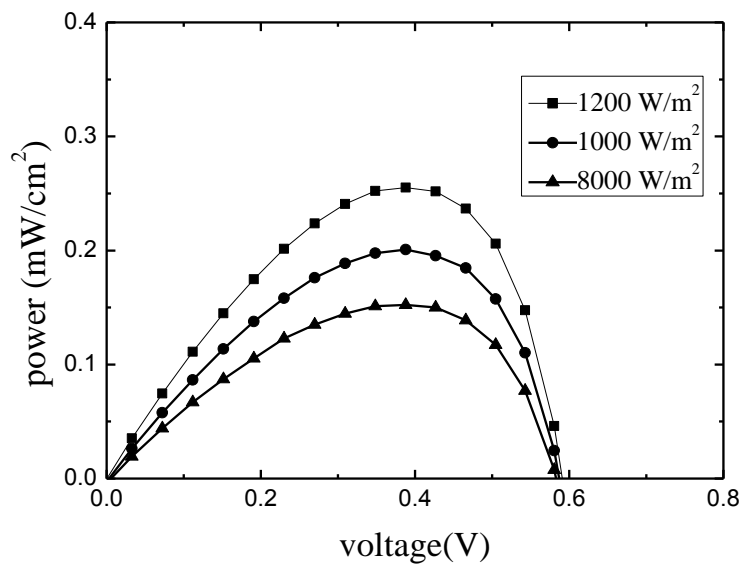


Figure 4.54. Power - voltage characteristics curves of the DSSCs sensitized by Pomegranate at different light intensities.

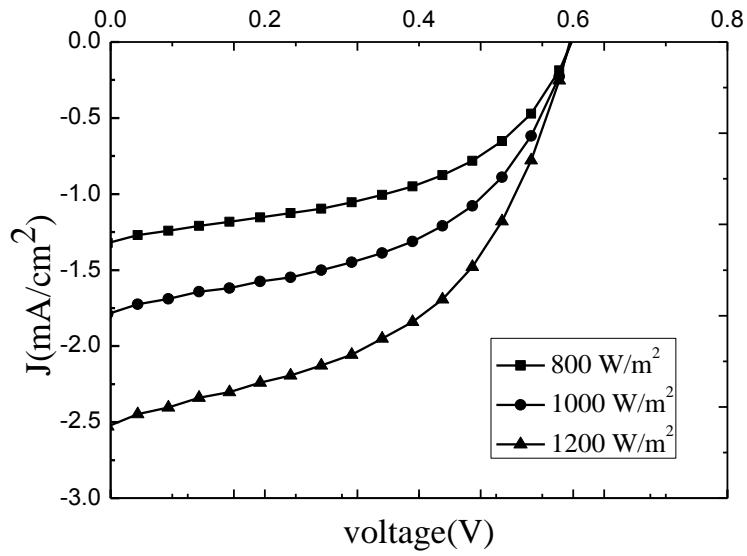


Figure 4.55. Current density–voltage characteristics curves for the DSSCs sensitized by Bananas at different light intensities.

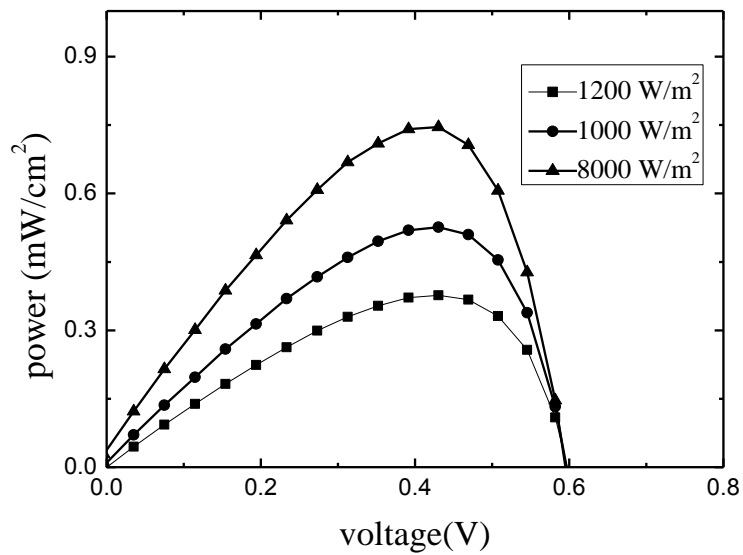


Figure 4.56. Power - voltage characteristics curves of the DSSCs sensitized by Bananas at different light intensities.

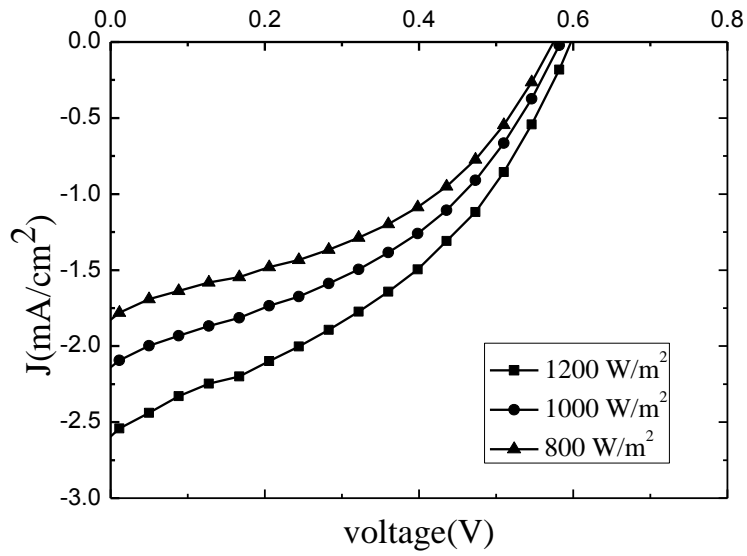


Figure 4.57. Current density–voltage characteristics curves for the DSSCs sensitized by Guava at different light intensities.

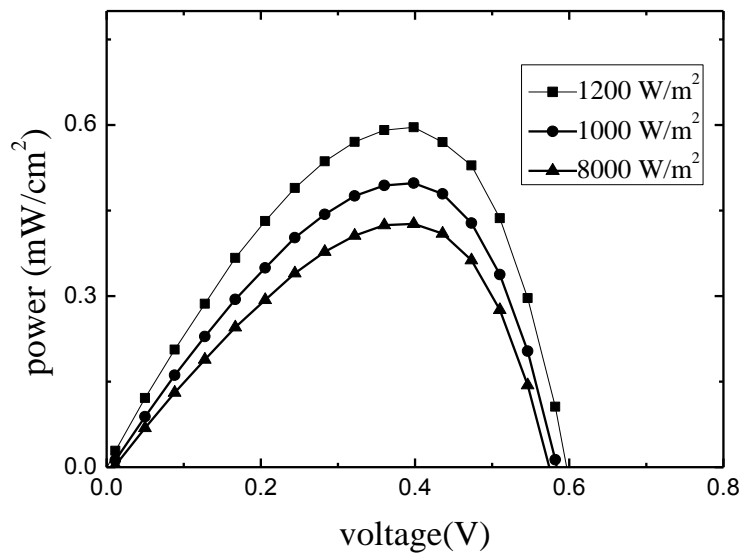


Figure 4.58. Power - voltage characteristics curves of the DSSCs sensitized by Guava at different light intensities.

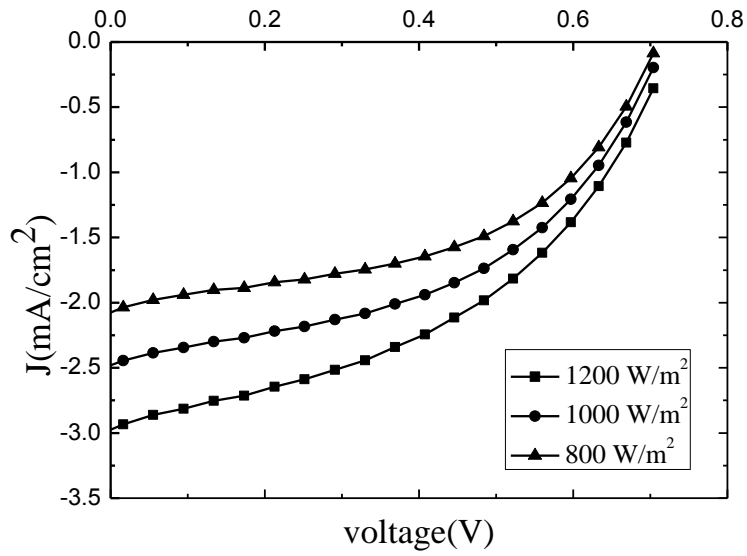


Figure 4.59. Current density–voltage characteristics curves for the DSSCs sensitized by Fluoridation at different light intensities.

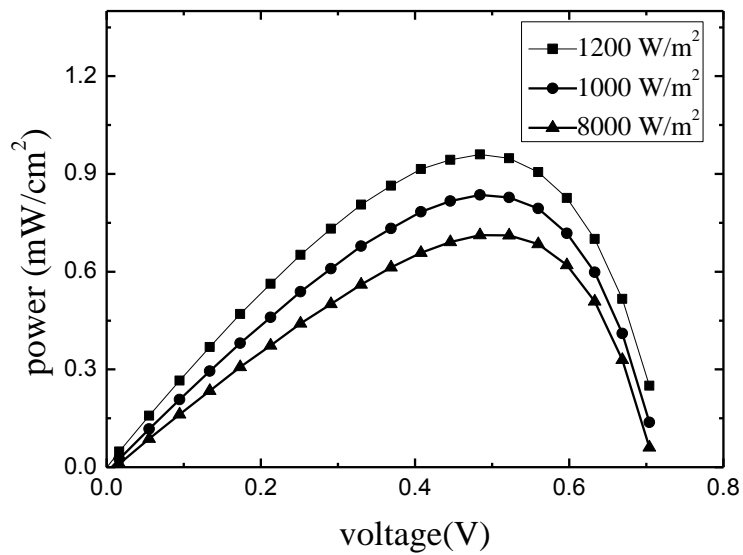


Figure 4.60. Power - voltage characteristics curves of the DSSCs sensitized by Fluoridation at different light intensities.

All the photovoltaic parameters of the fabricated DSSCs are listed in table 4.1. Values of (J_{sc}) and (V_{oc}) were determined from the J-V curves by estimating the (J- axis) and (V- axis) intercepts, respectively. The maximum power point is determined from the P-V curves from which J_m and V_m can be calculated. The fill factor and cell efficiency are calculated using Eq. (2.10) and Eq. (2.11), respectively. As can be seen from Table 4.1, the short circuit current density has a maximum value of 6.092 mA/cm² for the DSSC sensitized with the dye extracted from Mirabelle plums, and a minimum value of 0.95 mA/cm² for the DSSC sensitized with the dye extracted from Apricot. The DSSCs sensitized with Apple, Ziziphus jujuba, Berries, Mirabelle plums, and Peach, have relatively high values of the short circuit current density where the DSSCs sensitized with Apricot, Thyme, Mint, Shade tree, and Pomegranate have relatively low values of the short circuit current density. Moreover, the table shows that the short circuit current density increases with increasing the intensity of the incident light. These results for the J_{sc} are relatively higher than those obtained in [35,36,37]. In [35], DSSCs sensitized with Mango pericarp were fabricated and a short circuit current density of 2.69 mA/cm² was obtained. In [36], a short circuit current density of 3.59 mA/cm² was obtained for the DSSCs sensitized with sabdariffa. In [37], DSSCs sensitized with raspberries were fabricated and short a circuit current density of 0.360 mA/cm² was obtained.

The open circuit voltage ranges between 0.580 V for DSSCs sensitized with Mango extract and 0.703V for the cell dyed with Fluoridation. The DSSCs sensitized with Mint, Shade tree, Basil, Mango, and Pomegranate have relatively low values of the open circuit voltage whereas the DSSCs sensitized with Apricot, Apples, Ziziphus jujuba, Orange, and Fluoridation have relatively high values of the open circuit voltage. These results for the V_{oc} are relatively higher than those obtained in [35,36,37]. The fill factor of the fabricated cells changes from 32.3% to 63.5%. The highest fill factor was obtained for the DSSC sensitized with the extract of Victoria plums and the lowest fill factor was observed for the cell dyed with Mirabelle plums. The DSSCs sensitized with Apricot, Figs, Ziziphus jujuba, Basil, and Victoria plums have relatively high values of the fill factor. On the other hand, the DSSCs sensitized with Shade tree, Mirabelle plums, Peach, Pomegranate, and Guava have relatively low values of the fill factor. These results for the FF are relatively higher than those

obtained in [36,37]. The highest output power and efficiency were obtained for the DSSC sensitized with *Ziziphus jujuba* where the efficiency of the cell reached 1.032%. The DSSCs sensitized with *Ziziphus jujuba*, Berries, Mirabelle plums, Peach, and Fluoridation have relatively high values of the output power and efficiency whereas the DSSCs sensitized with Apricot, Thyme, Shade tree, Mango, and Pomegranate have relatively low values of the output power and efficiency. These results are much better than those obtained for the DSSCs sensitized by other natural dyes in pervious works [38]. The *Ziziphus jujuba* is the best natural dye were use, has values J_{sc} of 3.90 mA/cm^2 , V_{oc} of 0.661 V , $P_{max}=1.239 \text{ mW}$, $F.F=0.480$, and $\eta = 1.032\%$. Moreover, Table 3.2 shows the photoelectrochmical parameter of the DSSC sensitized with Ru complex, cis-dicyano-bis(2,2' -bipyridy 1-4,4' -dicarboxylic acid) ruthenium (II), Ruthenizer 505, (Solaronix, Switzerland), which is widely used in DSSC. As can be seen, V_{oc} of the DSSCs sensitized with the extract of Cream, Apricot, Figs, Apples, Sage, Thyme , Mint, *Ziziphus jujube*, Orange, Shade tree, Basil, Berries, Mirabelle plums, Victoria plums, Peach, Mango, Pomegranate, Bananas, Guava, and Fluoridation are very close to that work for the DCCSs sensitized Ru complex. The low efficiency mainly attributed to the low short circuit current.

As can be seen from table 4.1, The most of the fabricated cells have good open circuit voltage compared to the DSSCs sensitized by other natural dye in pervious works [35]. The fill factor for most of the cells have low values compared to the DSSCs sensitized by other natural dyes in pervious works [36].

The low values of η in our cells may be due to the fast charge recombination rate, loss resulting from the increase traffic of the electron [38], or incompatibility between the energy of the excited state of the adsorbed dye and the conduction band edge of TiO_2 . Moreover, the ground state of dye molecule could be considerably shifted with respect to the redox potential of Γ/I_3^- .

Low fill factor suggests that there is a large series resistance or a low shunt resistance in the cell. Series resistance arises from ohmic resistance, poor connection between material interfaces and low mobility of electrolyte. Low shunt resistance indicates that the current has alternative ways of crossing the cell other than the desired one, e.g. if

the TiO₂ electrode is in direct contact with counter electrode. In section 4.3, the values of shunt resistance and series resistance for some of the fabricated cells are shown.

If the thickness of the film is increased, more light can be harvested. But, at the same time, the distance the electron have to travel to reach the FTO layer increases and the probability of recombination also increases.

The used plants to extract the natural dyes in this work Table 4.1 shows the natural dyes as well as the corresponding open circuit voltage (V_{OC}) and short current (I_{SC}) of the (DSSC). Table 4.1 indicates that different dye has different absorption wave of light and the different corresponding open circuit voltage illustrates that the different combination of TiO₂ and dyes built also the different energy gaps. Different energy gaps of solar cells cause the different open circuit voltage. Moreover, the natural dyes extracted from the various plants have complicate mixed constituents, which causes the absorption wave of light not single.

The low P_{max} values come from the DSSC sensitized by the extracts natural dyes which ascribes to weakly bond between their dye molecule and TiO₂ film which is in consistent with the above discussions. Although nature dye chlorophyll play a key role in the photosynthesis ability in plant body, the ability cannot result in good photo-to-electric conversion in DSSC, because of no available bonds between the dyes molecular and TiO₂ film, through which electrons can transport from excited dyes molecule to TiO₂ film. Obviously, as a photo sensitizer, the interaction and bond between sensitizer (dye) and sensitizer (TiO₂ film) is very important in enhancing the photoelectric conversion efficiency of DSSC.

Natural dyes can be bound to the surface of the nanocrystalline-TiO₂ film, facilitating the injection of electrons from the excited state of natural dyes to the conduction band of TiO₂. Portico solvents such as ethanol are suitable as a rinsing solvent for the preparation of the electrodes that exhibit high cell performance, while water had an adverse effect.

Therefore, the natural dye shows potential to be used as green energy generator. In future, the use of TiO₂ film from the paste type to a thin film is suggested, as it will improve the connectivity between the TiO₂ film and dye. Natural dye based cells appear to be limited by low V_{oc} and a large decrease in photocurrent, probably due to

dye degradation. Finding different additives for improving V_{oc} might result in larger conversion efficiencies. Although the efficiencies obtained with these natural dyes are still below the current requirements for large scale practical application, the results are encouraging and may boost additional studies oriented to the search of new natural sensitizers and to the optimization of solar cell components compatible with such dyes.

Therefore, these natural dyes extracts are potentially capable of replacing some of the man made dyes used as sensitizer in nanocrystalline TiO_2 photovoltaic cells. Both the preparation of nanocrystalline TiO_2 layer and the nature of redoxing electrolyte must be optimized to enhance collection efficiency of the cell. We do suggest other nanostructure configurations such as nanocrystalline rods or dendrimers structures. Other large bandgap semiconductors might be used instead TiO_2 . Other factors during dye extraction such as solvent choice, temperature of extraction, and pH of the extracted dye solution must be investigated.

Due to the following advantages of DSSC over semiconductor based solar cells: bifacial configuration, efficiency less sensitive to angle of incidence, transparency for power windows, and color variation by selection of the dye; DSSC are expected to be a choice in building integrated photovoltaics . Also, success in fabrication of flexible substrate and screen printing of wide bandgap nanostructured semiconductor materials will facilitate mass production and commercialization of DSSC.

Table 4.1. Photovoltaic parameters of the DSSCs sensitized by natural dyes.

Dye	Intensity of light	J_{sc} (mA/cm²)	V_{oc} (V)	J_m (mA/cm²)	V_m (V)	P_{max} (mW)	FF	H %
Cream	1200 W/m ²	2.721	0.620	1.761	0.421	0.700	0.410	0.580
	1000 W/m ²	2.281	0.610	1.451	0.421	0.607	0.440	0.607
	800 W/m ²	1.930	0.600	1.290	0.421	0.530	0.460	0.661
Apricot	1200 W/m ²	0.951	0.630	0.701	0.470	0.330	0.550	0.275
	1000 W/m ²	0.771	0.620	0.561	0.470	0.260	0.551	0.261
	800 W/m ²	0.650	0.610	0.471	0.470	0.220	0.554	0.275
Figs	1200 W/m ²	3.001	0.596	2.100	0.406	0.848	0.474	0.706
	1000 W/m ²	2.091	0.596	1.500	0.438	0.642	0.515	0.642
	800 W/m ²	1.391	0.596	1.070	0.442	0.459	0.459	0.573
Apples	1200 W/m ²	3.251	0.651	2.001	0.421	0.835	0.395	0.351
	1000 W/m ²	2.750	0.641	1.750	0.421	0.726	0.412	0.420
	800 W/m ²	2.320	0.631	1.450	0.421	0.634	0.433	0.525

Dye	Intensity of light	J_{sc} (mA/cm²)	V_{oc} (V)	J_m (mA/cm²)	V_m (V)	P_{max} (mW)	FF	η %
Sage	1200 W/m ²	1.561	0.621	1.027	0.433	0.442	0.436	0.368
	1000 W/m ²	1.301	0.607	0.865	0.433	0.372	0.471	0.372
	800 W/m ²	1.061	0.596	0.683	0.434	0.302	0.478	0.377
Thyme	1200 W/m ²	0.956	0.604	0.603	0.425	0.257	0.476	0.229
	1000 W/m ²	0.712	0.596	0.444	0.425	0.187	0.440	0.187
	800 W/m ²	0.515	0.575	0.318	0.402	0.126	0.425	0.157
Mint	1200 W/m ²	1.131	0.590	0.670	0.387	0.258	0.386	0.215
	1000 W/m ²	0.980	0.579	0.587	0.387	0.227	0.400	0.227
	800 W/m ²	0.780	0.567	0.476	0.387	0.183	0.413	0.228
Ziziphus jujuba	1200 W/m ²	3.901	0.661	2.948	0.420	1.239	0.480	1.032
	1000 W/m ²	3.180	0.652	2.305	0.470	1.077	0.519	1.077
	800 W/m ²	2.670	0.646	1.982	0.470	0.925	0.536	1.156

Dye	Intensity of light	J_{sc} (mA/cm²)	V_{oc} (V)	J_m (mA/cm²)	V_m (V)	P_{max} (mW)	FF	η %
Orange	1200 W/m²	2.314	0.660	1.490	0.460	0.683	0.447	0.569
	1000 W/m²	1.745	0.660	1.147	0.460	0.517	0.448	0.517
	800 W/m²	1.438	0.660	0.920	0.460	0.423	0.445	0.528
Shade tree	1200 W/m²	1.043	0.596	0.598	0.386	0.230	0.369	0.191
	1000 W/m²	0.801	0.578	0.423	0.386	0.162	0.350	0.162
	800 W/m²	0.628	0.567	0.309	0.386	0.118	0.331	0.147
Basil	1200 W/m²	1.720	0.581	1.035	0.472	0.483	0.483	0.402
	1000 W/m²	1.398	0.581	0.950	0.431	0.409	0.499	0.409
	800 W/m²	1.094	0.581	0.742	0.431	0.318	0.500	0.395
Berries	1200 W/m²	4.256	0.601	2.644	0.411	1.077	0.421	0.897
	1000 W/m²	3.573	0.595	2.285	0.411	0.939	0.441	0.939
	800 W/m²	2.815	0.583	1.998	0.411	0.804	0.489	1.005

Dye	Intensity of light	J_{sc} (mA/cm ²)	V_{oc} (V)	J_m (mA/cm ²)	V_m (V)	P_{max} (mW)	FF	η %
Mirabelle plums	12000 W/m ²	6.092	0.583	3.366	0.330	1.134	0.322	0.945
	1000 W/m ²	5.164	0.573	2.877	0.330	0.958	0.323	0.958
	800 W/m ²	4.311	0.563	2.558	0.330	0.845	0.348	1.056
Victoria plums	1200 W/m ²	1.452	0.603	1.096	0.515	0.556	0.635	0.463
	1000 W/m ²	1.383	0.687	0.981	0.515	0.501	0.527	0.501
	800 W/m ²	1.201	0.671	0.845	0.515	0.431	0.534	0.583
Peach	1200 W/m ²	3.512	0.617	2.144	0.395	0.864	0.351	0.720
	1000 W/m ²	2.555	0.611	1.675	0.395	0.659	0.422	0.659
	800 W/m ²	1.962	0.606	1.295	0.395	0.513	0.431	0.641
Mango	1200 W/m ²	1.243	0.480	0.827	0.391	0.321	0.538	0.267
	1000 W/m ²	1.037	0.570	0.696	0.391	0.269	0.455	0.269
	800 W/m ²	0.878	0.560	0.582	0.391	0.225	0.457	0.281

Dye	Intensity of light	J_{sc} (mA/cm²)	V_{oc} (V)	J_m (mA/cm²)	V_m (V)	P_{max} (mW)	FF	η %
Pomegranate	1200 W/m²	1.129	0.581	0.656	0.391	0.225	0.343	0.212
	1000 W/m²	0.907	0.581	0.514	0.391	0.200	0.379	0.200
	800 W/m²	0.725	0.581	0.395	0.391	0.152	0.360	0.156
Bananas	1200 W/m²	2.501	0.596	1.722	0.429	0.745	0.499	0.620
	1000 W/m²	1.770	0.596	1.214	0.429	0.522	0.492	0.522
	800 W/m²	1.306	0.596	0.882	0.429	0.378	0.485	0.472
Guava	1200 W/m²	2.594	0.592	1.491	0.400	0.595	0.388	0.495
	1000 W/m²	2.130	0.582	1.243	0.400	0.498	0.401	0.498
	800 W/m²	1.811	0.572	1.070	0.400	0.425	0.410	0.531
Fluoridation	1200 W/m²	2.965	0.703	1.982	0.483	0.958	0.459	0.798
	1000 W/m²	2.474	0.703	1.731	0.483	0.835	0.480	0.835
	800 W/m²	2.077	0.703	1.491	0.483	0.712	0.487	0.890
Ru	1200W/m²	12.5	0.600	10.22	0.381	3.14	0.4604	2.58

4.2 Chemical Dyes as Photosensitizers For Dye Sensitized Solar Cell

4.2.1 Absorption Spectra of Chemical Dyes

Figures 4.61 through 4.68 show the UV–VIS absorption spectra of the chemical dyes listed in table 3.2.

Figure 4.61 shows the absorption spectrum of Eosin Y using ethanol as a solvent. There is an absorption peak at about 520.4 nm. Figure. 4.62 shows the absorption spectrum of Aniline Blue which exhibits an absorption a peak at 624.8 nm. Figure 4.63 shows that the Bromophenol Blue has an absorption peak at 426.3 nm for ethyl alcohol solvent. The absorption spectrum of Alcian Blue is shown in Figure. 4.64. The absorption spectrum curve shows two peaks at 624.2 nm and 671.5 nm. As can be seen from Fig. 4.65, the absorption spectrum curve shows a peak at 654.4nm for the Methyl Orange. Fig. 4.66 reveals that Crystal Violet extract has an absorption peak in the visible light region at 587.7nm. Fast Green dissolved in ethyl alcohol shows a peak at 619.8nm in Fig 4.67 Finally, in Fig. 4.68, it is shown that Carbol Fuchsin extract has a very sharp peak at 550.6nm.

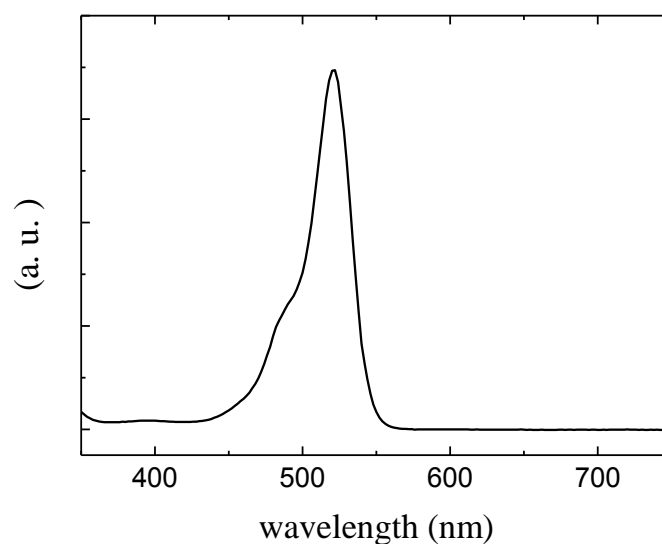


Figure 4.61. The absorption spectrum of the Eosin Y dissolved in ethyl alcohol.

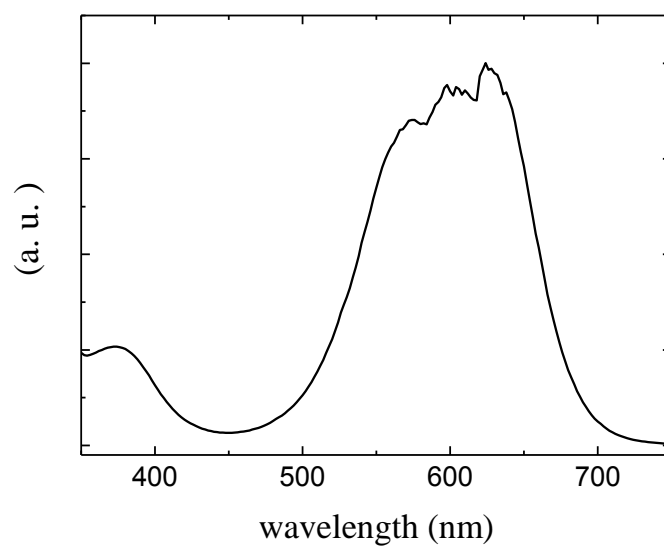


Figure 4.62. The absorption spectrum of Aniline Blue dissolved in ethyl alcohol.

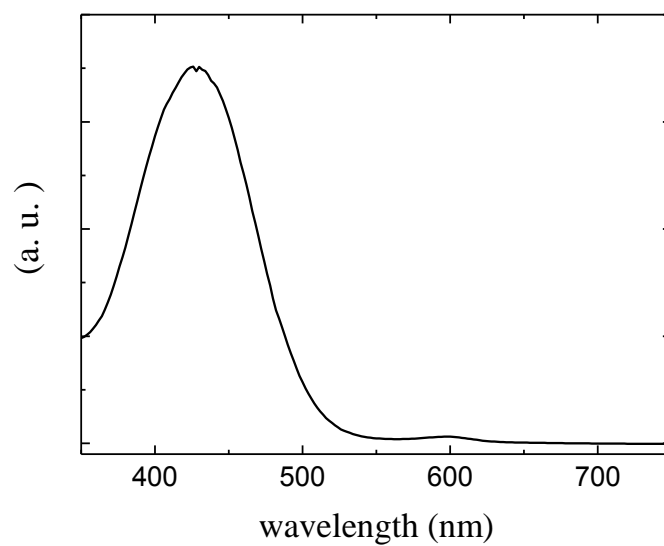


Figure 4.63. The absorption spectrum of the Bromophenol Blue dissolved in ethyl alcohol.

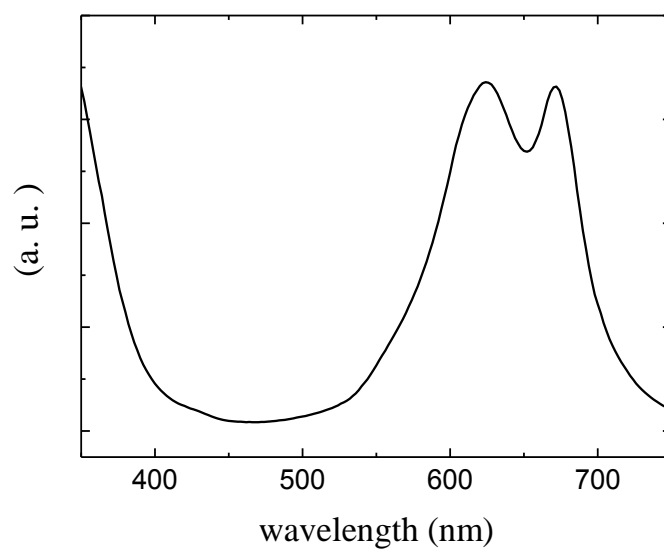


Figure 4.64. The absorption spectrum of the Alcian Blue dissolved in ethyl alcohol.

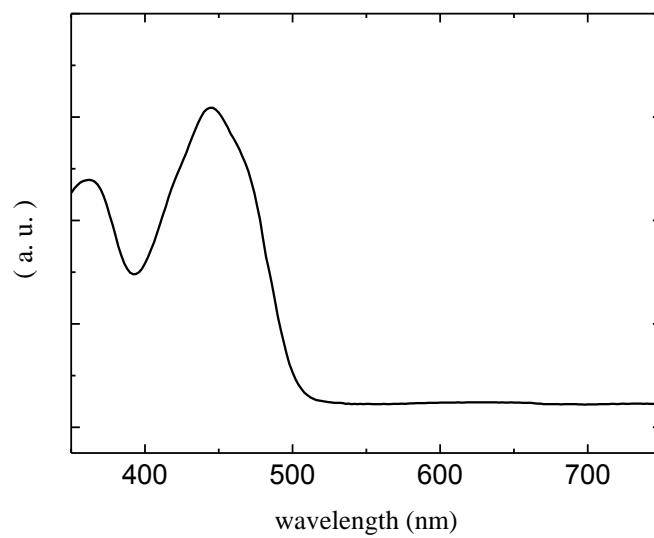


Figure 4.65. The absorption spectrum of the Methyl Orange dissolved in ethyl alcohol.

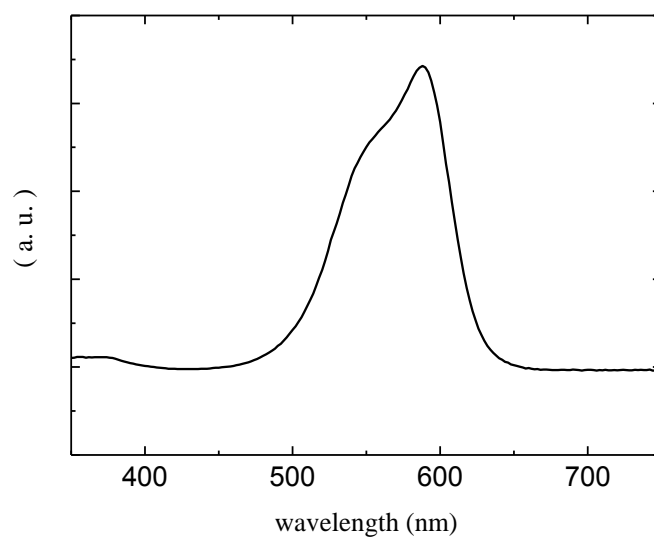


Figure 4.66. The absorption spectrum of the Crystal Violet dissolved in ethyl alcohol .

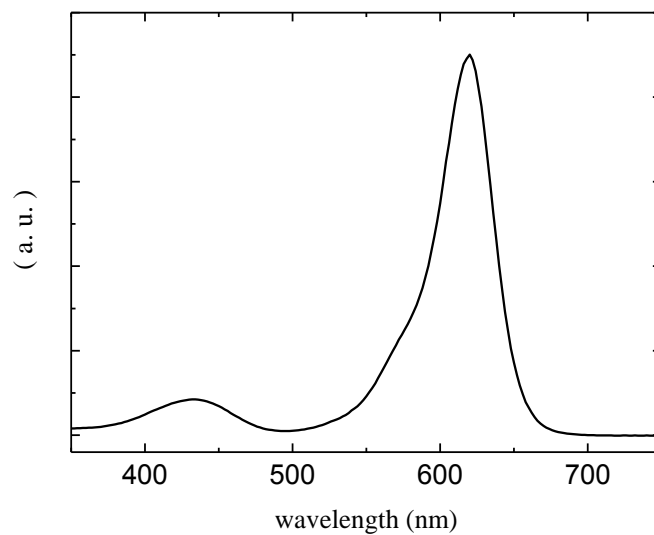


Figure 4.67. The absorption spectrum of the Fast Green dissolved in ethyl alcohol .

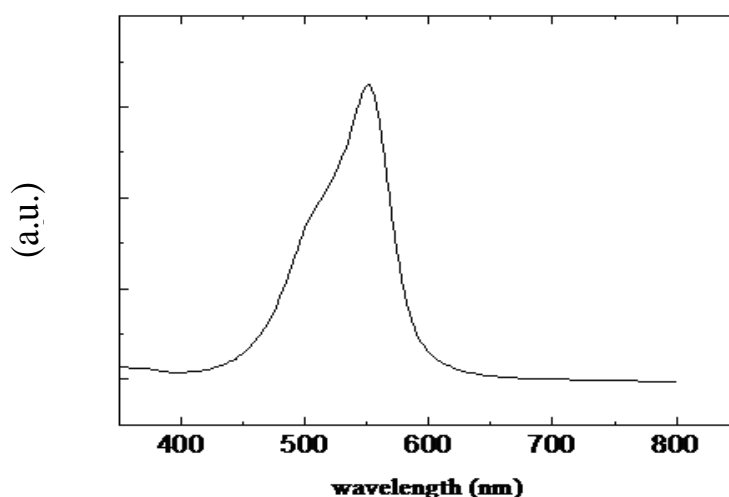


Figure 4.68. The absorption spectrum of the Carbol Fuchsin dissolved in ethyl alcohol.

4.2.2. Photovoltaic Parameters of Dye Sensitized Solar Cells Sensitized with Chemical Dyes

In the following, the results obtained for the DSSCs sensitized the eight chemical dyes and with platinum as a counter electrode are presented. For each dye, the measured current density J versus the voltage V is plotted at three different light intensities (1200 W/m^2 , 1000 W/m^2 , and 800 W/m^2). For each J-V curve, the output power (P) is calculated and plotted versus the voltage. Figure 4.69 shows the measured current density versus the voltage of the cell sensitized by Eosin Y at light intensities 800 W/m^2 , 1000 W/m^2 , and 1200 W/m^2 . The output power is then calculated for each experimental point by simply multiplying the individual current and voltage of that point. The calculated power as a function of the voltage applied to the cell is plotted in Fig. 4.70. Figures 4.69, 4.71, 4.73, 4.75, 4.77, 4.79, 4.81, and 4.83 show the J-V characteristic curves obtained for the fabricated DSSC using Aniline Blue, Bromophenol Blue, Alcian Blue, Methyl Orange, Crystal Violet, Fast Green, and Carbol Fuchsin. Each figure shows the results obtained under illumination of the cell by three different intensities. In a similar manner, Figs. 4.70, 4.72, 4.74, 4.76, 4.78, 4.80, 4.82 and 4.84 show the calculated power versus the voltage for the cells fabricated these dyes in the same order mentioned above.

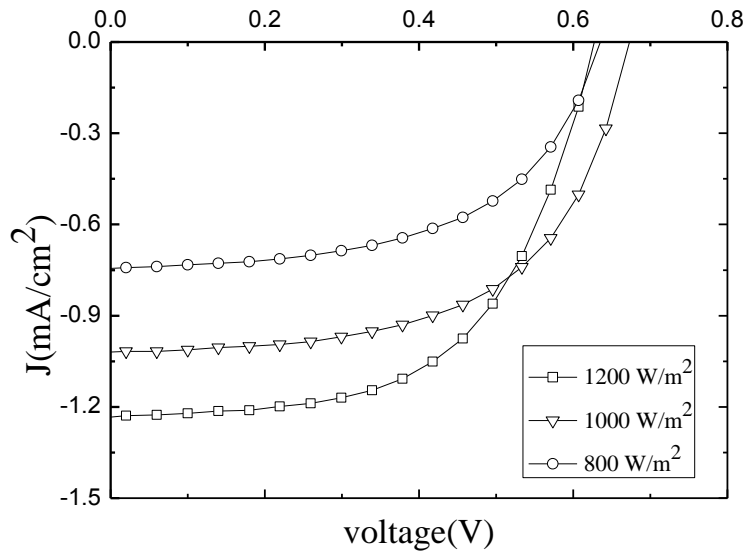


Figure 4.69. Current density–voltage curves for the DSSC sensitized by Eosin Y at different light intensities.

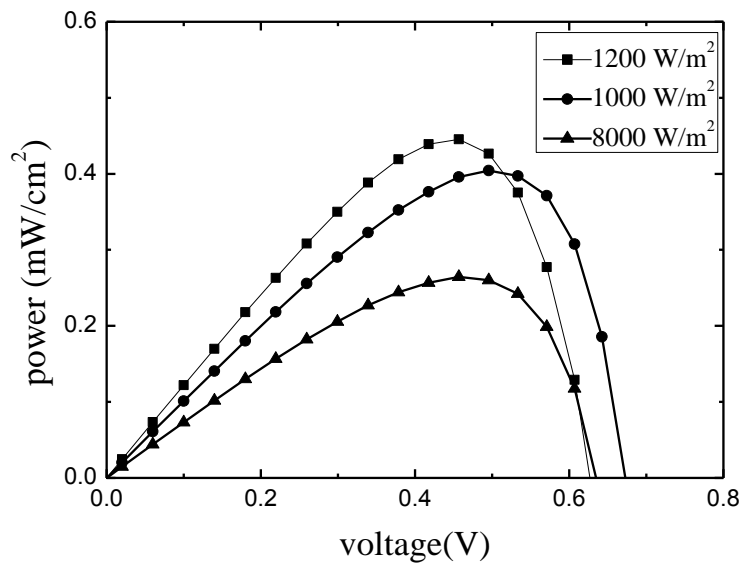


Figure 4.70. Power - voltage characteristics of the DSSC sensitized by Eosin Y at different light intensities.

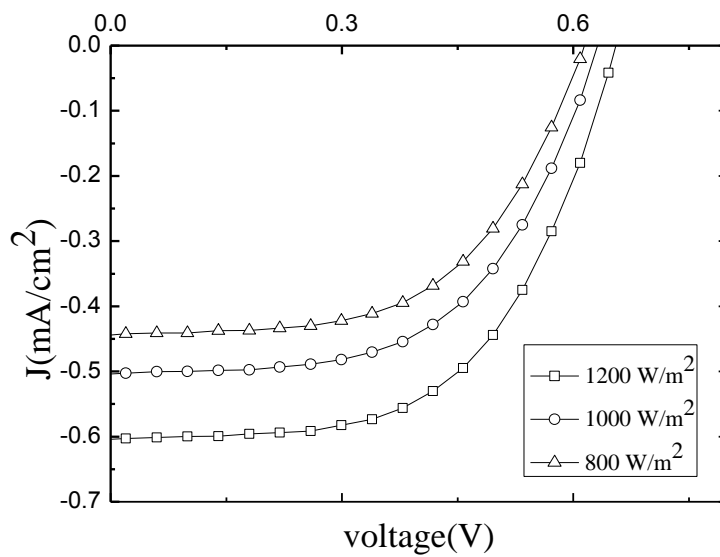


Figure 4.71. Current density–voltage curves for the DSSC sensitized by Aniline Blue at different light intensities.

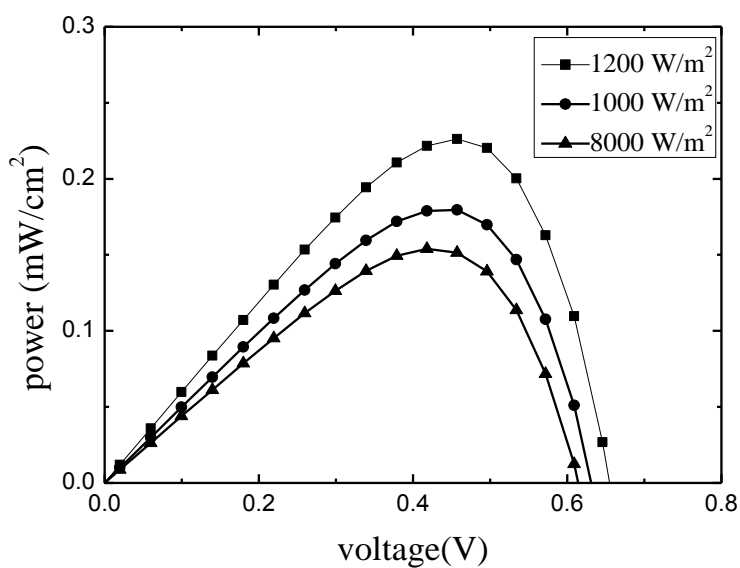


Figure 4.72. Power - voltage characteristics of the DSSC sensitized by Aniline Blue at different light intensities.

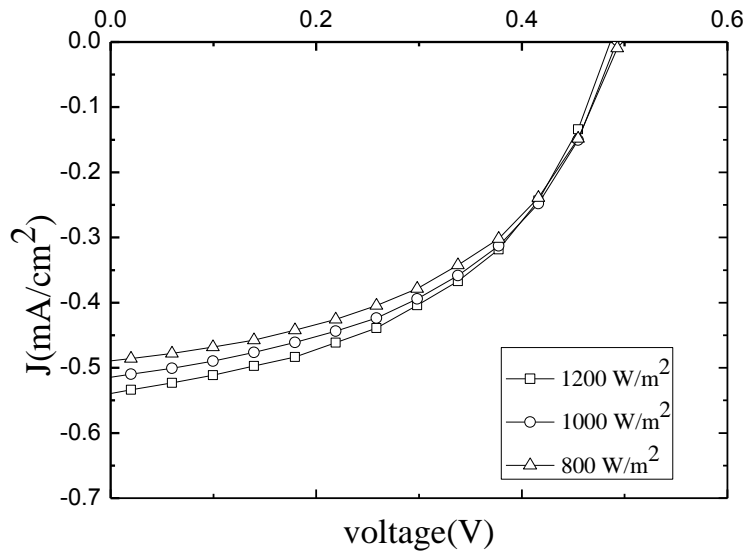


Figure 4.73. Current density–voltage curves for the DSSC sensitized by Bromopheol Blue at different light intensities.

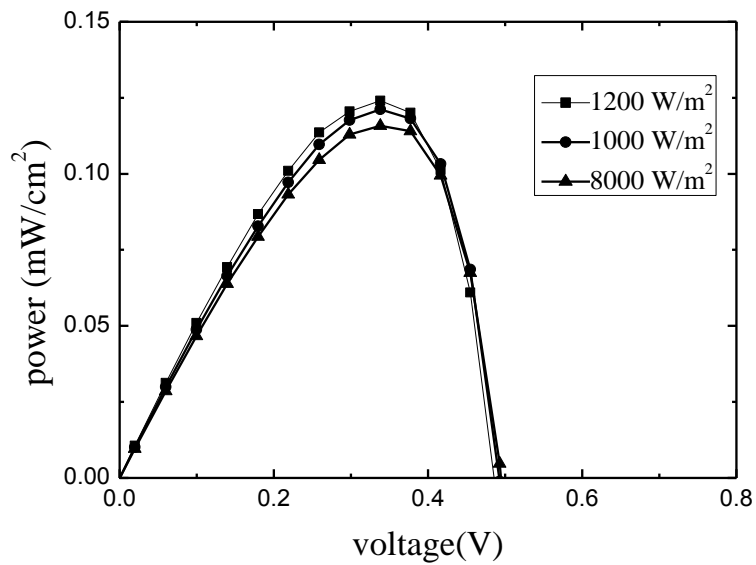


Figure 4.74. Power - voltage characteristics of the DSSC sensitized by Bromopheol Blue at different light intensities.

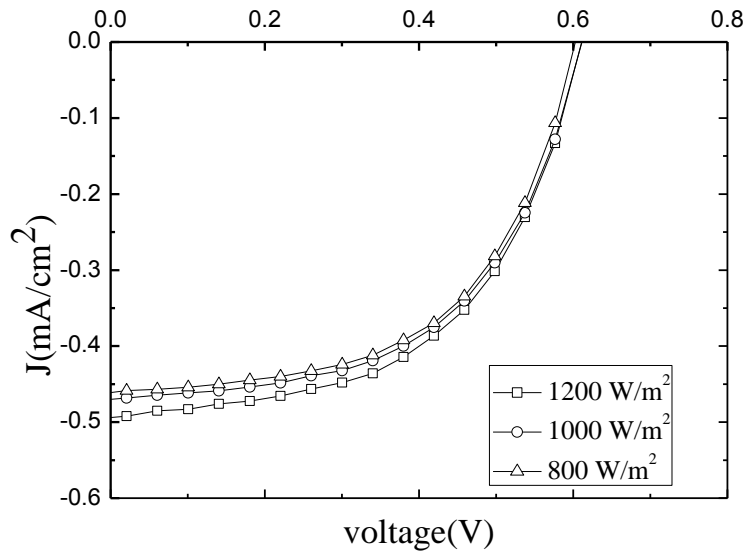


Figure 4.75. Current density–voltage curves for the DSSC sensitized by Alcian Blue at different light intensities.

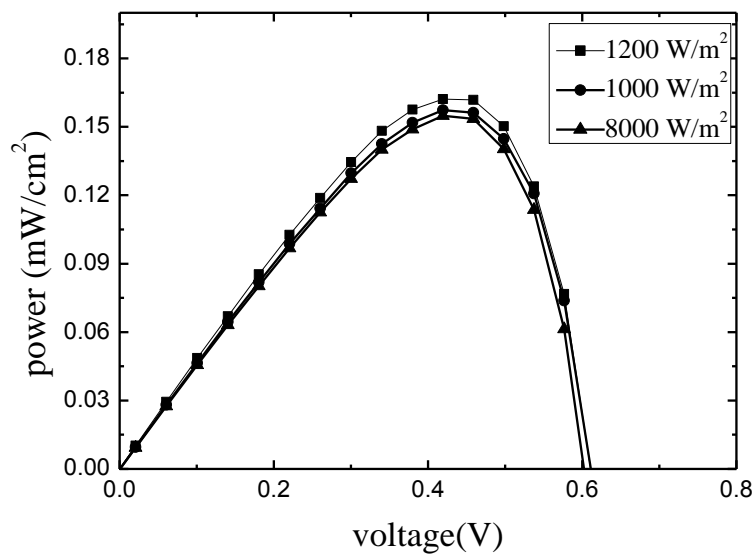


Figure 4.76. Power - voltage characteristics of the DSSC sensitized by Alcian Blue at different light intensities.

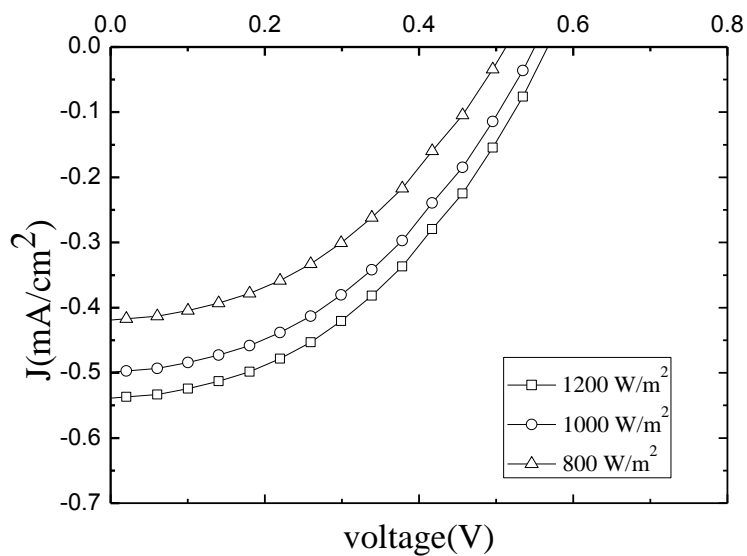


Figure 4.77. Current density–voltage curves for the DSSC sensitized by Methyl Orange at different light intensities.

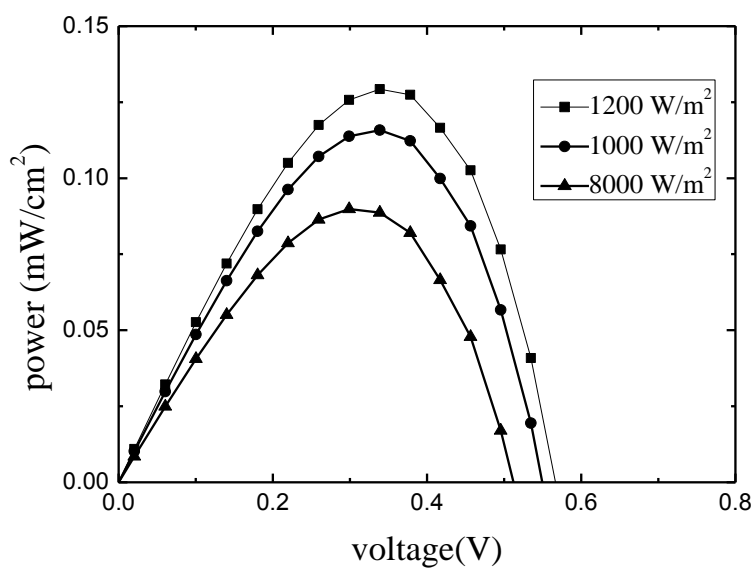


Figure 4.78. Power - voltage characteristics of the DSSC sensitized by Methyl Orange at different light intensities.

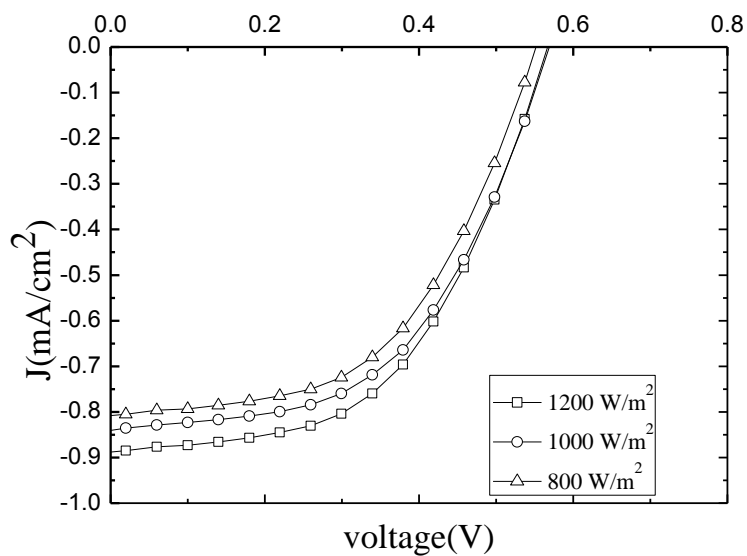


Figure 4.79. Current density–voltage curves for the DSSC sensitized by Crystal Violet at different light intensities.

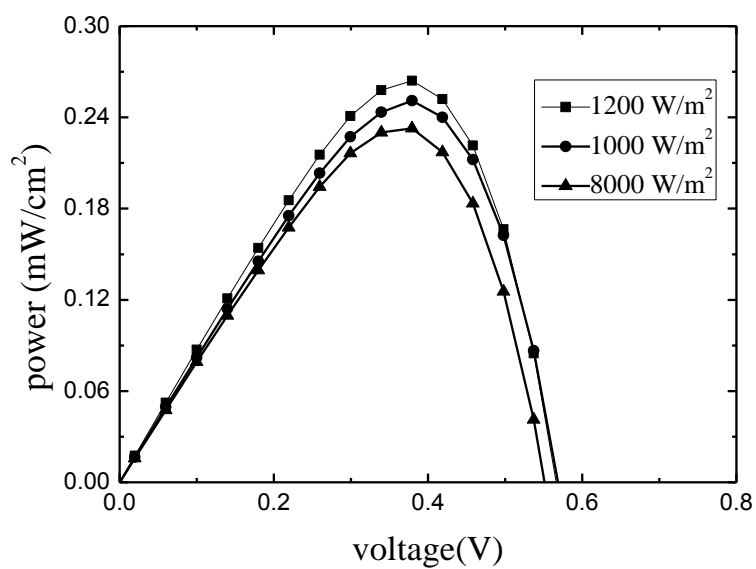


Figure 4.80. Power - voltage characteristics of the DSSC sensitized by Crystal Violet at different light intensities.

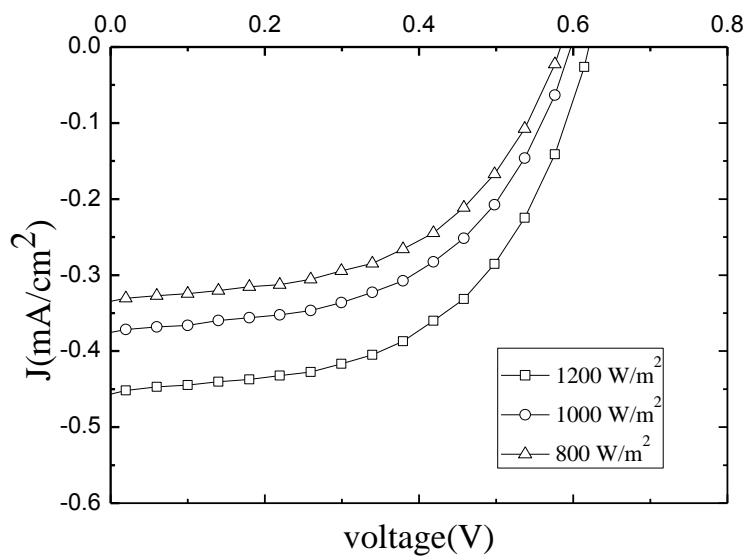


Figure 4.81. Current density–voltage curves for the DSSC sensitized by Fast Green at different light intensities.

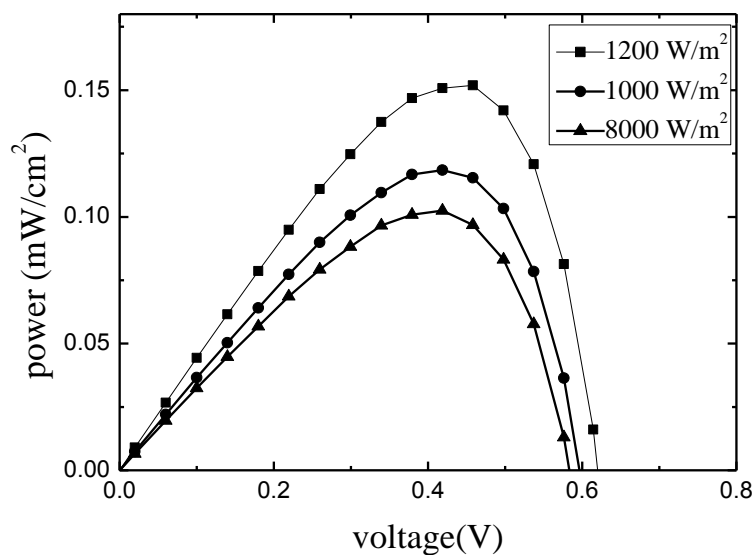


Figure 4.82. Power - voltage characteristics of the DSSC sensitized by Fast Green at different light intensities.

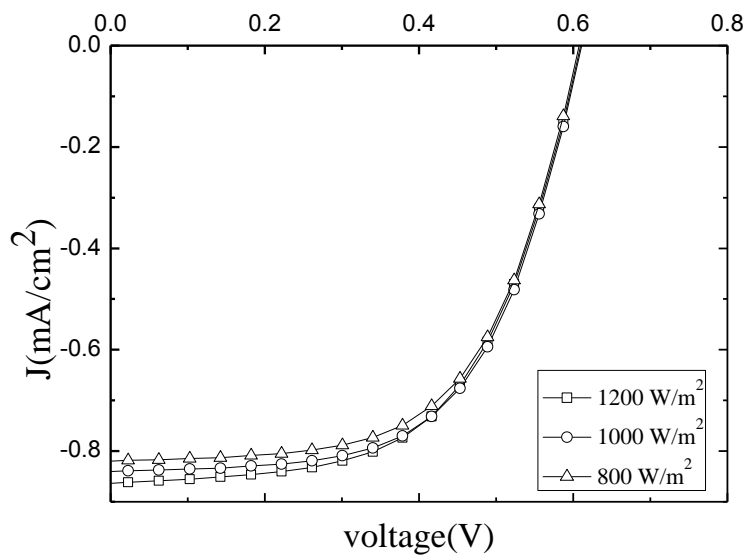


Figure 4.83. Current density–voltage curves for the DSSC sensitized by Carbol Fuchsin at different light intensities.

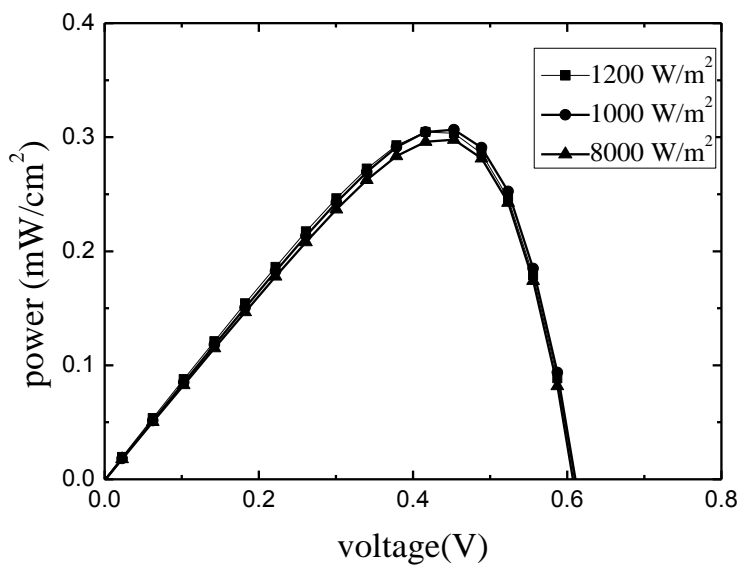


Figure 4.84. Power - voltage characteristics of the DSSC sensitized by Carbol Fuchsin at different light intensities.

All the photovoltaic parameters of the fabricated DSSCs are listed in table 4.2. Each cell was examined under three illuminations (1200 W/m^2 , 1000 W/m^2 , 800 W/m^2). Values of J_{sc} and V_{oc} were determined from the J-V curves, by finding the intercepts of the J- axis and V- axis intercepts, respectively. The maximum power point is determined from the P-V curves from which J_m and V_m can be calculated. The fill factor and cell efficiency are the calculated using Eq. (2.10) and Eq. (2.11), respectively. From table 4.2, the best performance was obtained for cell dyed with Eosin Y which has the following results, $J_{sc} = 1.23 \text{ mA/cm}^2$, $V_{oc}=0.63 \text{ V}$, $P_{max}= 0.44 \text{ mW/cm}^2$, $F.F=0.52$, and $\eta =0.34\%$. As can be seen from Table 4.2, the short circuit current density has a maximum value of 1.230 mA/cm^2 for the DSSCs sensitized with the Eosin Y, and a minimum value of 0.456 mA/cm^2 for the DSSCs sensitized with the Fast Green. The DSSCs sensitized Eosin Y, Crystal Violet, and Carbol Fuchsin exhibit high values of the short circuit current density whereas the DSSCs sensitized with Alcian Blue, Methyl Orange, and Fast Green have relatively low values of the short circuit current density. Moreover, the table shows that the short circuit current density increases with increasing the intensity of the incident light. The open circuit voltage ranges between 0.565 V for the DSSCs sensitized with Bromophenol Blue extract and 0.653 V for the cell dyed with Aniline. The fill factor of the fabricated cells changes from 43.0% to 60.2% . The highest fill factor was obtained for the DSSC sensitized with the extract of Alcian Blue and the lowest fill factor was observed for the cell dyed with Methyl Blue. The highest output power and efficiency were obtained for the DSSC sensitized with Eosin Y where the efficiency of the cell reached 0.336% . The DSSCs sensitized with Eosin Y, Crystal Violet, and Carbol Fuchsin have relatively high values of the output power and efficiency whereas the DSSCs sensitized with Methyl Orange, Bromophenol Blue, and Fast Green, have relatively low values of the output power and efficiency. These results are comparable than those obtained for the DSSCs sensitized by other chemical dyes in pervious works [39]. The low values of (I_{sc}) in our cells may be due to the fast charge recombination rate, loss resulting from the increase traffic of the electron, or incompatibility between the energy of the excited state of the adsorbed dye and the conduction band edge of TiO_2 .

Table 4.2. Photovoltaic parameters of the fabricated DSSCs

Dye	Intensity of light	J_{sc} (mA/cm ²)	V_{oc} (V)	J_m (mA/cm ²)	V_m (V)	P_{max} (mW)	FF	η %
Eosin Y	1200 W/m ²	1.230	0.630	1.021	0.439	0.440	0.521	0.336
	1000 W/m ²	1.020	0.671	0.787	0.509	0.339	0.581	0.399
	800 W/m ²	0.747	0.633	0.537	0.484	0.261	0.551	0.236
Anilin blue	1200 W/m ²	0.604	0.653	0.497	0.457	0.261	0.575	0.186
	1000 W/m ²	0.505	0.630	0.410	0.438	0.224	0.564	0.177
	800 W/m ²	0.444	0.612	0.346	0.441	0.177	0.561	0.190
Bromopheol blue	1200 W/m ²	0.537	0.565	0.370	0.337	0.123	0.469	0.102
	1000 W/m ²	0.513	0.549	0.350	0.337	0.120	0.479	0.120
	800 W/m ²	0.487	0.521	0.347	0.337	0.115	0.494	0.143
Alcian blue	1200 W/m ²	0.492	0.601	0.369	0.483	0.162	0.602	0.135
	1000 W/m ²	0.470	0.600	0.358	0.483	0.156	0.556	0.156
	800 W/m ²	0.460	0.599	0.351	0.483	0.153	0.557	0.191

Dye	Intensity of light	J_{sc} (mA/cm²)	V_{oc} (V)	J_m (mA/cm²)	V_m (V)	P_{max} (mW)	FF	η %
Methyl orange	1200 W/m²	0.537	0.565	0.383	0.341	0.129	0.430	0.108
	1000 W/m²	0.500	0.549	0.341	0.341	0.115	0.424	0.115
	800 W/m²	0.417	0.421	0.287	0.341	0.089	0.417	0.112
Crystal violet	1200 W/m²	0.885	0.567	0.695	0.377	0.263	0.450	0.219
	1000 W/m²	0.839	0.566	0.665	0.377	0.249	0.526	0.249
	800 W/m²	0.805	0.549	0.613	0.373	0.232	0.524	0.290
Fast green	1200 W/m²	0.456	0.619	0.333	0.459	0.151	0.541	0.127
	1000 W/m²	0.374	0.600	0.288	0.416	0.117	0.533	0.117
	800 W/m²	0.333	0.581	0.246	0.416	0.101	0.528	0.127
Carbol fuchsin	1200 W/m²	0.861	0.610	0.704	0.436	0.305	0.584	0.255
	1000 W/m²	0.841	0.608	0.700	0.436	0.303	0.596	0.303
	800 W/m²	0.821	0.606	0.680	0.436	0.297	0.596	0.371

4.3 Results and Discussions of Electrochemical Impedance Spectroscopy

Electrochemical impedance spectroscopy was measured for three cells using Autolab device, for the DSSCs sensitized by Berries, Mirabelle plums, and Peach

(A) FRA measurement for the DSSC using Berries as a sensitizer with photovoltaic parameter $J_{sc} = 2.85 \text{ mA/cm}^2$, $V_{oc} = 0.583 \text{ V}$, $FF = 48.9\%$, and $\eta = 1.005\%$.

- FRA measurement potentiostatic scan have three types: FRA frequency scan, electrochemical circle fit, and fit and simulation data

(1) FRA frequency scan has three curves are:

(i) Nyquist $-Z''$ vs Z'

(ii) Bode modulus

(iii) Bode phase

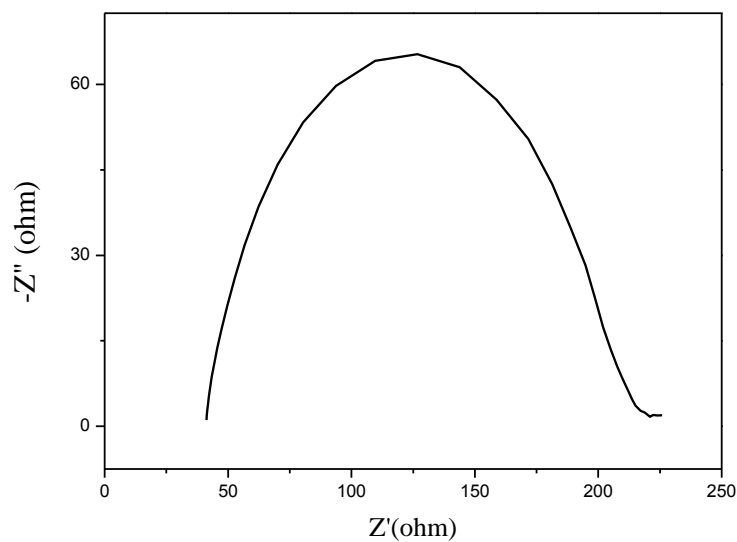


Fig 4.85. Nyquist curve for the DSSC sensitized by Berries

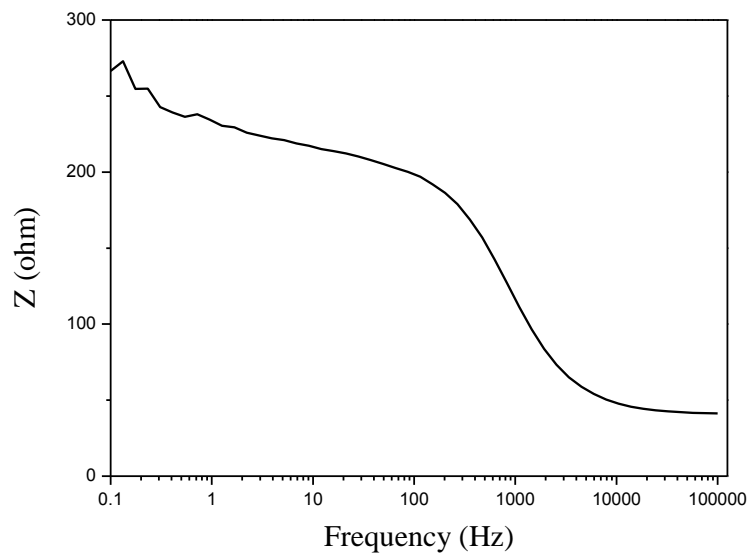


Fig 4.86. Bode modulus for the DSSC sensitized by Berries.

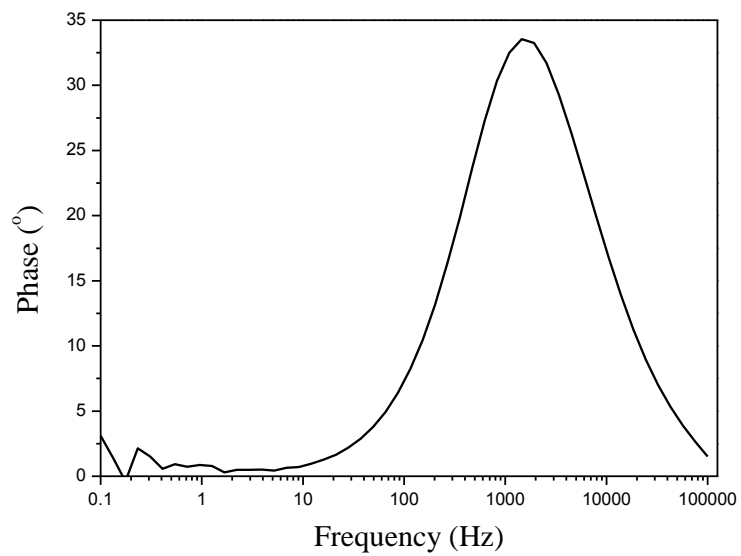


Fig 4.87. Bode phase curve for the DSSC sensitized by Berries

(2) Electrochemical circle fit was obtained

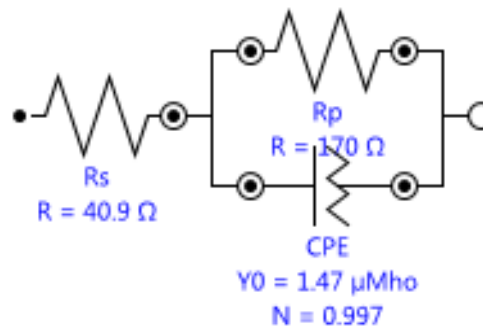


Fig 4.88. The equivalent circuit for the DSSC sensitized by Berries.

From the simulation and fitted data Fig 4.88, we can obtain R_s (electronic resistance) = 40.9Ω , R_p (charge-transfer resistance) = 170Ω ,and Q , constant phase element with $Y_0=1.47\mu\text{Mho}$, and $n= 0.997$ CPE may be replaced by pseudo capacitance by E.q. (5.17) $C=1.44\ \mu\text{F}$, then Fig 4.88. become

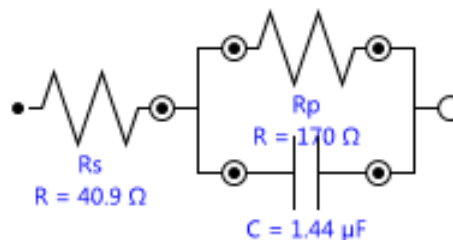


Fig 4.89. The equivalent circuit for DSSC sensitized by Berries with replace CPE with pseudo capacitance.

(3) Fit and simulation

The simulation tool can be used to calculate the expected behavior of a user-defined equivalent circuit. To use the simulation tool, the equivalent circuit must first be defined, in the same way as for the fitting procedure. However, the fit or simulation parameter in the control interface must be set to "Simulation". The simulation is performed automatically and the results are immediately available for plotting.

Figure 4.90. shows an example of simulated data, compared to the initial measured data points used in this example.

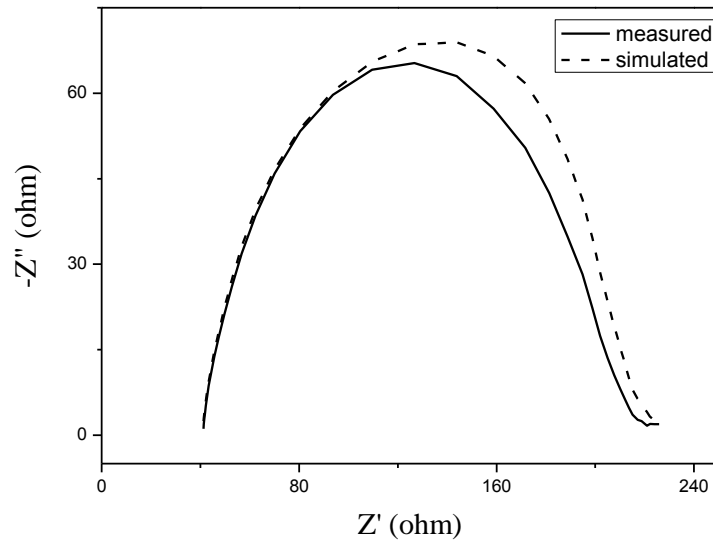


Fig 4.90. Nyquist curve for simulated values, and measured data points

(A) FRA measurement for the DSSC using Mirabelle plums as sensitizer with photovoltaic parameter $J_{sc} = 4.31 \text{ mA/cm}^2$, $V_{oc} = 0.563 \text{ V}$, $FF = 34.8\%$, and $\eta = 1.056\%$.

(1) FRA frequency scan has the following curves

- (i) Nyquist $-Z''$ vs Z'
- (ii) Bode modulus
- (iii) Bode phase

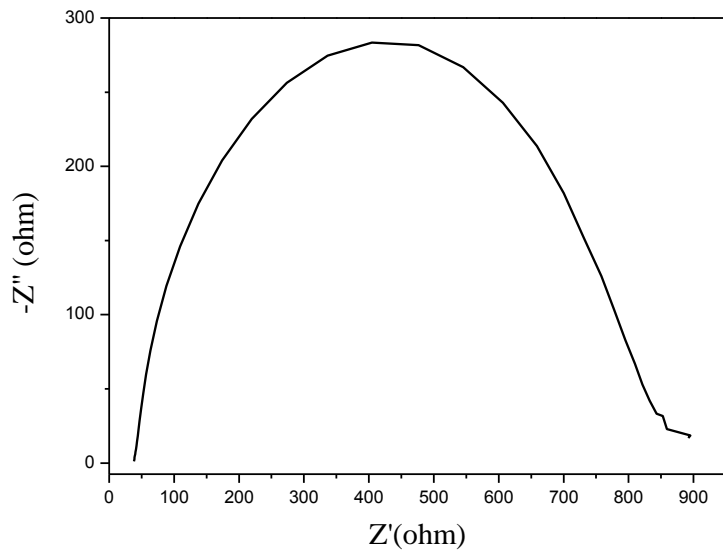
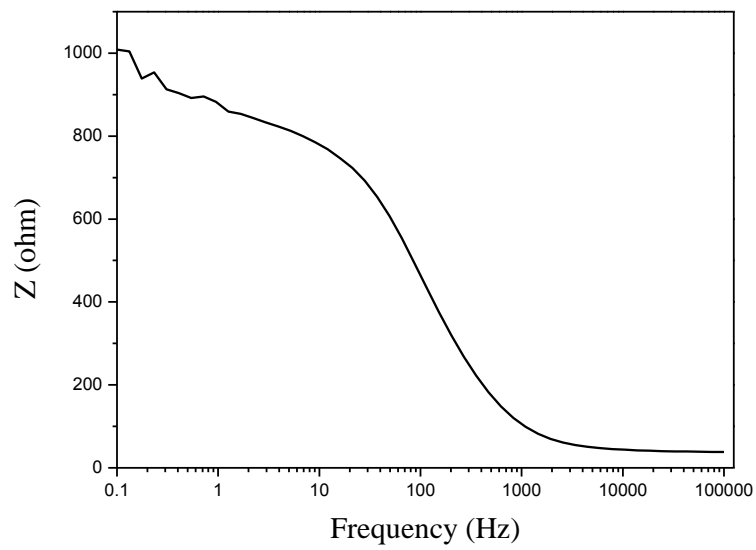


Fig 4.91. Nyquist curve for the DSSC sensitized by Mirabelle



plums

Fig 4.92. Bode modulus for the DSSC sensitized by Mirabelle plums.

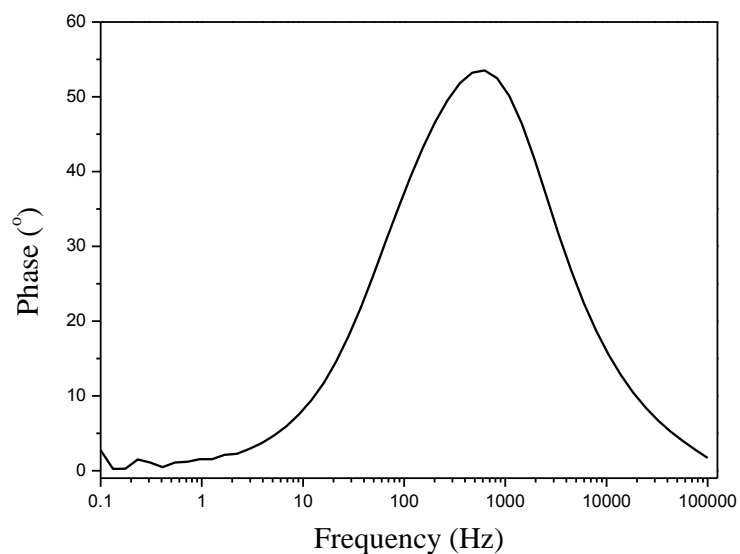


Fig 4.93. Bode phase for the DSSCs sensitized by Mirabelle plums.

(2) Electrochemical circle fit were obtained

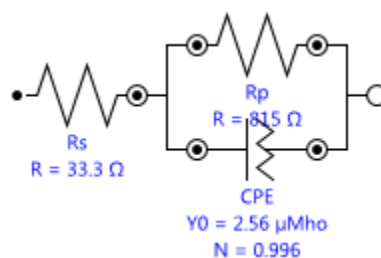


Fig 4.94. The equivalent circuit for the DSSC sensitized by Mirabelle plums.

From the Fig 4.94. we can obtain R_s (electronic resistance) = 33.3Ω , R_p (charge-transfer resistance) = 815Ω ,and Q , constant phase element with $Y_0 = 2.56 \mu\text{Mho}$, and $n = 0.996$ CPE can be replaced with pseudo capacitance $C = 2.50 \mu\text{F}$, then Fig 4.94 become

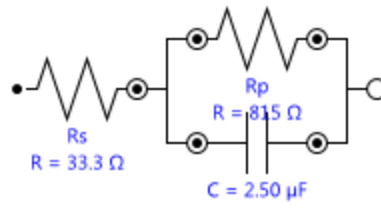


Fig 4.95. The equivalent circuit for the DSSC sensitized by Mirabelle plums with replacing CPE with pseudo capacitance.

(3) Fit and simulation

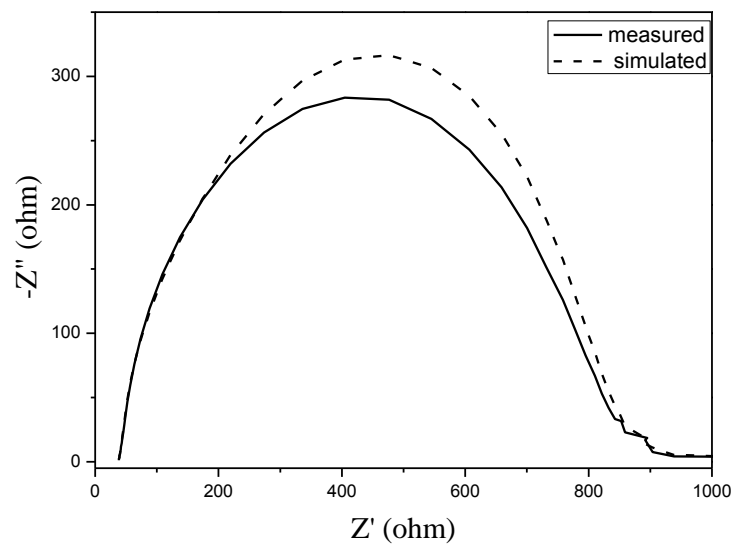


Fig 4.96. Nyquist curve for simulated values and measured data point

(B) FRA measurement for the DSSC using Peach as a sensitizer with photovoltaic parameter $J_{sc} = 3.512 \text{ mA/cm}^2$, $V_{oc} = 0.617 \text{ V}$, $FF = 35.1 \%$, and $\eta = 0.72 \%$.

As mentioned before, three curve should be consider.

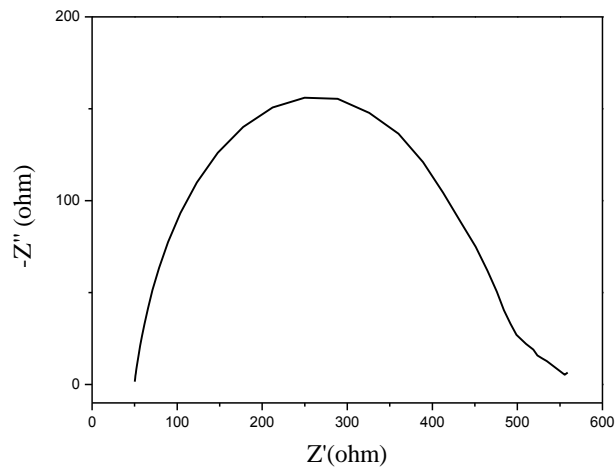


Fig 4.97. Nyquist curve for the DSSC sensitized by Peach.

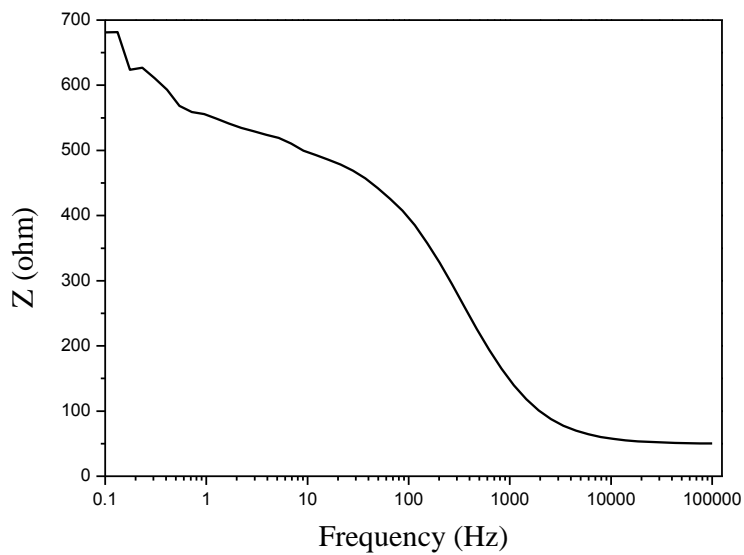


Fig 4.98. Bode modulus curve for the DSSC sensitized by Peach.

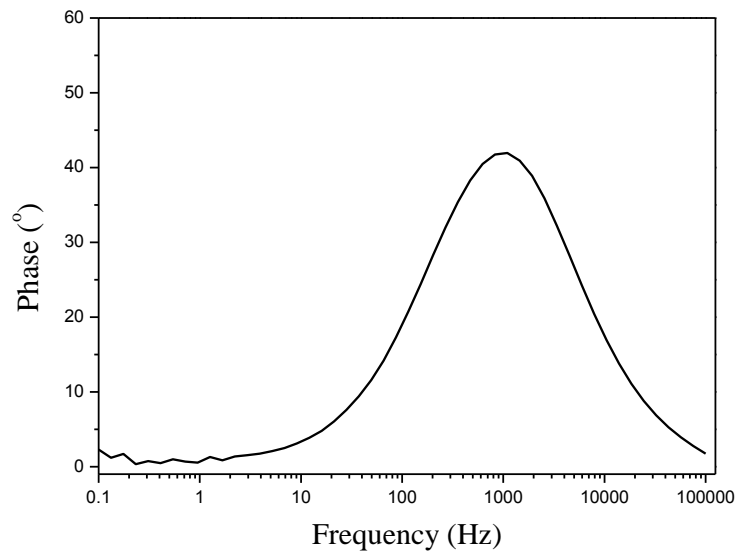


Fig 4.99. Bode phase curve for the DSSC sensitized by Peach.

(2) Electrochemical circle fit

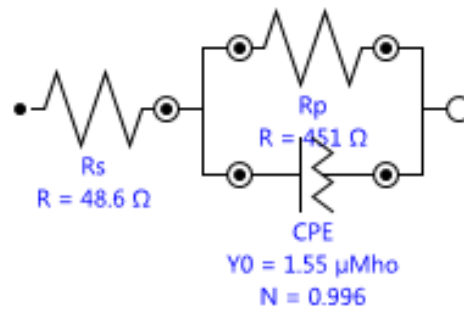


Fig 4.100. The equivalent circuit for DSSCs sensitized by Peach.

From the Fig. 4.100, we can obtain R_s (electronic resistance) = 48.6Ω , R_p (charge-transfer resistance) = 451Ω ,and Q , constant phase element with $Y_0=1.55 \mu\text{Mho}$, and $n= 0.996$ replacing CPE with pseudo capacitance $C =2.51 \mu\text{F}$, Fig. 4.100 become

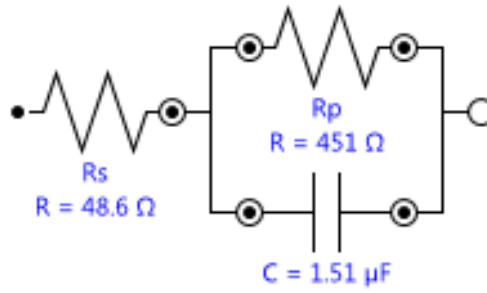


Fig 4.101. The equivalent circuit for the DSSC sensitized by Peach. with replacing CPE with pseudo capacitance.

(3) Fit and simulation

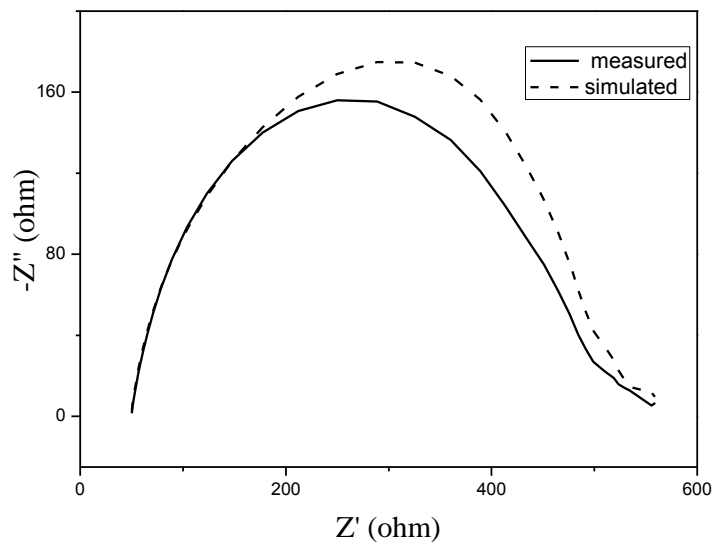


Fig 4.103. Nyquist curve for simulated values, and measured data point

CAPTER FIVE

Conclusions

The main aim of this thesis was to study the fabrication and characterization of dye sensitized solar cell using natural and synthetic dye. The characterization of the dye sensitized solar cells was main focus of attention in this thesis. The characterization was not limited to the actual cells but also the source materials i.e. TiO₂ past and dye and, photoelectrode and counterelectrode different parts of the cell were separately characterized , the benefits used in this work.

The natural dyes were extracted from leaves of plants. The TiO₂ layer was dyed using twenty natural dyes, A set of dye-sensitized solar cells were assembled using ethanol dye solvent and platinum as a back electrode, and eight chemical dyes were used as sensitizers for DSSCs. These dyes are Alcian Blue, Crystal Violet, Eosin Y, Carbol Fuchsin, Aniline Blue, Methyl Orange, Fast Green and Bromophenol Blue. The fabricated cells were examined under three different light intensities, the impedance spectroscopy of three natural dyes cells were measured and equivalent circuit was found.

The following results have been obtained Using ethyl alcohol as a solvent and platinum as a back electrode the results were founded as, the J_{sc} from 0.951 mA/cm² to 6.092 mA/cm² and V_{oc} from 0.573V to 0.703V for natural dyes, the best performance was obtained for the DSSC sensitized with Ziziphus jujuba with parameter $J_{sc} = 2.671$ mA/cm², $V_{oc} = 0.646$ V, $J_m = 1.982$ mA/cm², $V_m = 0.470$ V, FF = 53.6 %, and $\eta = 1.156$ %.

The DSSC fabricated chemical dyes were examined, and we were used platinum as back electrode and ethyl alcohol as solvent of dyes the results were founded as, the J_{sc} from 0.456 mA/cm² to 1.230 mA/cm² and V_{oc} from 0.565 V to 0.653V and the best performance was obtained for the DSSC sensitized with Eosin Y with parameter $J_{sc} = 2.671$ mA/cm², $V_{oc} = 0.646$ V, $J_m = 1.982$ mA/cm², $V_m = 0.470$ V, FF = 53.6 %, and $\eta = 0.399$ %.

These results clearly show that the application of natural dye to DSSCs as a photosensitizer is promising for the realization of high cell performance, low-cost production, and non-toxicity. It should be emphasized here that natural dyes from food are better for human health than synthetic dyes.

References

- [1] R.L. Sizmann, P. Köpke and R. Busen, "Solar power plants", 17-83, editor: C.-J. Winter, R.L. Sizmann and L.L. Vant-Hull, "Solar Radiation Conversion" Springer-Verlag, Berlin, Heidelberg, (1991).
- [2] H. A. McCARTNEY and M. H. UNSWORTH " Spectral distribution of solar radiation. I: direct radiation" *Quart. J. R. Met. Soc.*, VOL.104, PP. 699-718, (1978),
- [3] K.. Peippo, Aurinkosähköjärjestelmien käytön ja mitoituksen perusteita, NEMO-raportti 23, ISSN 0785-644X, ISBN 951-22-1342-7, Teknillinen korkeakoulu, in Finnish, (1992).
- [4] Motiva, <http://www.motiva.fi/tietopankki/asuminen/asu-kul-sahko.html>, available on 16.12.2001.
- [5] M. Gutschner and S. Nowak, "Potential and implementation of building-integrated photovoltaics on the local level - case studies and comparison of urban and rural areas in Switzerland", 16th European Photovoltaic Solar Energy Conference, 1-5 May, (2000).
- [6] L. L. Kazmerski, "Photovoltaics: A Review of Cell and Module Technologies", *Renewable and Sustainable Energy Reviews*, Vol. 1 No. 1, pp. 71-170, (1997).
- [7] M. A. Green, "Solar Cell Efficiency Tables", *Prog. Photovolt. Res. Appl.*, vol, 9, pp.287-293, (2001).
- [8] A. Shah, P. orres, R. Tscharnner, N. Wyrsh & H. Keppner "Photovoltaic Technology: The Case for Thin-Film Solar Cells", *Science*, Vol. 285 No. 5427, pp. 692-8, (1999).
- [9] A. Goetzberger, C. Hebling, Photovoltaic materials, past, present and future, *Solar energy material and solar cells*, Vol.62, No. 13, pp.1-19,(2000).
- [10] D. Meissner, Solar Technology –" Photoelectrochemical Solar Energy Conversion, *Ullmann's Encyclopedia of Industrial Chemistry*", Sixth Edition, Electronic Release, (1999).
- [11] B. O'Regan and M. Grätzel, "A low-cost, high-efficiency solar cell based on dyesensitized colloidal TiO₂ films" *Naturr*, vol. 353, No. 6346, pp. 737 – 740, (1991).

- [12] K. Wongcharee, V. Meeyoo, S. Chavadej, "Dye-sensitized solar cell using natural dyes extracted from rosella and blue pea flowers", *Sol. Energ. Mat. Sol.* Vol. 91, No. 7, pp. 566–571. (2007).
- [13] G. Calogero and G. D. Marco, "Red Sicilian orange and purple eggplant fruits as natural sensitizers for dye-sensitized solar cells," *Solar Energy Materials and Solar Cells*, vol. 92, no. 11, pp. 1341–1346, (2008).
- [14] Tsung-Wei Lin, Jun-Ren Lin, Sheng-You Tsai, Jing-Nang Lee, and Chen-Ching Ting, "Absorption Spectra Analysis of Natural Dyes for Applications in Dye-Sensitized Nano Solar Cells", *National Conference on Theoretical and Applied Mechanics*, Vol, 96, pp, 21-22, (2007).
- [15] P. Luo, H. Niu, G. Zheng, X. Bai, M. Zhang, W. Wang, "From salmon pink to blue natural sensitizers for solar cells: *Canna indica* L., *Salvia splendens*, cowberry and *Solanum nigrum* L.", *Spectrochim. Acta Part A* Vol. 74 pp. 936–942, (2009)
- [16] Huizhi Zhou, Liqiong Wu, Yurong Gao, Tingli Ma " Dye-sensitized solar cells using 20 natural dyes as sensitizers" *Journal of Photochemistry and Photobiology A: Chemistry*, Vol. 219, No. 2, pp.188–194 (2011)
- [17] R. G. Gordon, "Criteria for Choosing Transparent Conductors," *MRS Bulletin*, vol. 25, No.8, pp. 52-57, August (2000).
- [18] A. Hagfeldt and M. Grätzel, "Light-Induced Redox Reactions in Nanocrystalline Systems," *Chemical Reviews*, Vol. 95, No. 1, pp. 49-68, (1995).
- [19] K. Kalyanasundaram, M. Grätzel, "Applications of functionalized transition metal complexes in photonic and optoelectronic devices," *Coordination Chemistry Reviews*, Vol. 177, No. 1, pp. 347–414, (1998).
- [20] A. Hagfeldt , M. Grätzel , *Molecular Photovoltaics*, *Acc. Chem. Res.*, Vol. 33, No. 5, pp. 269-277, (2000).
- [21] M. A. Green, N.J. , " *Operating Principles, Technology, and System Applications*, Englewood Cliffs", Prentice, Solar Cells -Hall, (1982).

- [22] G. Wolfbauer et al., "A channel flow cell system specifically designed to test the efficiency of redox shuttles in dye sensitized solar cells", *SOL EN MAT*, vol, 70, No.1, pp. 85-101, (2000).
- [23] A. Hauch, R. Kern, J. Ferber, A. Georg, J. Luther, "Characterization of the Electrolyt-Solid Interfaces of Dye-sensitized Solar Cells by Means of Impedance spectroscopy", 2nd world conference and exhibition on photovoltaic solar conversion Vienna, Austria, (1998).
- [24] N. Papageorgiony, W. F. Maier, M. Grätzel, An Iodide/Triiodide Reduction Electron catalyst for Aqueous and Organic Media, *J. Electrochem. soc.*, Vol.144, No. 3, pp. 876-884, (1997).
- [25] A. Tolvanen, "Characterization and manufacturing techniques of dye sensitized solar cell", Master of science in technology, HELSINKI UNIVERSITY OF TECHNOLOGY, (FINLAND) , (2003).
- [26] J. Nelson, " The Physics of Solar Cell", Imperial College Press, London, pp. 13-16, (2003).
- [27] D.G. Wolfbauer, " The Electrochemistry of Dye sensitized solar cell ,their sensitizer and their redox shuttles", Department of chemistry, monash, clayton3168, Melbourne, Australia, (1997).
- [28] G. Smestad et al., " Testing of dye-sensitized TiO₂ solar cells I: Experimental photocurrent output and conversion efficiencies", *Solar Energy Materials & Solar Cells*, Vol. 32, No. 3, pp. 259-272, (1994).
- [29] S. Hao, J. Wu, Y. Huang, and J. Lin, "Natural dyes as photosensitizers for dye-sensitized solar cell" *Solar Energy*, vol. 80, No. 2, pp. 209–214, (2006).
- [30] Raistrick ID, "Application of impedance spectroscopy to materials science", *Ann Rev Mater Sci*, vol, 16, pp. 343–70, (1986)
- [31] Barsoukov E, Macdonald JR, "Impedance spectroscopy theory, experiment, and applications". 2nd edn. John Wiley & Sons, Hoboken, NJ, (2005).
- [32] Bard AJ, Faulkner LR, " Electrochemical methods: fundamentals and application", Wiley, New York, (1980).

- [33] Research Solutions and Resources LLC (2009) The constant phase element (CPE). <http://www.consultrsr.com/resources/eis/cpe1.htm>. Accessed, (2009).
- [34] Z. Stoynov, D. Vladikova, " Differential impedance analysis", Marin Drinov Academic Publishing House, Bulgaria, (2005).
- [35] A.R. Hernández-Martínez, M. Estevez , S. Vargas, F. Quintanilla, R. Rodríguez, "Natural Pigment-Based Dye-Sensitized Solar Cells", Vol 10, No 1, 2011
- [36] Sancun Hao, Jihuai Wu, Yunfang Huang, Jianming Lin " Natural dyes as photosensitizers for dye-sensitized solar cell " Solar Energy vol. 80, No.2, pp.209–214, (2006)
- [37] Khalil Ebrahim Jasim, Sains Malaysia "Natural Dye-Sensitized Solar Cell Based on Nanocrystalline TiO₂ ", (Sel Suria Terpeka Pewarna Semula Jadi Berasaskan Nanohablur TiO₂) Vol. 41, No.8, pp. 1011–1016 (2012)
- [38] J. Halme, " Dye-sensitized nanostructured and organic photovoltaic cells: technical review and preliminary tests", Master of science in technology, HELSINKI UNIVERSITY OF TECHNOLOGY, (FINLAND), 2002.
- [39] Wei Hao Lai, Yen Hsun Su , Lay Gaik Teoh, , Min Hsiung Hon, " Commercial and natural dyes as photosensitizers for a water-based dye-sensitized solar cell loaded with gold nanoparticles" Journal of Photochemistry and Photobiology A: Chemistry Vol. 195, No. 2-3, pp.307–313,(2008)